A GEOPHYSICAL INVESTIGATION OF DEWATERING STRUCTURES IN WESTERN LAKE SUPERIOR

A THESIS
SUBMITTED TO THE FACULTY OF THE GRADUATE SCHOOL
OF THE UNIVERSITY OF MINNESOTA
BY

DANIEL JAY GUSTAFSON

IN PARTIAL FULFILLMENT OF THE REQUIREMENTS
FOR THE DEGREE OF
MASTER OF SCIENCE

DR. NIGEL WATTRUS & DR. JOHN SWENSON

JANUARY, 2012

Acknowledgements

I would like to take this opportunity to acknowledge and thank those who provided me with invaluable assistance and support throughout this project:

I thank my advisors, Nigel Wattrus and John Swenson for their guidance and their patients throughout my graduate studies. Their continued feedback and advice have made this project and its completion a reality. Additionally I would like to thank the captain and crew of the R/V Blue Heron for their assistance in the collection of the geophysical data used for this project. I have enjoyed the many cruises we have had together and will miss being out on the big water.

To my fellow graduate students, I thank you for your friendship and support, especially Jessica Gary and Josh Allen. I wish you all the best going forward.

Finally a special thank you goes to Nigel Wattrus for offering me such a great thesis topic and the opportunity to conduct geophysical research in four countries on three continents, in addition to the half-dozen Blue Heron cruises.

Abstract

Irregular ring shaped depressions are widely developed on the floor of Lake Superior. They are typically between 200 and 300 meters across. The troughs that define these rings are typically 10 to 30 meters wide and up to five meters deep. High resolution multibeam bathymetric data show that the lake floor rings are actually chains of individual bathymetric pocks. In Lake Superior bathymetric pocks have been observed as isolated features, irregular polygonal rings, and closely grouped ring networks. The Lake Superior basin contains sediments deposited during the last deglaciation of the basin. The glacial and post-glacial sediments sit atop Precambrian basement rocks. These bathymetric ring features have not been commonly reported elsewhere. Pockmarks, however, have been observed globally and are typically the result of expelled fluids or gases.

A series of high resolution, single-channel seismic data sets were collected in addition to high resolution multibeam bathymetry to test the working hypothesis that Lake Superior's rings are the result of sediment dewatering. The vast depth of the Thunder Bay trough provides an ideal location to study these features, protected from wave base erosion.

The results confirm the existence of three types of dewatering structures associated with the lake floor rings. These features include two deep-sourced and one shallow dewatering structure(s). The evidence suggests that the rings were produced by the expulsion of fluid from the lake floor at, or close to, the

termination of glaciolacustrine deposition in the basin. This places the formation of these unusual features around the time of the last eastward overflow from Lake Agassiz directly into Lake Superior. Abrupt lake level change linked to the Agassiz overflow is believed to have triggered basin wide expulsion of pore water leading to the formation of the lake floor rings.

Table of Contents

List of Tables

List of Figures

Chapter 1: Introduction

One of the first papers describing pockmarks was a paper published in 1970 by King and MacLean. In this paper the authors describe pockmarks on the Scotian Shelf that they attribute to the seafloor expulsion of fluids or gas. Since then, pockmarks have been described worldwide in marine and lacustrine sediments. Interest in these features is commonly motivated by the fact that they are often associated with deep-sourced thermogenic gas (Sahling, 2008; Davy et al., 2010). Although frequently associated with gas expulsion (Judd and Hovland, 2007), pockmark formation has also been associated with fluid expulsion (Moernaut et al., 2010; Plaza-Faverola et al., 2011; Reiche et al., 2011). ROV and submersible observations have documented the development of biological communities in association with these features (Hovland and Judd, 1988; Hovland et al., 1992). Presumably, these communities are at least in part, supported by the fluids and gasses released from the sea-floor at these sites (Hovland and Judd, 1988).

Ring-shaped depressions were first described in Lake Superior by Berkson and Clay (1973) who associated them with syneresis in the fine-grained lake floor sediments. Flood and Johnson (1984) later described ring and crescent shaped pockmarks on the lake floor off the Keweenaw Peninsula. They attributed them to dewatering of the glaciolacustrine sediments underlying the lakefloor.

Sidescan and multibeam sonar imagery has revealed that much of the lake floor of Lake Superior, below wave base (the depth to which large storms

reach) is covered by fields of giant ring-shaped depressions (Wattrus pers. comm.) These are often as much as 300 meters across, up to 5 meters deep and have ring widths of more than 25 m. The lake floor inside a ring is at the same general elevation as the lake floor outside the ring. The rings occur both as isolated structures as well as irregular networks. There is no evidence that when grouped in networks, the rings ever intersect each other (Wattrus pers. comm.). Multibeam data reveals that the rings are actually irregular polygons that are composed of chains of pockmarks/pits (Wattrus et al., 2005)**.**

The sediments below the lake floor are mostly the product of deposition during and since the last deglaciation of the basin (Dell, 1972, 1974; Johnson, 1980). The boundary between the late-glacial and post-glacial “Holocene” is typically unconformable. Cartwright et al. (2004) conducted a pseudo-3D high frequency single channel seismic survey in western Lake Superior with a 28 kHz echosounder that revealed that the surface rings are expressed on the Holocene boundary. They interpreted the lake floor rings to be the surface expression of an immature polygonal fault system.

High frequency CHIRP sub-bottom data collected in the Thunder Bay Trough show evidence of dewatering structures in the glaciolacustrine section (Wattrus et al., 2005). These features include inverted *feather and chimney* structures that in some cases can be traced to buried pockmarks/rings at the top of the glaciolacustrine sediment package beneath the post glacial Holocene sediments.

This study sets out to test the following working hypotheses that:

a. The lake floor rings are comprised of polygonal ring-like chains of individual pockmarks.
b. Dewatering structures that terminate below or in close proximity to individual pockmarks, should be present in high resolution CHIRP profiles.
c. The lake floor bathymetric features are not controlled or influenced by the underlying till or bedrock topography.

The objectives of the study are to:

a. compile a detailed morphologic picture of the subsurface plumbing associated with the lake floor;
b. establish a relative chronology for their formation;
c. identify a likely mechanism that is responsible for their formation;
d. propose a rudimentary physical model that explains their formation.

This study is organized into five sections: background, methods, results, discussion, and conclusions. In chapter two the key aspects of the region's formation and recent geologic history are summarized. Particular emphasis is placed on the history of the final stages of the Laurentide Ice Sheet (LIS) and the linkage of overflows from Glacial Lake Agassiz with the Lake Superior Basin.

Chapter three reviews the various data and procedures used in this study. The processes employed in the acquisition and processing of all the data which were used in this study will be outlined in detail including: seismic reflection data; multibeam sonar data; and piston-core data.

Chapter four describes the results of the study. Unique seismic facies are identified based on reflector character, reflector configuration, and external geometry.

A detailed discussion of the results is given in chapter five. In this chapter, the seismic facies described in the previous chapter are geologically interpreted and possible relationships with glacial processes are presented. Several examples of the interpreted data, as well as isopach and depth maps are used to illustrate features of interest. At times the seismic data is somewhat ambiguous and alternate interpretations are provided and discussed.

Chapter six is a summarization of key results of this study. These include: the identification of three primary chimney (drainage structures); the description of the drainage structure's distribution in cross-section and map-view; the definition of the relationship of these features with individual geological facies; the identification of a favored dewatering trigger; a proposed physical model; and suggestions for future research.

Chapter 2: Background

2.1 Geologic Setting

The bedrock geology of the Superior basin is dominated by the rocks of the Superior Province and Keweenawan Supergroup. The Superior Province is sub-divided into three sub-provinces: the granite-greenstone terrains of the Wabigoon and Wawa sub-provinces, and the metasedimentary schists and gneisses of the Quetico sub-province (Card, 1990). The Keweenawan Supergroup is made up of the Duluth Complex (synrift-anorthosites), the North Shore Volcanics Group (basalts and rhyolites), and the Oronto and Bayfield Groups (post rift clastics) (Green, 1995; Ojakangas et al., 2001a; Ojakangas et al., 2001b). The Keweenawan Supergroup rocks are associated with a failed attempt to rift the continent that occurred approximately 1.1 billion years ago (Green, 1995).

The primary structural features of the Superior Basin are the Superior Syncline (Fig. 2.1), and normal/reactivated-reverse (Isle Royale, Thiel, Keweenaw) faults (Fig. 2.2) related to the Midcontinent Rift (Huber, 1975; Ojakangas and Dickas, 2002).

2.2 Quaternary History

Lake Superior Basin's most recent history is shaped by the complex relationships between the Laurentide Ice Sheet (LIS), meltwater and pro-glacial lakes associated with the LIS, isostatic rebound, and climate change

(Breckenridge, 2005; Sharpe, 2008; Gary, 2010). During the last glacial maximum, the Wisconsin Glacial Stage marked the last major advance of the Laurentide Ice Sheet. During this time period the Des Moines lobe advanced as far south as central Iowa before beginning it's final retreat ca.14,000 ^{14}C BP (Wright, 1971). In the Superior basin, Quaternary sediments rest unconformably atop Precambrian basement rocks, and are the result of repeated advance/retreat cycles of the Superior Lobe of the LIS. The Superior Lobe was a major agent of erosion and left little if any sediment record from prior to the last glacial maximum (Farrand, 1969; Breckenridge, 2005).

2.2.1 Glaciation

The advance of the Superior Lobe through the Superior basin from the northeast is denoted in the sediment record by a layer of red sandy-clayey till that is characterized by basalt, agate, felsite and sandstone clasts (Wright, 1973). The Superior Lobe advanced and retreated five times during the Wisconsian (Wright, 1971; Lowell, 1999). In chronological order the first four phases (Fig. 2.3) are: The St. Croix phase (~15.5 ka BP), which achieved the greatest southward advance of the Superior Lobe beyond the Superior Basin; the Automba phase (~14 ka BP); the Split Rock phase (~13 ka BP), and the Nickerson Phase (~12 ka BP) (Wright, 1973).

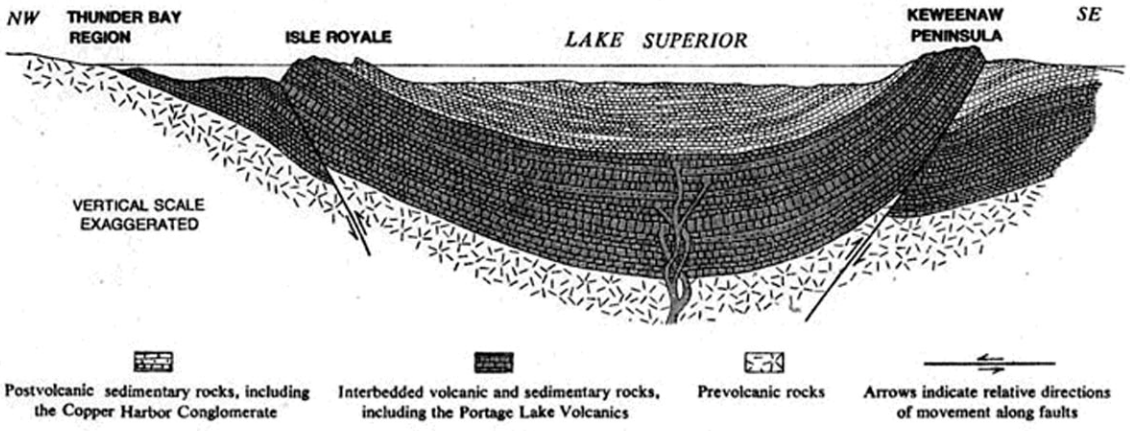

Figure 2.1 Superior Syncline geologic cross section. From Huber 1975.

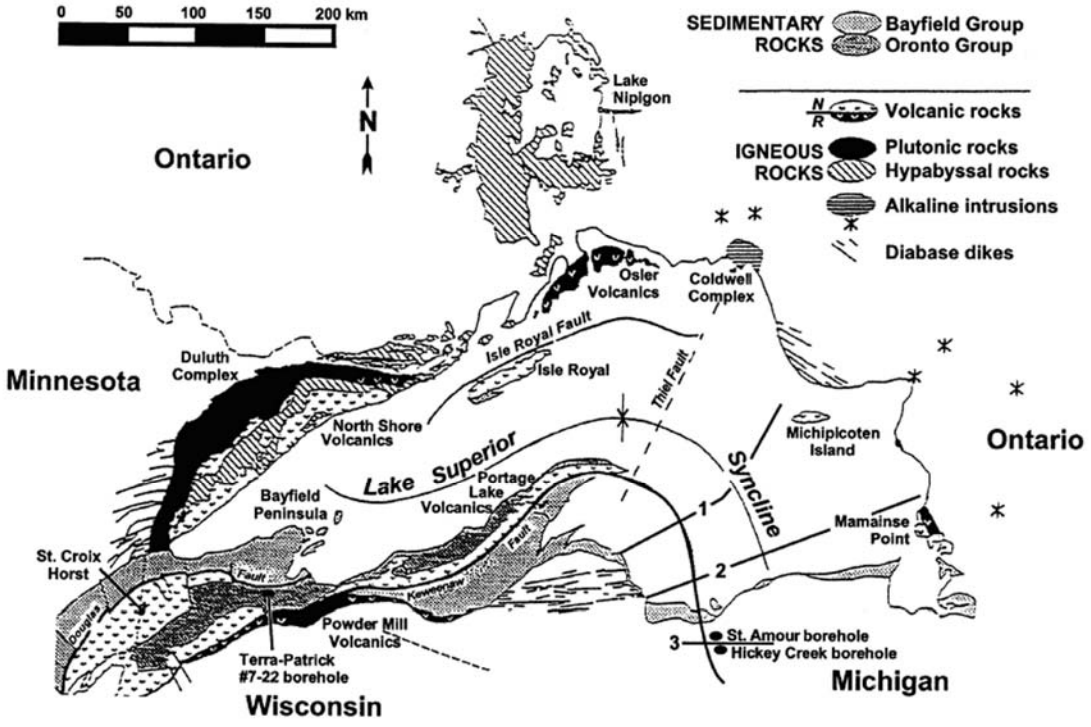

Figure 2.2 Lake Superior region geologic structure map. From Ojakangas and Dickas 2002.

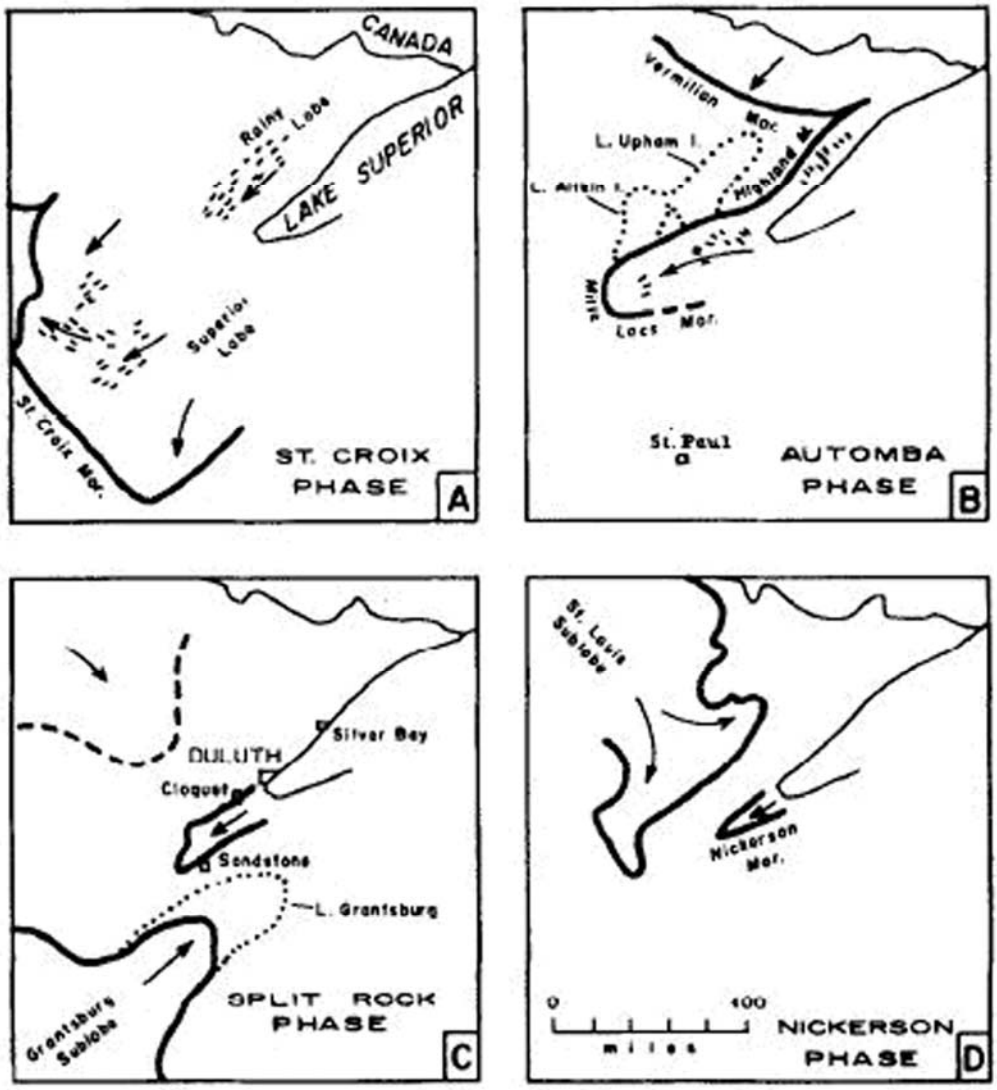

Figure 2.3 First four Superior Lobe Phases. The Marquette phase is not depicted. From Wright 1971.

The Marquette phase (~10 ka BP) marked the fifth and final re-advance of the Superior Lobe. It was identified with the discovery of a buried forest near Lake Gribben, Michigan in 1998 (Lowell et al., 1998). The Superior Lobe is

thought to be contained within the basin during the Marquette Phase, but the actual location of the ice margin of the Marquette advance is debated (Lowell, 1999; Mooers, 2005).

During the Automba phase, a series of small proglacial lakes formed within the low lying Superior basin along the margin of retreating Superior Lobe. Ultimately these small lakes coalesced to form Glacial Lake Duluth (Fig. 2.4) (Farrand, 1969; Carney, 1996). Lacustrine sediments deposited in these early proglacial lakes were likely completely removed or reworked during the later Split Rock, Nickerson, and Marquette phases of the Superior Lobe. Each time the ice margin retreated into the basin, proglacial lakes would have developed in the low land adjacent to the ice margin. The final retreat of the Superior Lobe left behind a series of recessional moraines and glacial tills. It is possible that sediments deposited during the Automba, Split Rock, Nickerson phases were preserved during the Marquette re-advance and remains undisturbed (in situ), below the glacial deposits left behind after the ice sheet's final retreat.

Seismic surveys in the western arm of Lake Superior have identified a series of thick moraine complexes crossing the lake floor from the Keweenaw Peninsula of Michigan to the Minnesota North Shore. These have been interpreted to represent the location of the ice margin as it paused during its final retreat towards Hudson Bay (Landmesser and Johnson, 1982). Evidence for Glacial Lake Duluth is preserved in weakly developed relict shorelines around the basin.

A sequence of lower post-Lake Duluth water levels developed (Fig. 2. 4) as the Superior Lobe retreated further northward exposing new lower drainage routes (Farrand and Drexler, 1985). During the Lake Minong Stage, lake level in the basin dropped ca. 40 meters below the present day lake level (Farrand, 1969). The lake level reached its lowest level, over 70 meters below its present level when the LIS retreated far enough north to allow the drainage of the basin through North Bay, Ontario. With the disappearance of the LIS from the region, isostatic rebound of the crust led to the rise of the outlet at North Bay causing the lake level to rise again. Lake Nipissing marked the onset of the current lake level approximately 5 ka BP as isostatic rebound re-established drainage from the basin at the current outlet at Sault Ste. Marie (Farrand and Drexler, 1985).

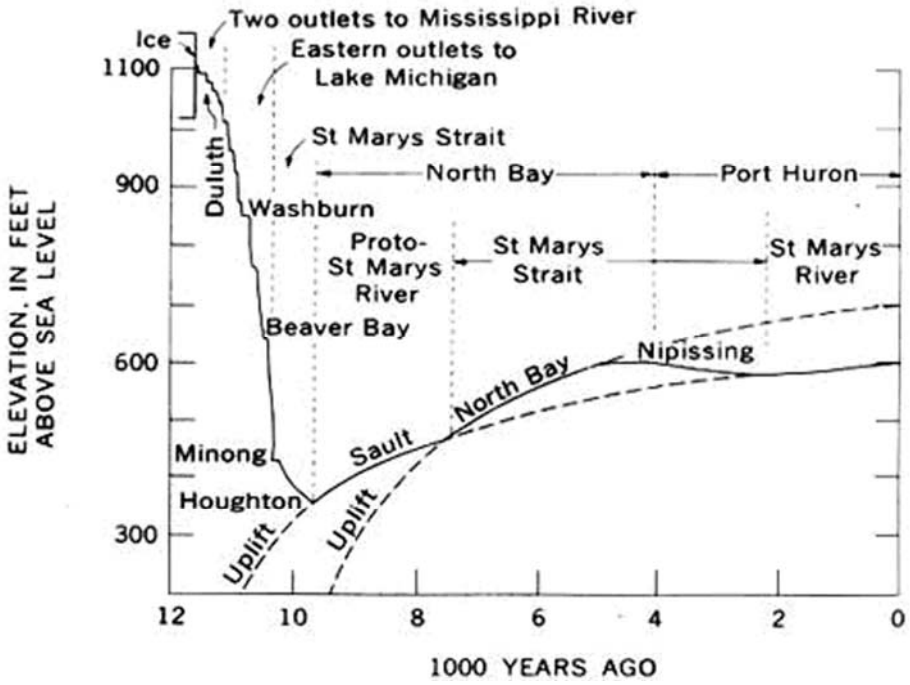

Figure 2.4 Lake Superior Basin lake level curves. Lake level curves prior to isostatic rebound. From Farrand and Drexler 1985.

2.2.2 Lake Superior Sediment Record

Our understanding of the soft-sediment record of Lake Superior dates to two coring programs undertaken in the 1960s. In the summers of 1961 and 1962, a deep drilling program undertaken by the University of Minnesota and the University of Michigan collected 11 sediment cores up to 200 meters in depth throughout the Superior basin, four of which terminated in bedrock. In 1967 and 1968 the Carnegie Institute collected over a hundred shallow (< 9 meters) Kullenberg sediment cores throughout the lake basin. William Farrand and his graduate student Carol Dell used these cores to develop a generalized sediment stratigraphy for the lake (Farrand, 1969; Dell, 1971). The generalized sediment record described by Dell (1972) consists of three primary sedimentary units: Glacial sediments; Glaciolacustrine sediments; and Post-Glacial sediments. Lake Superior's sediment record is depicted and described in Figure 2.5. The specific characteristics of these units are listed below.

2.2.2.1 Glacial Sediments

Glacial sediments (primarily clayey tills) associated with the advance and the retreat of the Superior Lobe rest unconformably on top of the Precambrian basement rocks and cover almost the entire lake basin (Breckenridge, 2005). At the bottom of this unit are clayey basal tills. Deposited on top of these basal tills are stratified red clays and silts with interbedded outwash sands, deposited near the wasting ice margin. These glacial deposits are ubiquitous throughout the

basin and of varied thicknesses. The thickness of the glacial package ranges between 12 and 60 meters.

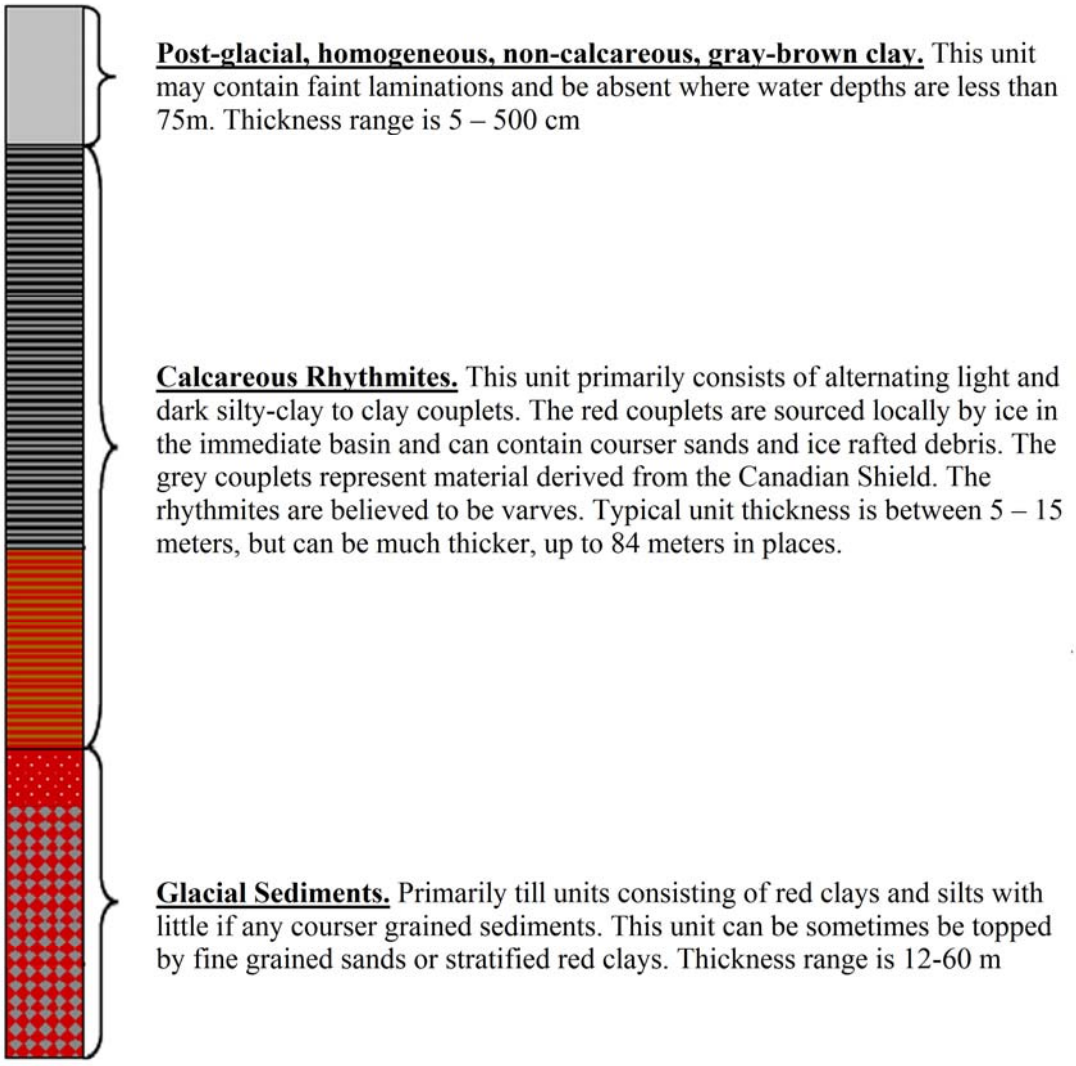

Figure 2.5 Generalized stratigraphic section of Lake Superior's soft sediment record. Modified from Gary, 2010.

2.2.2.2 Glaciolacustrine Sediments

The retreat of the Superior Lobe and the formation of proglacial Lake Duluth marked the onset of glaciolacustrine sedimentation within the Superior basin (Farrand, 1969). Deposited atop the glacial package is a sequence of glaciolacustrine red clay rhythmites (locally sourced from within the basin) that transition into gray clay rhythmites (believed to represent material derived from the Canadian Shield) (Breckenridge, 2005). These have been interpreted to be annual varves (Farrand, 1969; Dell, 1971; Mothersill, 1979 Breckenridge, 2005). The absence of datable material in the rhythmites prohibits the use of radiocarbon dating to confirm that they are annual varves. Measurable differences in calcite:dolomite ratios between the light-dark couplets have been interpreted to represent reduced sedimentation rates during the dark-winter layers that resulted in the dissolution of carbonates, compared to the light-summer layers. This led Dell (1974) to interpret the rhythmites to be an annual record (varves). There is no discernible difference in grain size between light and dark layers, with an average grain size less than two μm (Farrand, 1969). The varves typically terminate abruptly against the overlying Holocene sediments (Breckenridge, 2005).

A dated wood fragment found in the basal sediments of Beaver Lake, MI suggests that rhythmite deposition began approximately ca. 10,550-11,000 cal. BP (Fisher and Whitman, 1999). Published paleomagnetic records of secular variation from Lake Superior suggest that varve deposition ceased approximately

9035 ± 170 Cal. BP (Breckenridge et al., 2004). Glaciolacustrine sedimentation rates were an order of magnitude higher than Holocene sedimentation rates (i.e. centimeter(s) vs. millimeters) (Breckenridge et al., 2004)

2.2.2.3 Post-Glacial Sediments

The gray varves generally terminate abruptly against post-glacial brown-gray homogenous post-glacial Holocene clays. The average wave base in Lake Superior was calculated to be approximately 100 meters by Johnson (1980). As a result, shallower areas of the lake may be non-depositional and these post-glacial sediments may not be present.

2.2.3 Glacial Lake Agassiz

Lake Agassiz was the largest proglacial lake associated with the LIS. At one point in time it covered over 260,000 square kilometers of the North American continent (Leverington et al., 2000). The Agassiz basin formed as the result of lithostatic loading of the North American continental crust by the Laurentide Ice Sheet. A large depression developed under the ice sheet, such that advancing ice lobes were thrust up-slope and wasting ice lobes ultimately retreated down-slope (Teller, 1995). Glacial Lake Agassiz first developed approximately 11,700 ^{14}C BP when the Des Moines Lobe retreated northward into the Agassiz Basin (Teller, 1985). Over the course of Lake Agassiz's 4000 year existence, the fluctuating margin of the LIS caused the opening and closing of various drainage pathways, (Fig. 2.6) effectively controlling lake level. The

multiple manifestations of Lake Agassiz are defined as a series of lake phases; in chronological order these are the Cass, Lockhart, Moorhead, Emerson, Nipigon, and Ojibway (Clayton and Moran, 1983; Teller, 1985).

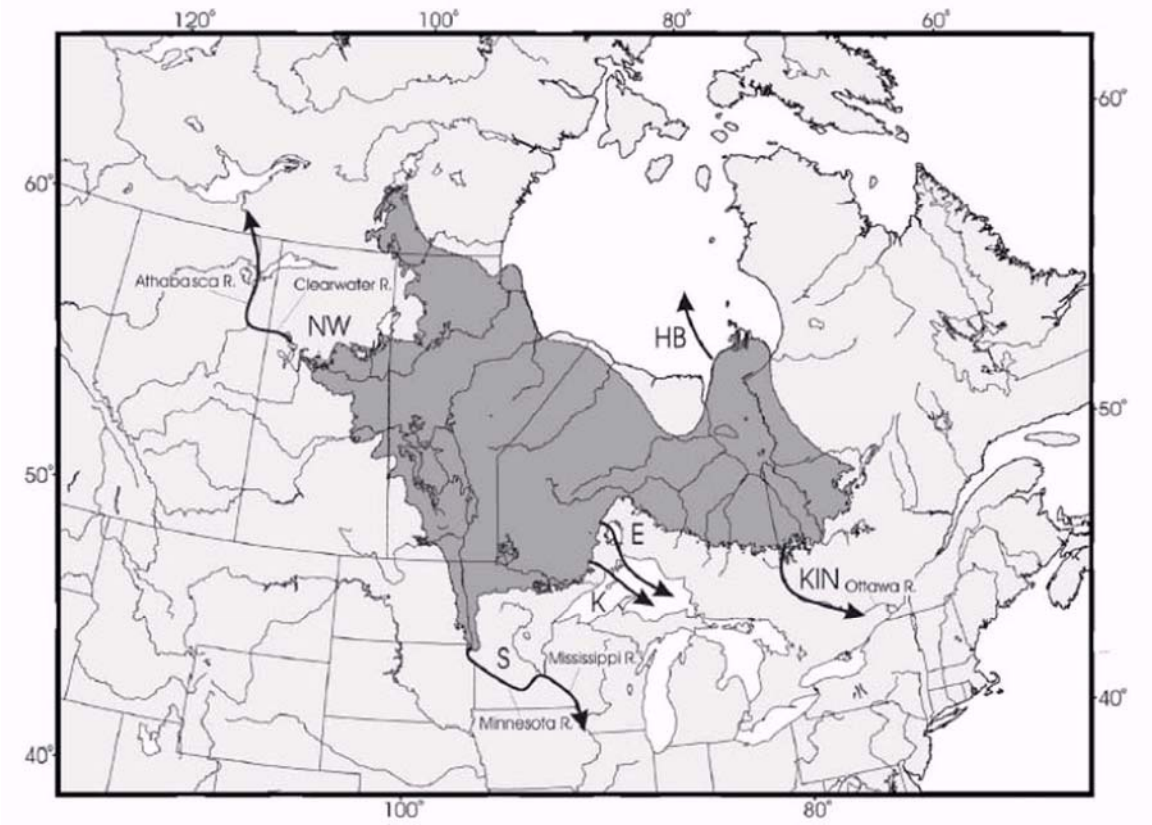

Figure 2.6 Total area covered by Glacial Lake Agassiz throughout the course of it's existence and proposed outlets. The marked outlets include: the Northwestern outlet (NW), Southern (S), Eastern Thunder Bay outlet (K), Eastern Nipigon basin outlet (E), Kinojevis outlet (KIN), and Hudson Bay outlet (HB). From Teller et al., 2005.

The Cass and Lockhart Phases were the earliest expressions of Lake Agassiz, when the Des Moines Lobe of the LIS first retreated into the basin. Lake Agassiz was repeatedly invaded by the Red River and James River Lobes, and

at times it was totally displaced by these ice advances (Farrand and Drexler, 1985). During the Cass and Lockhart Phases, Lake Agassiz overflow drained to the Gulf of Mexico by way of the Minnesota and Mississippi Rivers (Clayton and Moran, 1983; Farrand and Drexler, 1985; Fisher, 2002; Teller, 1995). At 10,800 ^{14}C BP, as the LIS margin wasted north of Thunder Bay, new lower eastward drainages developed terminating Agassiz overflow to the Gulf of Mexico (Teller, 1985; Fisher, 2002).

The opening of the eastern outlets marked the onset of the Moorhead Phase. During this phase, Agassiz overflow discharged eastward through the Nipigon basin into Lake Superior, then on to Lake Huron through Sault Ste. Marie (Drexler et al., 1983; Farrand and Drexler, 1985; Teller, 1985, 1995; Leverington, 2003). Re-advancing ice closed the eastward drainage routes and marked the beginning of the Emerson Phase (~9700 B.P).

The closure of the eastern outlets switched Agassiz overflow northwest towards the Arctic Ocean through Glacial Lake McConnell and the MacKenzie River basin, in addition to reactivating the Gulf of Mexico route (Teller, 1985; Smith, 1993; Fisher, 2002, 2006;).

When the ice retreat resumed, the eastern drainage routes reopened and Lake Agassiz entered its Nipigon Phase. During this phase, as the ice margin continued to retreat to the north, a series of lower drainages were opened. Each new drainage route resulted in vast quantities of fresh water being released into the Atlantic Ocean via the upper Great Lakes (Teller and Thorleifson, 1983;

Farrand and Drexler, 1985; Teller, 1985; Teller et al., 2002; Colman, 2002; Yu et al., 2010).

With the continued retreat of the ice margin northward, Lake Agassiz entered it's final phase – the Ojibway Phase. As a result, during this period, overflow from Agassiz was diverted east, bypassing Lake Superior, into proglacial Lake Ojibway, and down the Ottawa River Valley to the St. Lawrence Valley, where it was joined by overflow from the western Great Lakes. During the Ojibway Phase, Lake Agassiz no longer drained through any of the Great Lakes (Teller, 1985).

2.2.4 Implications of Lake Agassiz Overflow

The opening of eastern Agassiz drainage outlets resulted in multiple catastrophic discharges of several thousand cubic kilometers of freshwater to the North Atlantic Ocean (Clark, 2001; Teller et al., 2002; Yu et al., 2010). Modeling studies have shown that these large influxes of freshwater to the North Atlantic were capable of disrupting Atlantic meridional overturning (MOC), in turn reducing the production of North Atlantic Deep Water (NADW) (Clark, 2001; Teller et al., 2002; Zhang, 2004; Stouffer, 2007). Periods of cooler climate have been linked to decreased NADW production (Clark, 2001; Teller et al., 2002).

The Younger Dryas cooling event seen in Northern Europe has been linked to Agassiz overflow routed eastward through Thunder Bay (Broecker, 1989; Clark, 2001; Teller et al., 2002). This hypothesis was generally accepted

until recently, when critics suggested that the proposed Thunder Bay route was blocked by ice and did not open until after the Younger Dryas (Fisher, 2005; Lowell and Fisher, 2009; Lowell et al., 2009). Geophysical surveys conducted in 2008 and 2009 in the Thunder Bay trough documented the absence of erosional bedrock features and deltaic deposits at and near the mouth of Thunder Bay (Voytek, 2010). These features would be expected had catastrophic eastward Agassiz drainage occurred through Thunder Bay (Gary, 2010). The current consensus is that Agassiz overflow was routed through the MacKenzie River Basin to the Arctic prior to the Younger Dryas (Murton, 2010).

Chapter 3: Methods

3.1 Seismic Data Acquisition

The data used in this study were collected in the Thunder Bay Trough (Fig. 3.1) aboard the R/V Blue Heron in July 2009. The primary goal of this survey was to image Lake Superior's lake floor rings and any subsurface structures or plumbing associated with them.

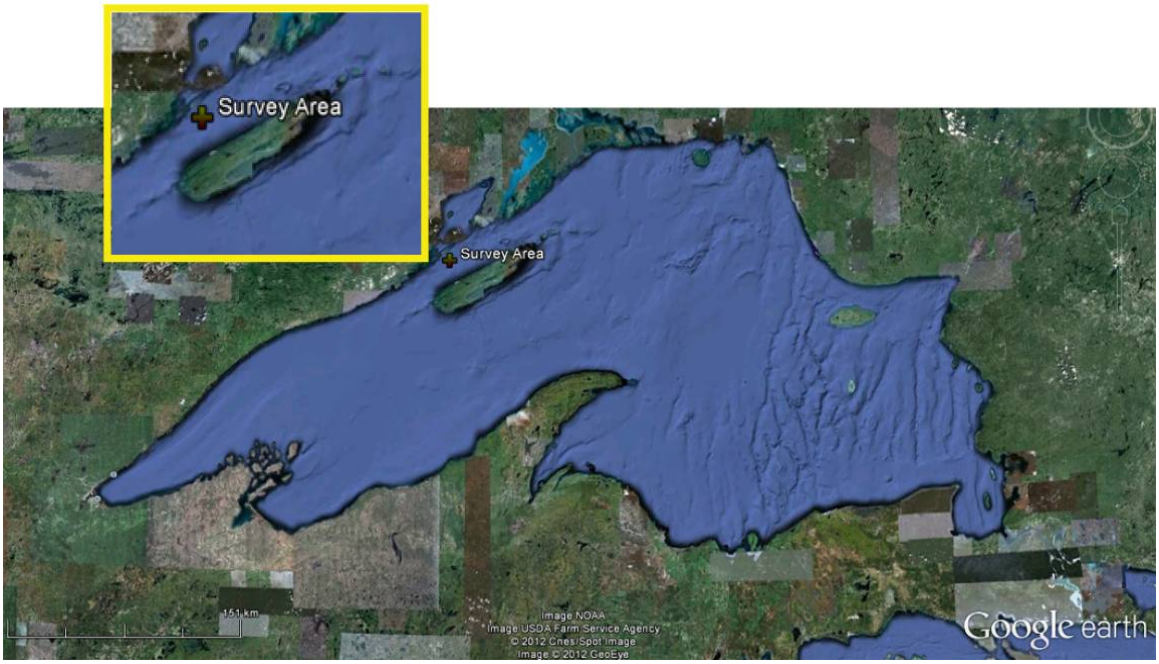

Figure 3.1 Survey location map with the general location of the survey area denoted with a cross. Image captured with *Google Earth*.

3.1.2 Instrumentation

A variety of seismic and acoustic observations were collected for this study. To best image potential small-scale plumbing structures beneath the lake floor rings, an Edgetech CHIRP high-frequency sub-bottom profiler was used as the primary seismic source. However, due to the CHIRP's inability to image the entire sediment record, a secondary single channel seismic (SCS) reflection survey was also acquired using a small airgun. This second data set made it possible to image the deep portions of the glaciolacustrine package and the underlying basal tills and bedrock albeit with lower resolution due to the lower frequency content of the airgun. Complementing the CHIRP and airgun data were high-resolution multibeam sonar and 28 KHz echosounder data.

Frequency analysis of the acquired airgun data shows that a majority of the airgun data is between 100 and 500 Hz, with a dominant frequency of 350 Hz, well below the survey’s Nyquist frequency of 5000 Hz. The vertical resolution limit of seismic data is roughly 1/4 to 1/2 of the dominant wavelength. Given an assumed near surface seismic velocity of 1500 m/s and a dominant frequency of 350 Hz, the vertical resolution associated with the airgun data is between two and four meters. The theoretical limit of the horizontal resolution (the minimum offset between two differentiable features on a reflector) is determined by the width of the Fresnel zone of the data. This is dependant on both the dominant wavelength and depth of the reflector. Given the acquisition characteristics of this survey, the width of the Fresnel zone associated with the airgun data is

approximately 45 meters for reflectors 200 meters below the source (average water depth in the survey area is 200 m).

The signal used by the CHIRP sup-bottom profiler employs a swept frequency (in this survey between 600 Hz and 12 KHz). The calculated vertical resolution associated with the CHIRP data is between ten centimeters and one meter. The horizontal resolution associated with the CHIRP data is approximately 17 meters in this survey. Even though this is high resolution data, care must be taken to not make inferences beyond the physical limits imposed by the employed source frequencies. Objects or subsurface targets below the described resolvable thresholds will not be imaged in the data.

CHIRP Sub-Bottom profiler (*EdgeTech, Boca Raton, FL*)

CHIRP sub-bottom data was acquired with an Edgetech SB-512 towfish using a 0.2 s pulse swept between 600 Hz-12 kHz. The towfish was towed at a constant depth and offset to minimize post acquisition processing. Data acquisition, processing and recording was controlled by Edgetech's Discover software. The processed data was digitally recorded in the JSF format and archived on DVDs. It was later converted to SEG-Y format for interpretation. Position information for this data was obtained from the R/V Blue Heron’s Furuno DGPS receiver. Since this position represents the location of the DGPS antenna on the boat and not the location of the actual towfish, echosounder data were also acquired with the R/V Blue Heron’s 28 kHz Knudsen profiler. This

information was used to correct the position of the CHIRP towfish in post-acquisition processing by matching bathymetric features in both datasets.

600B Airguns (*Bolt Technology, Norwalk, CT)*

A small airgun, equipped with a five-cubic-inch chamber, was used to acquire high-resolution single channel seismic (SCS) reflection data. A Benthos AQ-4 24-element hydrophone streamer was used to detect the reflected signal. A Geopulse Model 5210A analogue receiver was used to amplify and filter the output signal from the streamer. The data from the receiver was digitized and recorded in the industry standard SEG-Y format using the Triton Imaging SB-Logger high-resolution seismic acquisition system. In order to avoid aliasing problems the analogue signal was filtered with a high cut filter of 5 KHz before it was digitized at a sample rate of 10 kHz.

The survey was acquired with an average vessel speed of four knots. Firing at two second intervals, the airgun data was acquired with a shot spacing of approximately 2 meters. A recording duration of 0.75 seconds and an assumed seismic velocity of 1500 m/s allows for the potential imaging of reflectors up to 500 meters below the surface of the lake, which is well below the bedrock basement in this area.

240 KHz Reason SeaBat 8101 Multibeam

High resolution multibeam sonar bathymetry data were acquired using a Reson 8101 multibeam. This has a swath of 101 equi-angle beams, each 1.5^{o} wide, that provide a cross track aperture of +/- 75^{o}. It operates at 240 kHz and its ping rate is tied to the water depth below the transducer at nadir, position and motion (roll, pitch and yaw) information for the survey was obtained from an Applanix POS-MV 320 system. The data were recorded in industry standard XTF format using a Triton Imaging ISIS acquisition system. Sound velocity profiles, necessary to correct refraction artifacts in the data produced by speed of sound variations in the water column, were acquired periodically during the course of the survey with a SVPlus sound velocity profiler (AML Oceanographic, Sidney, BC Canada). Post-acquisition processing was performed using CARIS HIPS/SIPS.

Survey Management System

Hypack hydrographic survey management software was used to design and control the acquisition of the survey. The system received position information from the ship's navigation systems. A remote display was used to provide course correction information to the helmsman on the bridge. Using this system the ship's crew were able to keep the vessel on line within a few meters most of the time.

3.1.3 Survey Operations

The data were acquired using a pseudo-3D orthogonal-grid consisting of two sets (30 each) of ~North-South and ~East-West orthogonal lines. Survey lines were spaced 20 meters apart with an approximate length of 1.5 km. The pseudo-3D orthogonal grid covers ~360,000 m^2. The center of the grid is approximately located at 48º 02’ 47.9”N, 89º 08’ 13”W.

3.2 Seismic Data Processing

Post-acquisition processing of the data took place at the University of Minnesota Duluth Large Lakes Observatory (LLO). The high resolution SCS data were processed using SPW (Parallel Geoscience Corporation, Long Creek, OR), a seismic processing system used by university research groups and industry professionals. The processed seismic data were interpreted at the LLO using The Kingdom Suite TKS+ (IHS Technology, Houston, TX), a workstation-based industry standard seismic interpretation package.

The CHIRP data were processed during acquisition, the recorded data consists of envelope rather than full waveform data, therefore no post-acquisition signal processing was required. However, the CHIRP towfish was towed behind the survey vessel. This created a significant offset between the towfish, where the data were acquired, and the DGPS antenna, where ship’s position was calculated. To correct this offset the recorded location where the data was acquired needed to be shifted. Since the CHIRP automatically varies its firing

rate based on the distance to the lake floor below the towfish, the shot offset also varies with water depth below the towfish. This variable shot offset made it impossible to use a simple fixed offset to correct the CHIRP navigation data. To overcome the variable firing rate, accurate geometry data was imported from echosounder profiles collected with the ship's Knudsen echosounder whose position relative to the DGPS antenna is well know and corrected for. CHIRP and echosounder profiles were plotted in Kingdom at the same horizontal scale above and below one another. The profiles were then aligned using distinct bathymetric features. Once the correct shift was determined from the echosounder profiles (using a minimum of seven data points for each seismic line) and a new geometry definition dataset for the CHIRP data could be derived. This was then used to reload the CHIRP data placing it in the correct spatial location. The error associated with the interpolation process is comparable to the horizontal resolution of the CHIRP data.

Processing of the SCS data involved several steps, which are outlined in (Fig. 3.2). Geographic Lat-Long coordinates were converted to Universal Transverse Mercator (UTM) using the WGS 1984 standard for UTM zone 16. The data were resampled, corrected for spherical divergence and bandpass filtered. An early mute was applied to remove spurious noise in the water column. One of the most important processing steps often applied during post-acquisition processing is deconvolution. This may be used for several purposes. It can be used to shorten and simplify the wavelet to make interpretation easier (a process

known as spiking deconvolution); it also can be used to reduce the influence of multiples (reverberations) in the data. These are generated by a variety of different mechanisms and they are often divided into two general types with very different characteristics. Long-term multiples (such as water bottom multiples generated by energy reverberating in the water column) are not a major concern, as they usually arrive much later than the primary subsurface reflections of interest. Short-term multiples (such as “peg-leg” multiples) can be more problematic, since their arrival at the detector tend to be almost coincident with the primary reflection of interest.

Whether by design or just good fortune, the short-term surface ghost multiple was extremely faint. Subsequent attempts to remove the surface ghost were successful but also resulted in the loss of coherency within the upper portion of the data. The survey is relatively flat with the exception of the lake floor rings. Spiking deconvolution was applied to the airgun data in an attempt to simplify the appearance of the chaotic unit (later described as seismic facies B) with only limited success. The intent of the airgun data was to image (completely) the different sedimentary packages present in basin down to bedrock. This was accomplished without employing deconvolution.

3.3 Sediment Piston Core Acquisition and Processing

A ca. nine meter piston core was collected using a Kullenburg coring system with a gravity core trigger. It was labeled by established convention as

BH093-SPP09-SA-1K. The core was sectioned into seven ~ 1.2 meter long sections (BH093-SPP09-SA-1K-(1,2,3,4,5,6,7)) while aboard the R/V Blue Heron and put in cold storage at the Large Lakes Observatory. Metadata were collected at LacCore: National Lacustrine Core Facility located on the University of Minnesota's Twin Cities campus. The core(s) were processed whole and were not split for this project. The metadata collected included measurements of the sediment core's acoustic impedance, bulk density, magnetic susceptibility, and P-wave velocity.

X-radiography data were also acquired for the core. This was done at the XRF-Core Lab at the LLO. Matlab was used to plot the X-radiography images alongside the sediment core's acoustic impedance, bulk density, magnetic susceptibility, and P-wave velocity. When the core is sectioned in the field some material is inevitably lost at the ends, foam is inserted to prevent further destruction of the sediment core. This foam gives a meaningless metadata signal and is commonly removed. The gaps in the metadata represent sediment core sections where the core-liner is not filled with sediments.

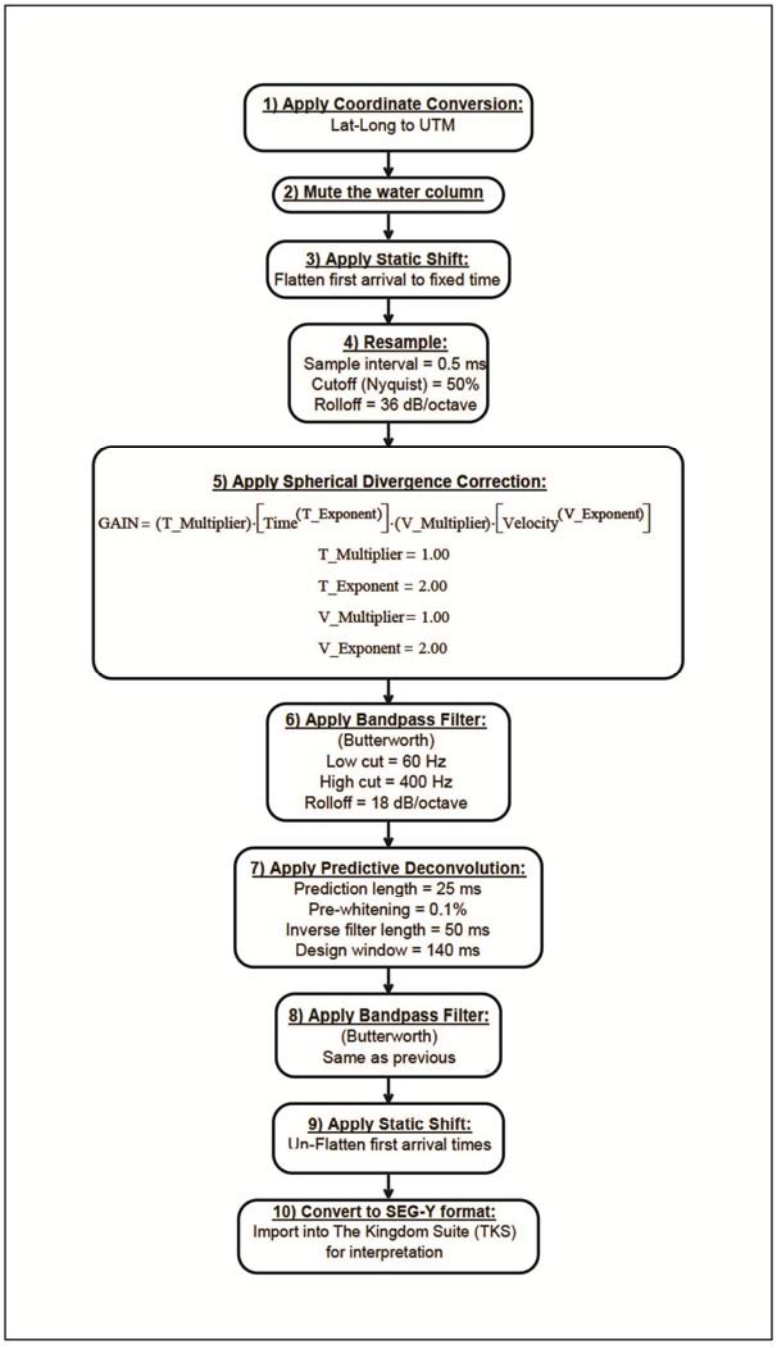

Figure 3.2 Data processing flow diagram. This flow diagram illustrates the general processing steps applied to the airgun data.

Chapter 4: Data

It is standard practice to describe geologic units or seismic facies beginning with those at depth and working towards the surface (bottom-to-top). Before addressing the observed seismic facies it is important to illustrate key structures on the lake floor, namely the lake floor rings. This is best accomplished by presenting the bathymetric data first, followed by the conventional presentation of seismic facies observed in this study.

4.1 Bathymetry Data

The survey area is covered with giant ring-shaped depressions, which can be over 300 meters across and as deep as 5 meters. The width of the ring trough is often more than 25 meters. Singular pocks/pits are also observed within the survey area. The multibeam data suggests that the lake floor rings are actually irregular polygons defined by individual pockmarks/pits (Fig. 4.1). The lake floor inside the ring is approximately the same elevation as the lake floor outside the ring. The rings are networked in the southeastern half of the survey area and there is no evidence that the rings ever intersect one another. The bathymetric relief is most significant along a northeast-southwest trend that runs diagonally through the survey area. These rings will be referred to when describing the location of various reflector anomalies observed in the four seismic facies in the following section.

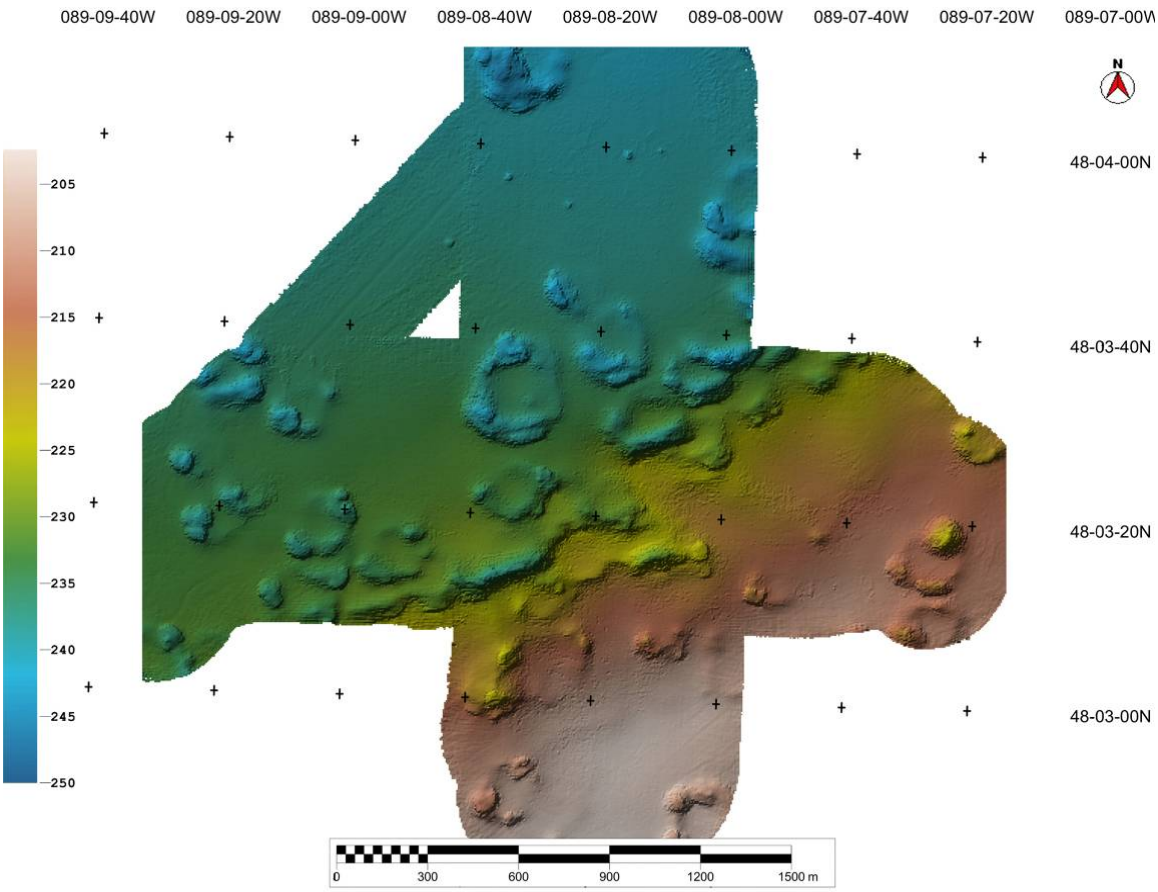

Figure 4.1 High Resolution Multibeam Bathymetry Data. The light is sourced 45^{o} above the horizon from the southeast. Depth to the lake floor is shown in the scaled color bar on the left in meters. Vertical exaggeration is 5X.

4.2 Core Metadata

The metadata is graphically presented in Figure 4.2. Light and dark layers are apparent in the sediment core X-radiography images. These light and dark couplets vary in size but are usually on the order of several centimeters in length. They also appear to correlate with peaks and troughs in the metadata. Though the metadata was collected it was not analyzed in this study.

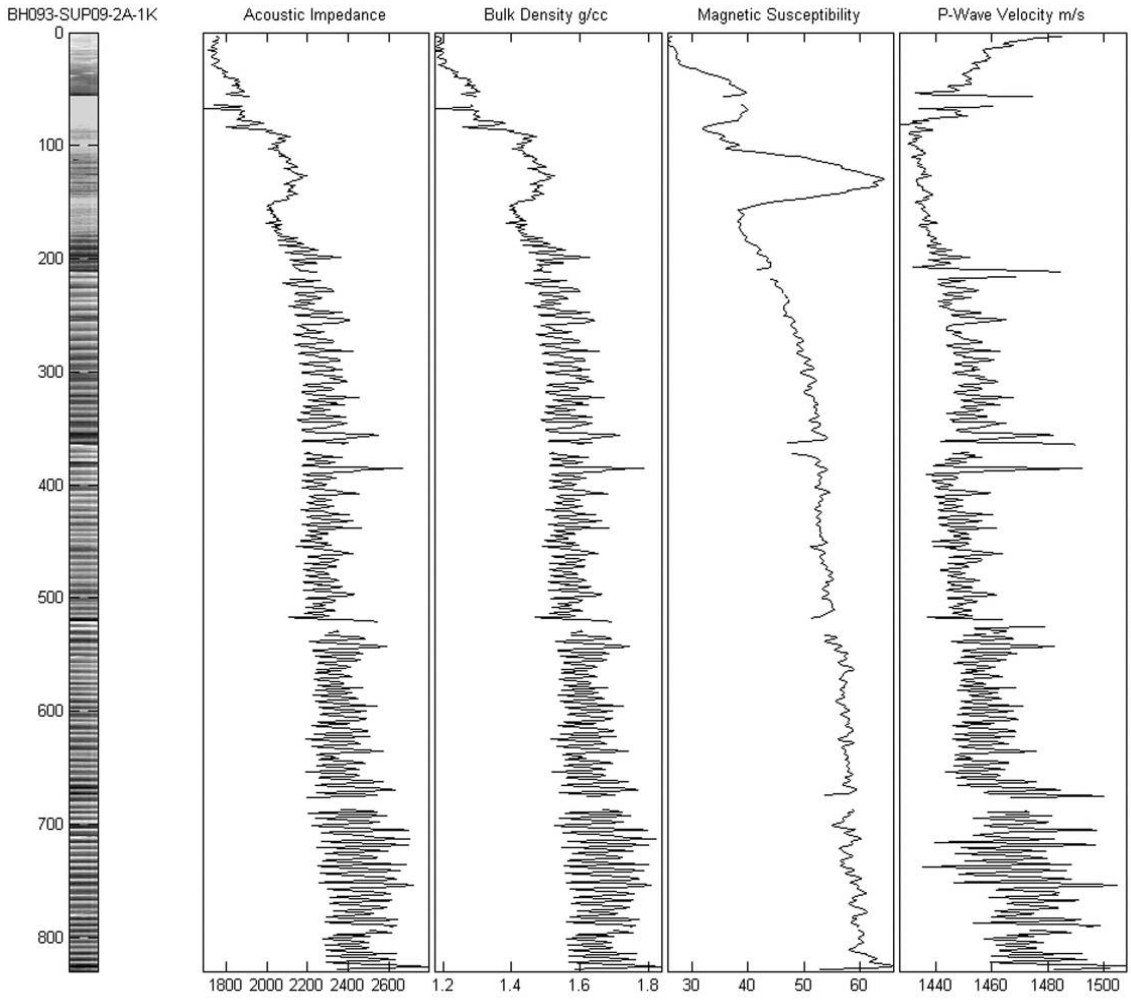

Figure 4.2 Piston core X-radiography images and metadata.

4.3 Seismic Interpretation Convention

Acoustic impedance contrasts within the subsurface sediments determine the character of a seismic-reflection profile. Seismic profiles are not necessarily a true representation of geologic cross sections. Changes in lithology or depositional environment are only imaged if they produce detectable changes in acoustic impedance. Seismic cross sections however, can be a good proxy for

subsurface geological structure when their interpretation is guided by a solid understanding of the geology of the area, and an understanding of plausible geological processes.

The interpretation method, conventions and nomenclature established by Stoker, Pheasant and Josenhans' "Seismic Methods and Interpretation" in *Glaciated Continental Margins: An Atlas of Acoustic Images (1997)* have been applied to the data used for this thesis. Three primary seismic-reflection characteristics are considered when identifying and interpreting seismic facies: Individual reflector character (i.e. reflector amplitude, continuity and frequency), reflector surface configuration and the external geometry of seismic facies or sequences. These three measures are described in detail in the following section.

4.3.1 Reflection Character

4.3.1.1 Reflection Amplitude

Classified as high, moderate, or low, reflection amplitude is determined by the acoustic impedance contrast between subsurface units. High-amplitude reflections are produced by large changes in acoustic impedance, which is often associated with a change in grain size or density. Conversely low-amplitude reflections are generated when the change in acoustic impedance is small. Lateral variations in amplitude along a single reflector can be indicative of

geological change along that reflector, such as a change in grain size and thus may be an indicator of proximity to the sediment source.

4.3.1.2 Reflection Frequency

Reflection frequency (or frequency repetition) is classified as broad, moderate, or narrow. Frequency is typically associated with bed thickness. Vertical changes in reflector frequency could indicate a unit boundary, whereas lateral changes could indicate a change within the seismic facies, such as a unit thinning or thickening. It does not necessarily mean that each reflection is indicative of a new lithological boundary.

4.3.1.3 Reflection continuity

Reflection continuity describes the lateral coherence of subsurface reflectors. Continuous reflectors are indicative of calm or low-energy depositional processes, conversely discontinuous reflectors are more often associated with high-energy depositional processes (Stoker et al., 1997).

4.3.2 Reflection Configuration

Three generalized reflection configurations are recognized in this dataset: stratified, chaotic and reflection-free (Fig. 4.3). Reflection configuration is also associated with depositional environment conditions (Stoker et al., 1997).

Stratified reflectors blanketing underlying topography could indicate a calm depositional environment with slow settling. Chaotic reflectors are indicative of a more dynamic depositional environment. Reflection-free (acoustically transparent) within seismic profiles often are indicative of a uniform homogenized lithological unit.

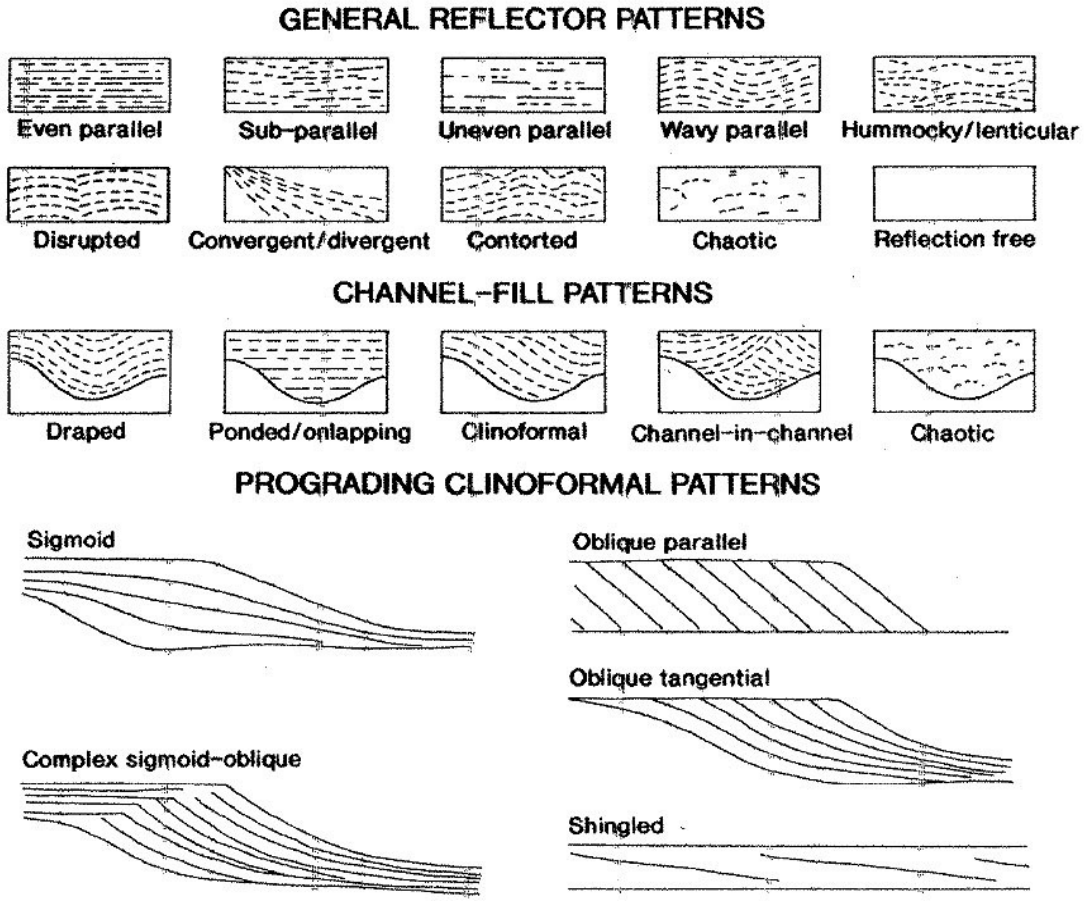

Figure 4.3 Examples of reflector configuration patterns. From Stoker et al., 1997.

4.3.3 External Geometry

External geometry provides a map-view of sub-surface facies through the interpolation between the survey lines and is limited by the relative density of survey lines. A map-plan view of subsurface facies and their spatial relationships with adjacent structures can be an important diagnostic tool when interpreting seismic data. Time maps that illustrate the external geometry (summarized in tables 4.1, 4.2, 4.3 and 4.4**)** will be included with each seismic interpretation below when applicable.

4.4 Seismic Interpretation

The data were loaded onto a workstation running IHS's Kingdom interpretation software. Inspection of the CHIRP and airgun SCS data identified four distinct seismic facies that were present throughout the survey area. These four seismic facies are labeled A, B, C and D from bottom to top (oldest to youngest) in the seismic section. A representative airgun SCS and CHIRP profile illustrating the typical form of each seismic facies recognized in each dataset is provided in Figures 4.4 and 4.5 respectively.

		Seismic Facies A
Reflection Character	Amplitude	Moderate to high amplitude toward the top of the facies, then fading to ambient noise as depth increases.
	Frequency	Broad
	Continuity	Continuous in most areas, although discontinuities are also common.
Reflection Configuration		Mostly stratified sub-parallel to uneven-parallel with some area of obliquely dipping parallel stratification with erosional truncations near the top.
External Geometry		Forms the acoustic basement throughout the survey area in the airgun-hydrophone data. Generally shallowest in the eastern portion of the survey area towards Isle Royale and deepest in the western portion of the survey area towards the Isle Royale Trough. There is a northeast-southwest trending synclinal structure that plunges to the southwest.

Table 4.1 Description of seismic facies A.

		Seismic Facies B
Reflection Character	Amplitude	Moderate to high
	Frequency	Moderate to broad
	Continuity	Predominately discontinuous
Reflection Configuration		Hummocky to semi-stratified
External Geometry		This facies blankets the entire survey area. Two parallel anticlinal structures plunge to the southwest. The facies thickens as it infils the northeast-southwest trending syncline structure. This facies is not imaged with the CHIRP system due to signal attenuation.

Table 4.2 Description of seismic facies B.

		Seismic Facies C
Reflection Character	Amplitude	High to moderate
	Frequency	Moderate to broad
	Continuity	Mostly continuous except for uppermost reflectors where numerous discontinuities occur.
Reflection Configuration		Stratified-parallel
External Geometry		This facies blankets the entire survey area and is uniformly imaged with the airgun-hydrophone system, but only partially imaged with the CHIRP system. This facies forms the acoustic basement in the CHIRP data. There is a good deal of relief in the upper facies section.

Table 4.3 Description of seismic facies C.

		Seismic Facies D
Reflection Character	Amplitude	High amplitude at upper boundary below which is facies is almost acoustically transparent.
	Frequency	Moderate at upper boundary
	Continuity	Stratified-parallel
Reflection Configuration		Nearly reflection free, except for the upper boundary and the facies interior under extreme gain.
External Geometry		This facies blankets the entire survey area and fills in relief described in facies C.

Table 4.4 Description of seismic facies D.

4.4.1 Seismic Facies A

The reflectors observed in seismic facies A are moderate to high amplitude but quickly fade to ambient noise as depth increases. They are mostly parallel to uneven-parallel with some areas of obliquely dipping parallel stratification with erosional truncations near the top. These reflectors define the acoustic basement throughout the survey area in the Airgun SCS data. This unit was not imaged by the CHIRP system. A time map (Fig. 4.6) created from the Airgun SCS data shows the topographic relief of this unit. There is a gently sloping ridge and corresponding trough running along a northeast-southwest trend.

4.4.2 Seismic Facies B

The reflectors observed in Seismic facies B can be described as: having high to moderate amplitudes; being moderate to broad in frequency; and being predominantly discontinuous. This facies blankets the entire survey area (bounded between facies A and C) and is uniformly imaged with the airgun-hydrophone system. This unit was not imaged with the CHIRP system due to signal attenuation. Seismic facies C thins above the ridge and thickens as it fills in the northeast-southwest trending trough observed in seismic facies A (Fig. 4.7). A time map (Fig. 4.8) created from the airgun SCS data shows the topographic relief of this unit. The surface morphology of this unit is dominated by two parallel synclinal structures that plunge to the northwest.

4.4.3 Seismic Facies C

The reflectors observed in seismic facies C can be described as: having high to moderate amplitudes; high frequency; and are generally continuous. The unit is well stratified and it's reflectors are largely parallel throughout the survey area. This is the thickest of the four described seismic facies (Fig. 4.9). It blankets the entire survey area and is uniformly imaged with the airgun-hydrophone system, but only partially imaged with the CHIRP system. This facies forms the acoustic basement in the CHIRP data. Several reflector anomalies are present within this unit and are described in detail below.

4.4.3.1 Reflector Anomalies

Abruptly truncated reflectors are visible within the upper 10 meters of CHIRP cross-sections. The truncations are typically abrupt and mark an unconformable boundary between seismic facies C and the unit above it. Maps made of the truncated reflectors reveal a series of circular voids (Fig. 4.10). The voids correlate with the locations of the ring structures observed in the multibeam data. It is important to note that reflectors are absent in the CHIRP data within the center of the rings.

The CHIRP profiles also show anomalous seismic chimneys. These anomalous structures are not visible in the airgun SCS data due to its relatively low frequency content. Three principle seismic chimney morphologies were observed in the high-resolution CHIRP profiles. An example of each of the three

distinct seismic chimney morphologies observed in this survey is shown in Figure 4.11(a,b,c). These structures commonly underlie the truncated reflectors within this unit. Seismic chimneys can be categorized as either being deep-sourced or shallow.

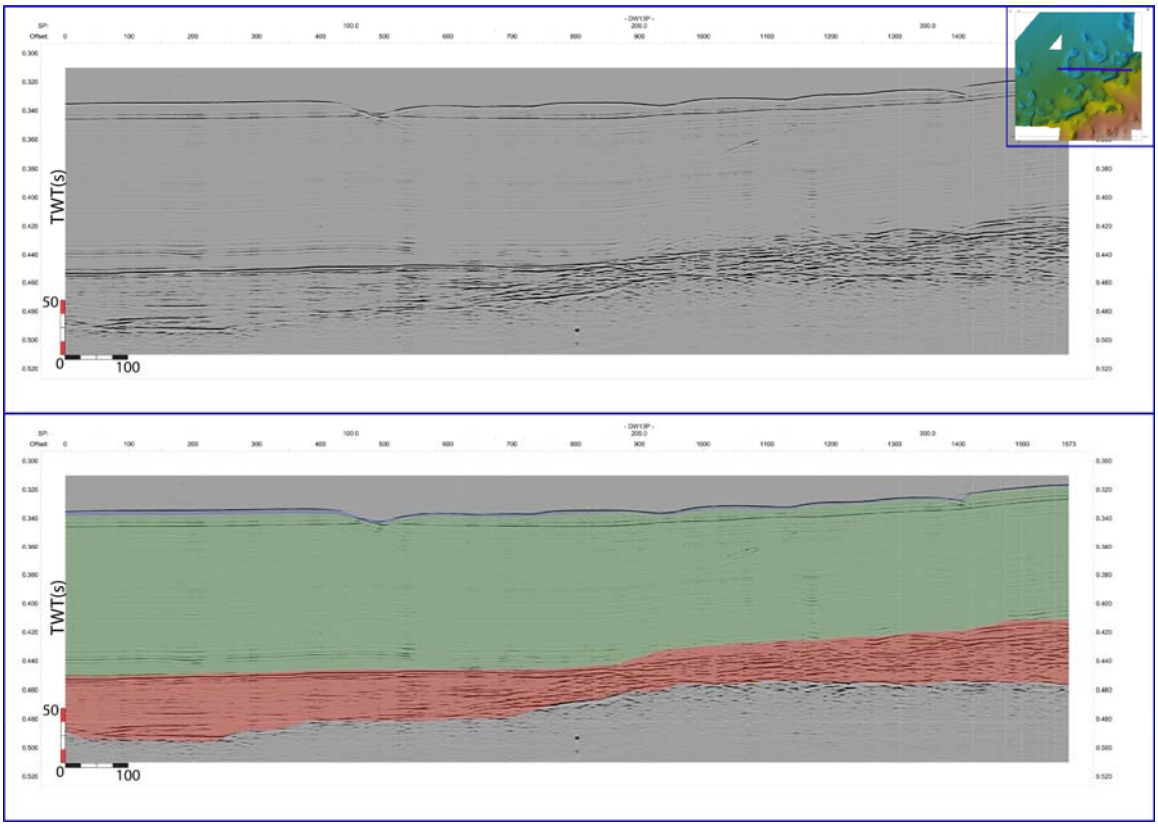

Figure 4.4 Typical airgun line in the survey area. This profile depicts seismic line DW13 collected off the southwest shore of Isle Royale. This east-west trending line runs from the Thunder Bay Trough towards Isle Royale. Offsets (lower horizontal scale) are given in meters, two-way travel time (left vertical scale) in seconds. The lower interpreted line (b) depicts the major facies identified in the survey area. The dark gray region at the bottom is identified as facies A. The red unit is identified as facies B. The green unit is identified as facies C. The blue unit is identified as facies A. These facies are described in tables 4.1, 4.2, 4.3 and 4.4. Note that the airgun and CHIRP survey lines are not the same length; this is the result of correcting the CHIRP geometry.

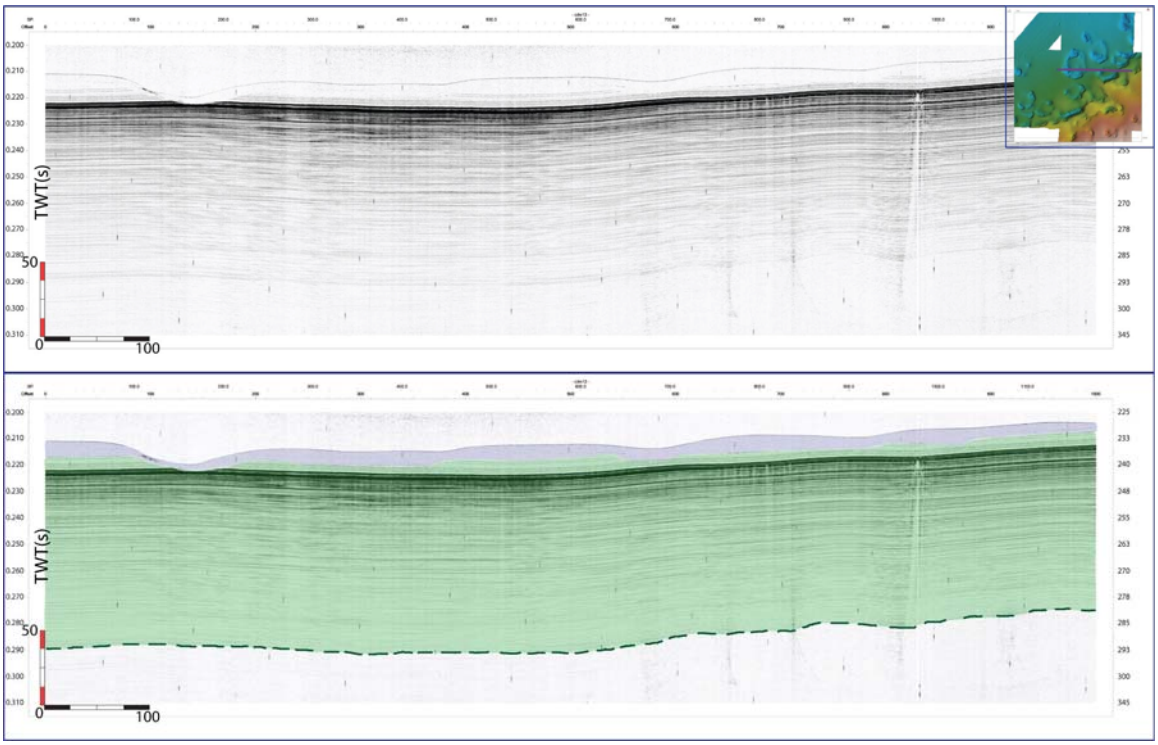

Figure 4.5 Typical CHIRP line in the survey area. This profile depicts seismic line cdw_13 collected in September 2009 off the southwest shore of Isle Royale (Location shown in Figure 3.1). This east-west trending line runs from the Thunder Bay Trough towards Isle Royale. Offsets (lower horizontal scale) are given in meters, two-way travel time (left vertical scale) in seconds, and depth (right vertical scale) is in meters. The interpreted line (b) depicts the major facies identified in the survey area. The green unit is facies C, which transitions into the acoustic basement due to signal attenuation. Facies C was not completely imaged by the CHIRP system, the deepest continuous-coherent reflector is denoted by the dashed green line. The blue unit is facies D. Descriptions of these units can be found in tables 4.3 and 4.4.

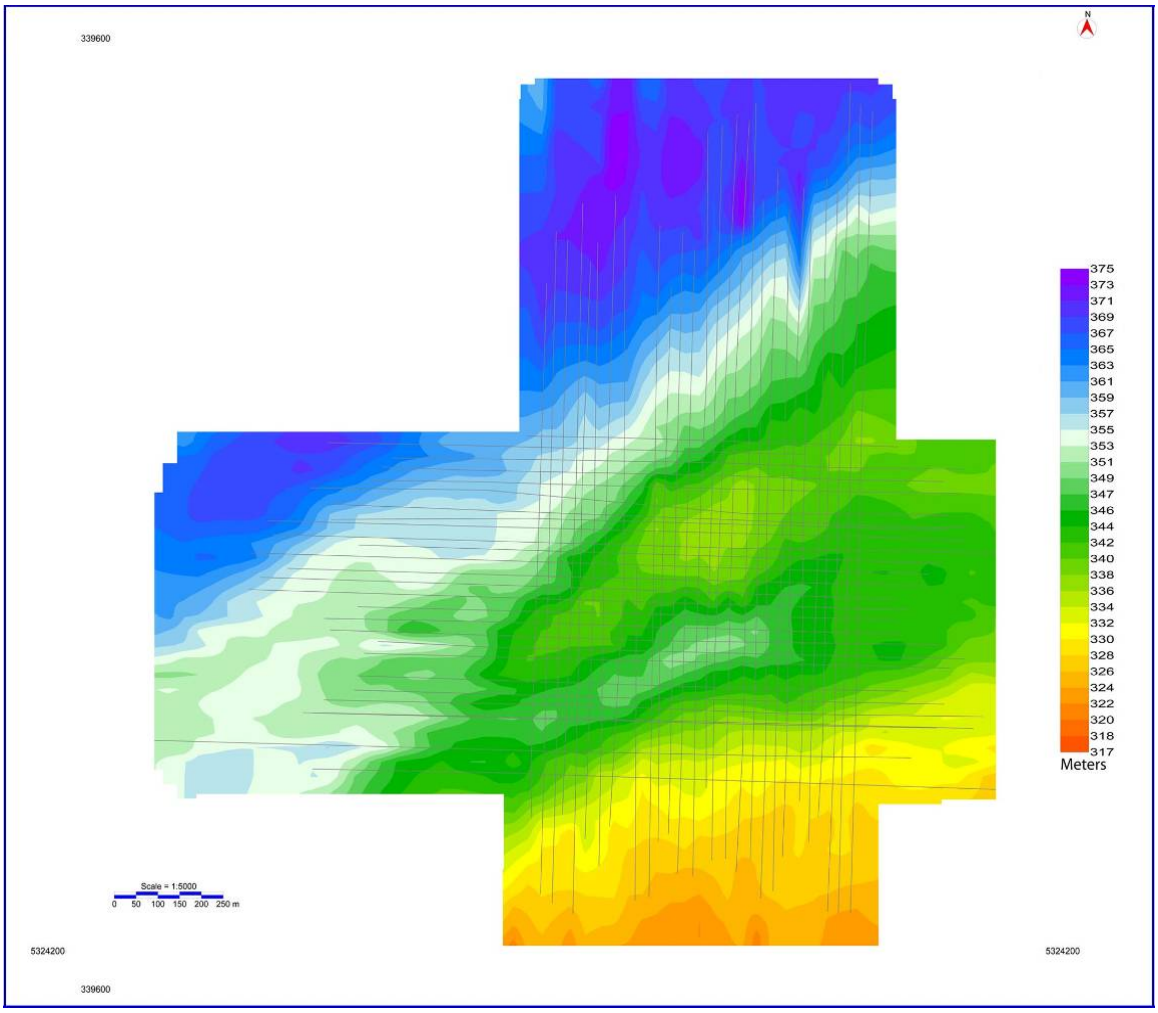

Figure 4.6 Seismic facies A surface topography time map. This time map was created in Kingdom Suite from the Airgun SCS data using the gradient projection gridding algorithm and an assumed seismic velocity if 1500 m/s. Depths to the gridded surface are shown in the color bar on the right in meters.

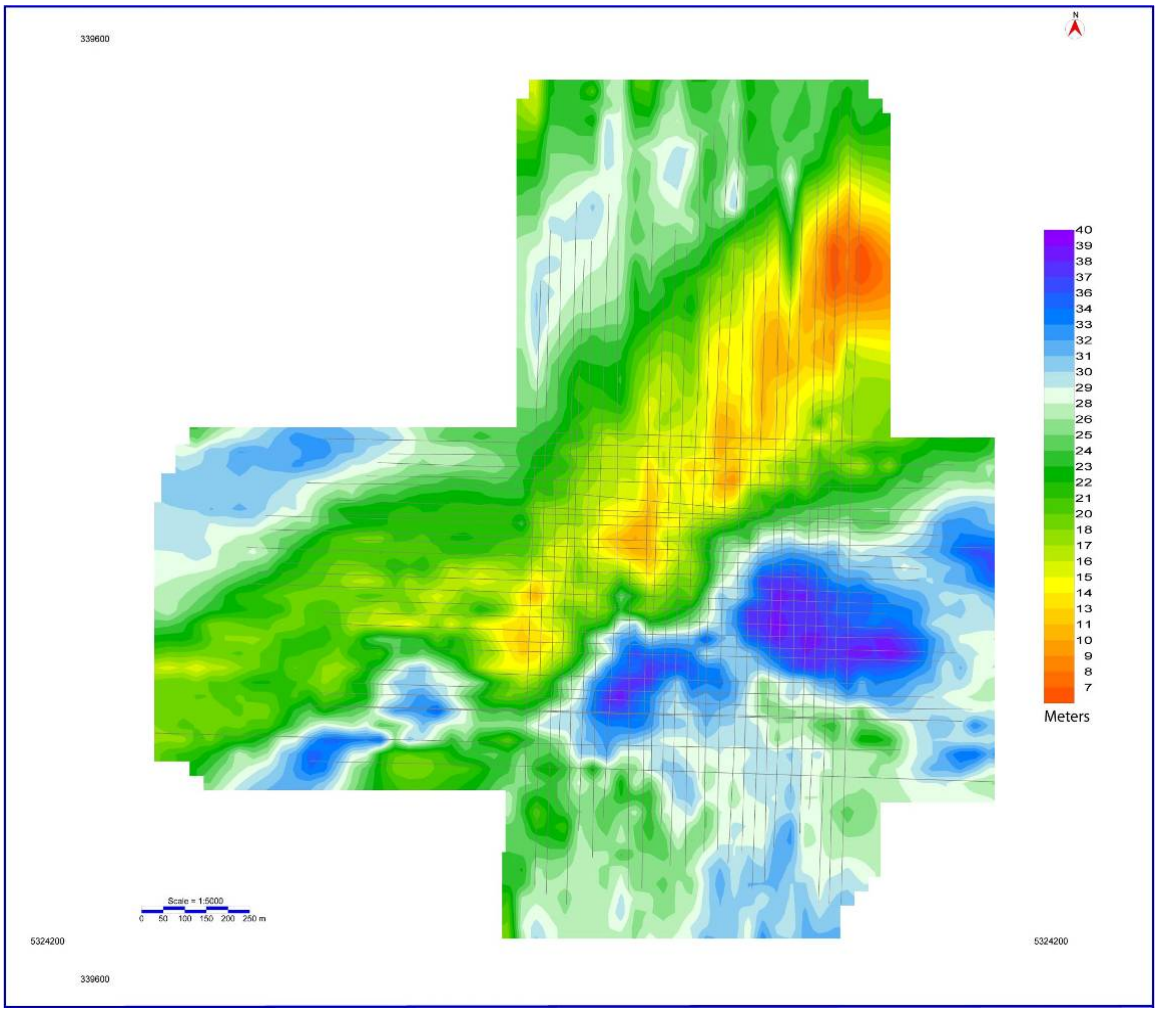

Figure 4.7 Seismic facies B isopach map. This isopach map was created in Kingdom Suite using an assumed seismic velocity of 1500 m/s. Unit thicknesses are given in the scale bar on the right in meters.

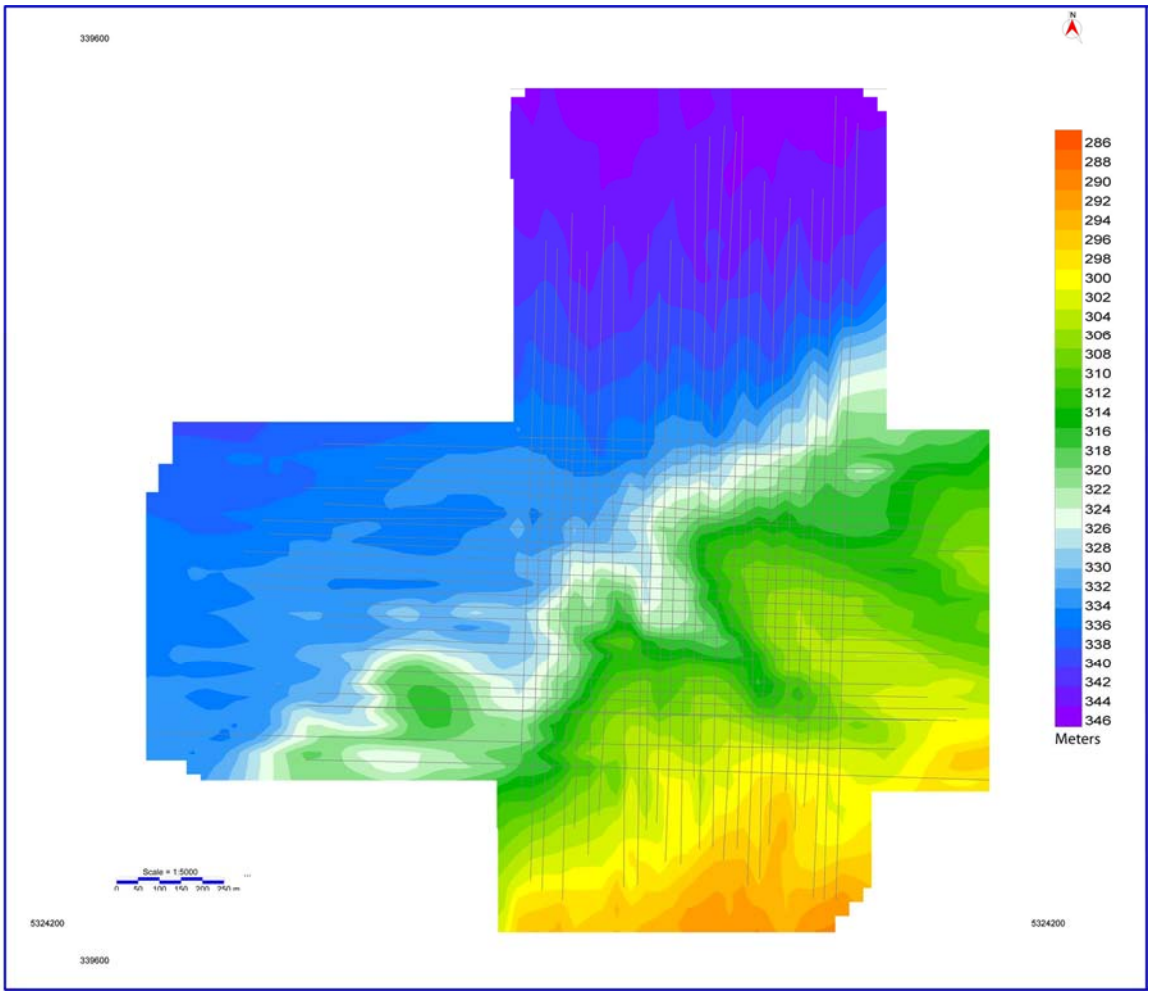

Figure 4.8 Seismic facies B surface topography time map. This time map was created in Kingdom Suite from the Airgun SCS data using the gradient projection gridding algorithm and an assumed seismic velocity if 1500 m/s. Depths to the gridded surface are shown in the color bar on the right in meters.

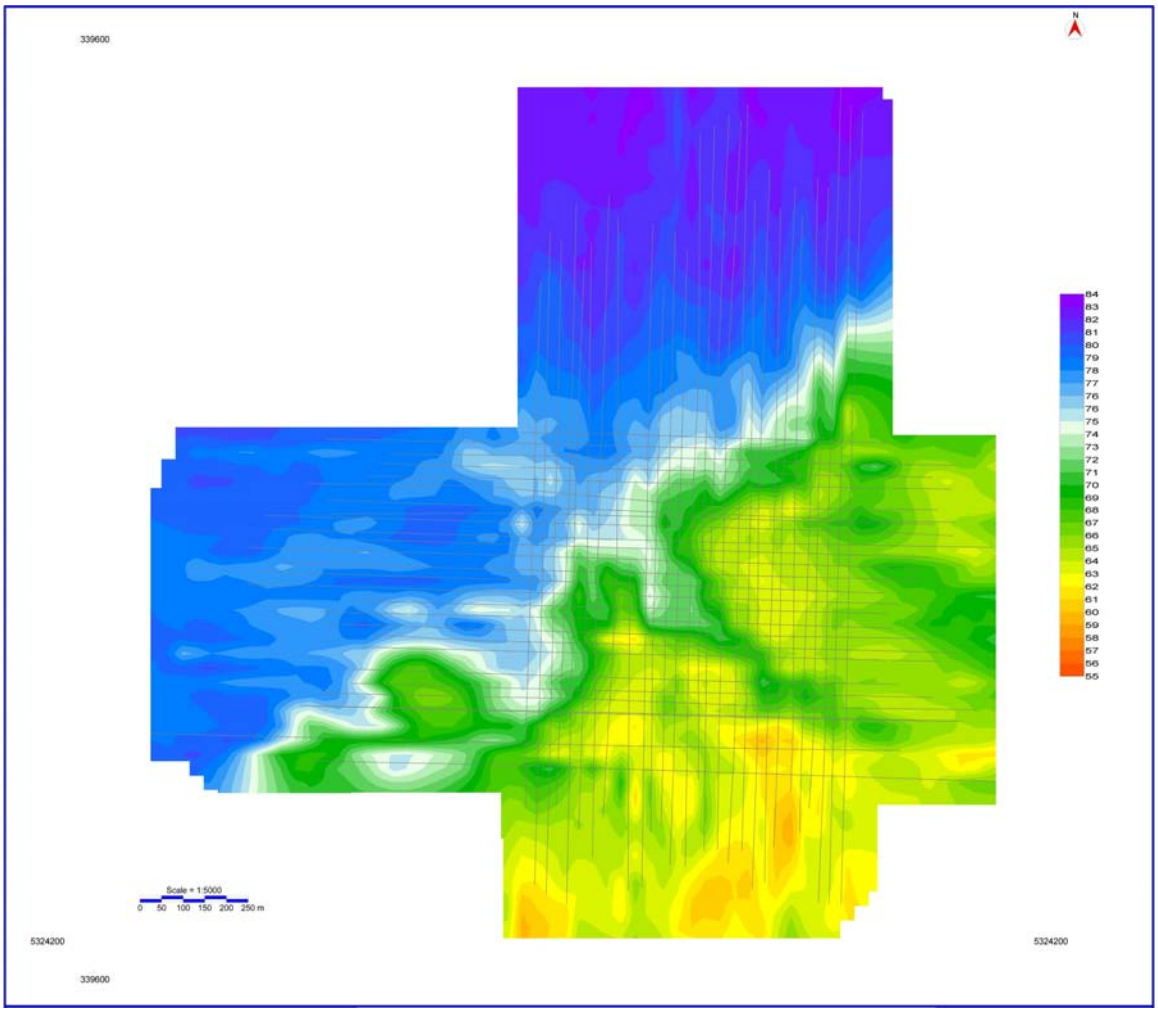

Figure 4.9 Seismic facies C isopach map. This isopach map was created in Kingdom Suite using an assumed seismic velocity of 1500 m/s. Unit thicknesses are given in the scale bar on the right in meters.

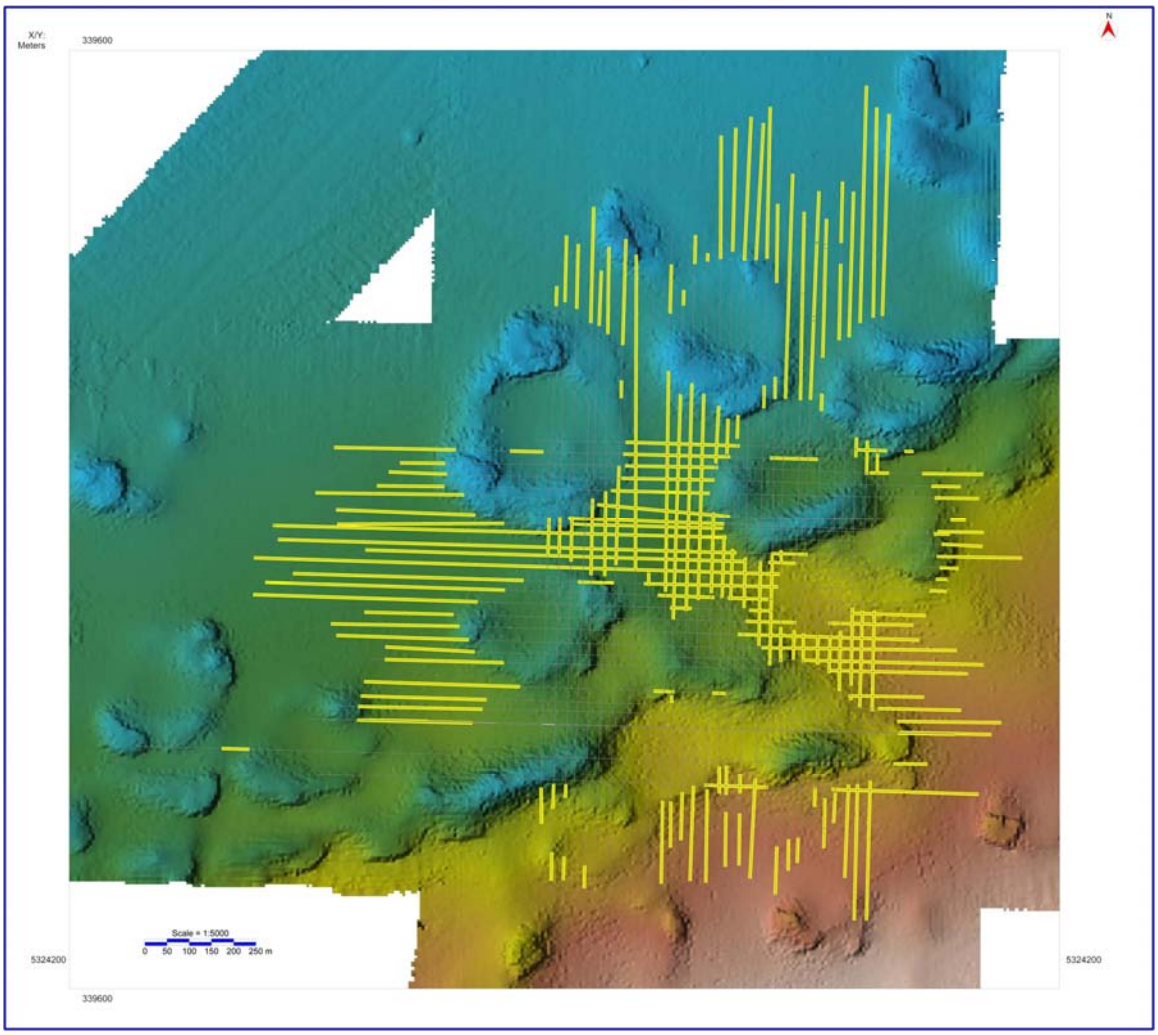

Figure 4.10 GL1 reflector map. The locations where reflector GL1 (the top of seismic facies C) have been overlain atop the bathymetry map. This map shows where reflector GL1 has been observed to be present. Several ring shaped voids are defined by the absence of GL1. The voids appear to be directly over several of the lake floor rings observed in the bathymetric data.

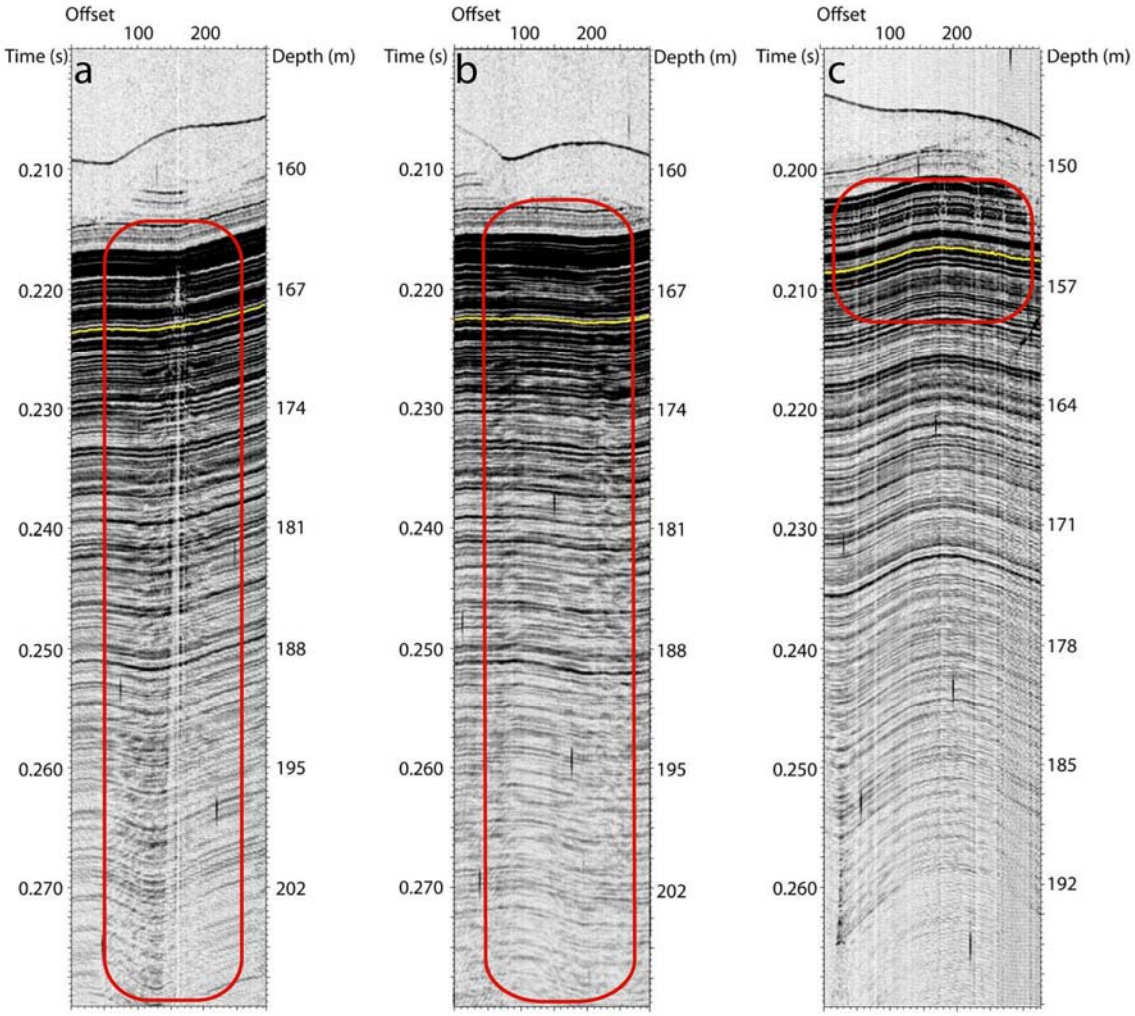

Figure 4.11a,b,c Chimney structure examples. These are typical examples of the three different types of chimney structures observed in the CHIRP data. Lateral offset is shown at the top of each of the three figures. The vertical scale is given in milliseconds (left vertical axis) and meters (right vertical axis). (A) Deep chimney contained within a red rectangle. (B) Diffuse chimney contained within a red rectangle. (C) Several short chimneys contained within a red rectangle.

4.4.3.1.1 Deep-Sourced Structures

4.4.3.1.1.1 Deep Chimneys

Deep chimney structures are sometimes described as looking like an inverted feather/quill structure (Wattrus, pers. comm.) Figure 4.11a depicts a deep-chimney structure. To be classified as a deep-chimney, the structure must have a well-defined coherent central-shaft with adjoining disturbed/upturned reflectors and extend to some depth. The disturbed or upturned reflectors appear to be overprinted on top of the existing stratified-parallel reflectors. In this survey, deep-sourced chimneys are imaged down to the (CHIRP system's) acoustic basement. The upper termination of the central shaft of a deep chimney often occurs at the unconformable boundary between seismic facies C and the overlying seismic facies D. These structures are often found beneath areas where reflectors have been abruptly truncated.

The central shafts of these features vary in appearance, but they typically appear as high-amplitude vertical columns 20-30 meters across, bounded by narrower low-amplitude columns on either side. Well defined and coherent central-shafts often transition into acoustically-blanked columns as it approaches the acoustic basement. The width of the zone of disturbed/upturned reflectors on either side of the central shaft varies in size but is typically 100-150 meters across on each side.

The three-dimensional character of these types of structures is illustrated by two orthogonal CHIRP survey lines (cdw13 and cdw41) that intersect a well

defined deep chimney in the northeast corner of the survey area. The intersection of the lines is indicated by the vertical red line in each CHIRP profile (Fig. 4.12a,b,c). These two CHIRP profiles illustrate that at least some of the deep chimneys are somewhat symmetrical. In cross-section the central shaft is approximately the same width in either direction. The peripheral disturbed/upturned reflectors also appear to be similar in both breadth and depth. This orthogonal-symmetry is suggestive of radial symmetry. However, without additional survey lines intersecting the same structure at another angle, radial symmetry can only be assumed and is not definitely proven.

Even though this is high-resolution data, the ability to resolve structures and their spatial distribution is limited by the spacing of the survey transects and the horizontal resolution of the CHIRP data. In this example, the Fresnel zone is approximately half the width of the central shaft. The deep chimneys observed in this study are dimensionally very similar in breadth and depth. This does not support varying scales of deep-chimneys among the deep chimneys, however, smaller chimneys may not have been imaged because of the limited resolution of the CHIRP data.

A second problem with the interpretation of this data is that there is no guarantee that the survey transects cut directly across the center of the feature. An example of this is CHIRP profile cdw22. Figure 4.13 is a cross-sectional profile of cdw22 which shows what could be interpreted to be a very weak central shaft with peripheral disturbed/upturned reflectors. This could be the result of a

survey line tangentially intersecting a central shaft or a separate feature in itself. Since the pseudo -3D survey was acquired with a survey line spacing of ~20 m, it is likely that in some cases the central shaft is missed altogether and only the adjoining disturbed/upturned portion of the deep chimney is intersected by a line.

Maps constructed of the locations of these deep-chimneys show that they align themselves along two linear trends. These linear trends appear to correlate with two plunging synclinal structures observed in the upper surface of seismic facies B (Fig. 4.14). It should also be noted that deep chimneys are not found in clusters in this survey.

4.4.3.1.1.2 Diffuse Chimneys

Figure 4.11.b depicts an example of a diffuse chimney structure. These are characterized by a vertical column of acoustic turbidity that is laterally bounded zones of disturbed/angled reflectors on either side. These are the most nebulous and difficult to characterize of the three chimney structures. They are deep-sourced features that often extend to the acoustic basement. These features typically have upper terminations that occur below the unconformable boundary between seismic facies C and D. They are often found beneath areas with truncated reflectors.

Picking/identifying the diffuse chimneys can be somewhat subjective in that their selection could influenced by truncated reflectors within the same profile. To minimize any potential bias that may be imparted by bathymetric relief,

diffuse chimneys were mapped, without referencing any bathymetric data, by marking the disturbed/angled reflectors observed along their edges at depth within the cross section. A survey base map on which the endpoints for suspected diffuse chimneys are plotted show that they roughly outline the ring structures seen in the bathymetry (Fig. 4.15).

4.4.3.1.1.3 Shallow (Short) Chimneys

Figure 4.11c depicts a cluster of short-chimneys, which are similar to classic chimneys in that they have a well defined central shaft, usually 10-15 meters wide. Short chimneys are much shallower structures, usually observed within the upper five meters of seismic facies C. These structures also typically terminate below what is interpreted to be the unconformable boundary between seismic facies C and D, and they are often found beneath areas with truncated reflectors. Short chimneys are by far the most seismically-diverse and often subtle chimney structures observed in this study. Some features are readily identified as short chimneys while others are barely visible. A base map depicts the locations of the observed short chimneys within the survey area (Fig. 4.16). They are color coded to delineate those that are unambiguous (black) and those that are more suspect (white). They are most densely populated in the southeast half the survey area.

4.4.4 Seismic Facies D

Seismic facies D is characterized by a high amplitude reflector that occurs at the upper boundary of the unit (sediment-water interface) and becoming almost acoustically transparent below that. Internal reflections can be seen when high amounts of gain are applied to the data. These internal reflections are typically found in close proximity to both the lake floor rings and chimney structures mentioned above. A time map for seismic facies D is not necessary because high-resolution multibeam data is available for this surface. Seismic facies D rests unconformably on top of seismic facies C throughout the survey area and is of relatively uniform thickness (1-5 meters), except that it thins within the lake floor rings (Fig. 4.17).

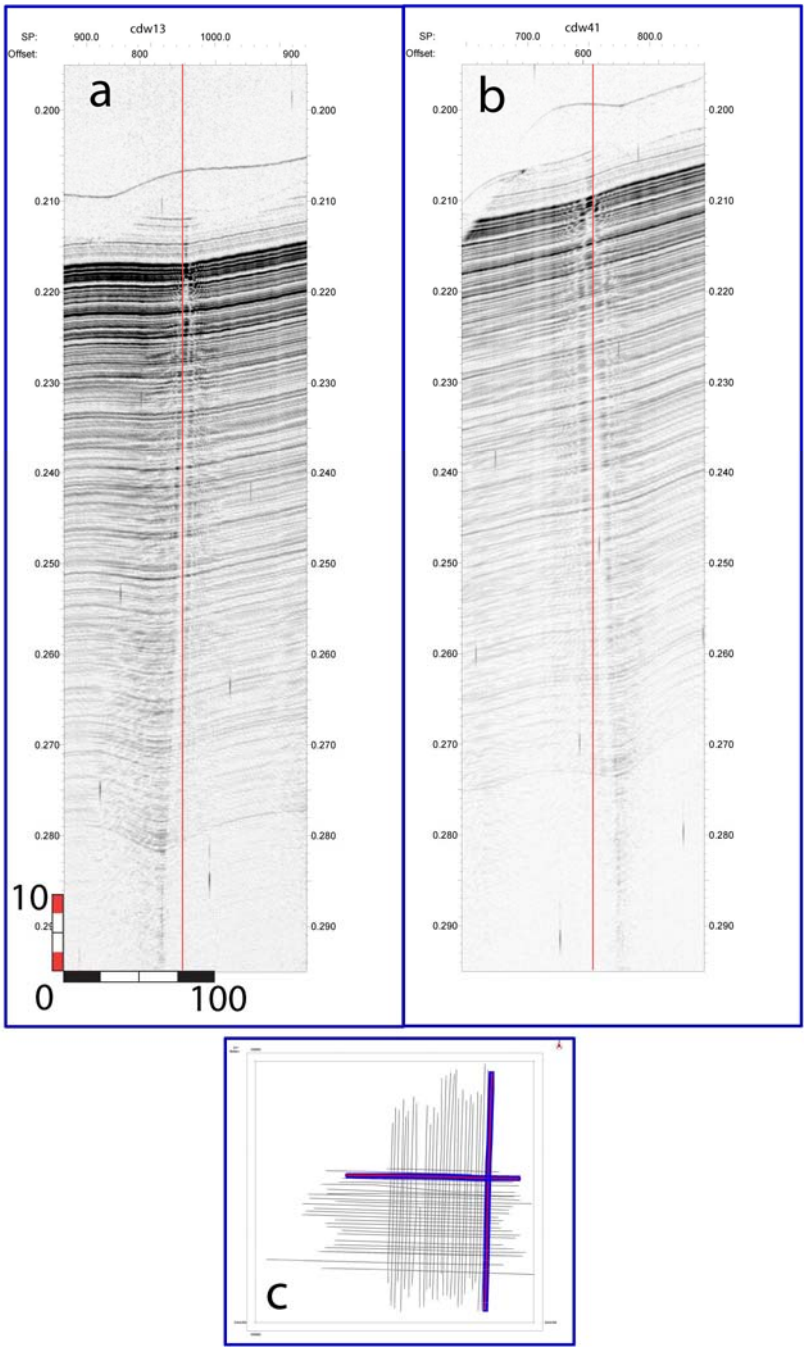

Figure 4.12a,b,c 3D-deep chimney. Two orthoganal CHIRP profiles (cdw13(A) and cdw41(B)) that intersect a deep chimney structure and illustrating their approximate 3D morphology. These two rings intersect in the northeast corner of the survey area (C).

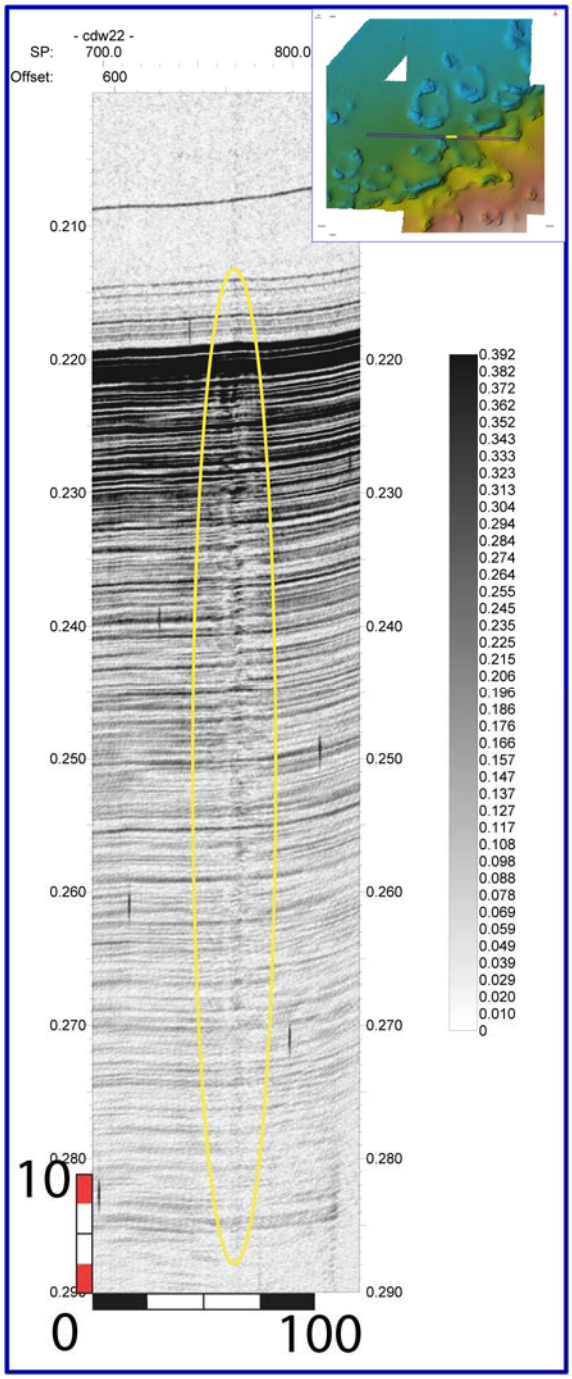

Figure 4.13 Possible tangentially intersected chimney. A weak central shaft bounded by upturned/disturbed reflectors is highlighted by the yellow ellipse. A scale bar (in meters) is provided in the lower left corner.

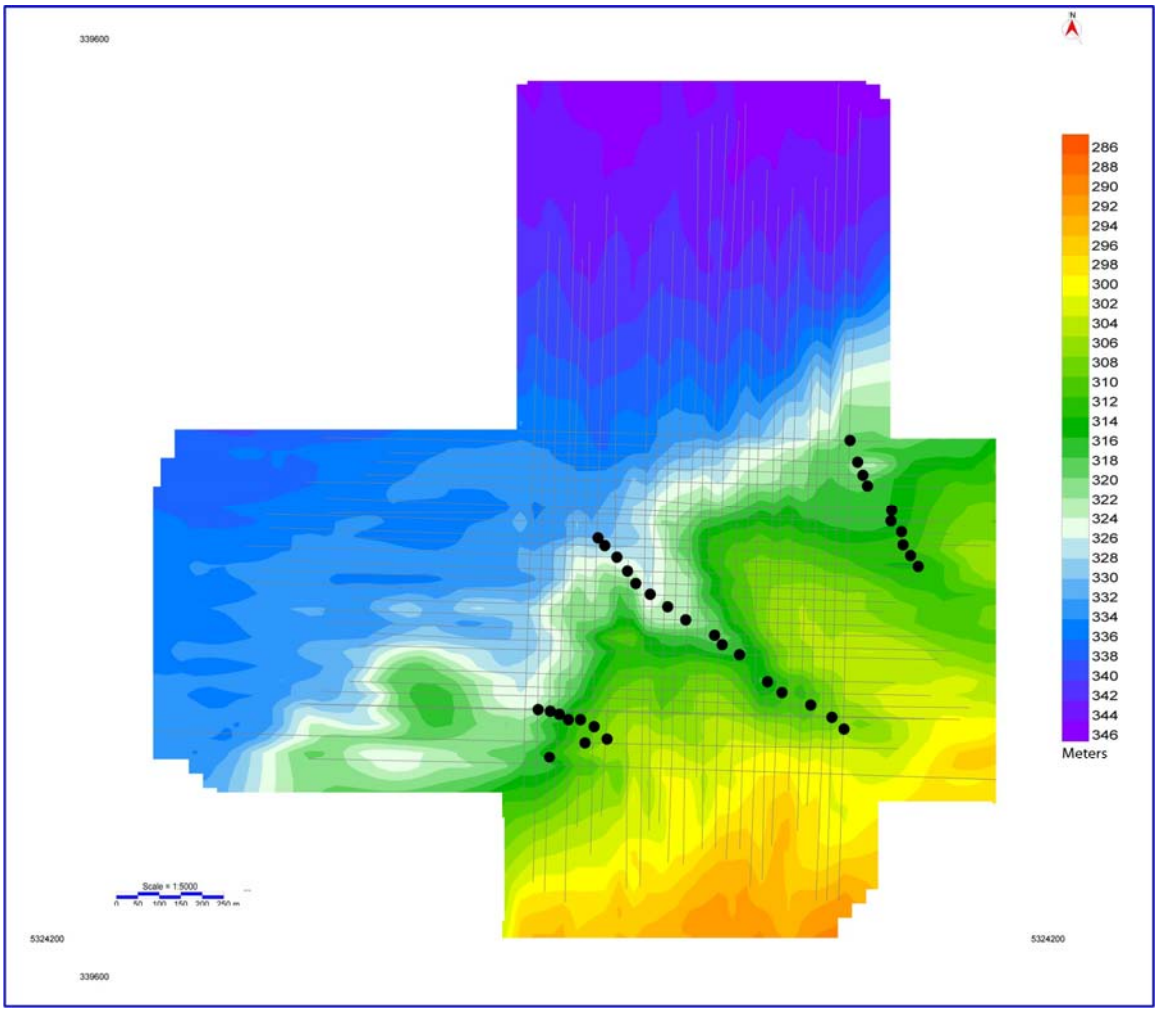

Figure 4.14 Deep chimney location map. Seismic facies C time map (fig. 4.8) with the location of deep chimney structures marked by black circles.

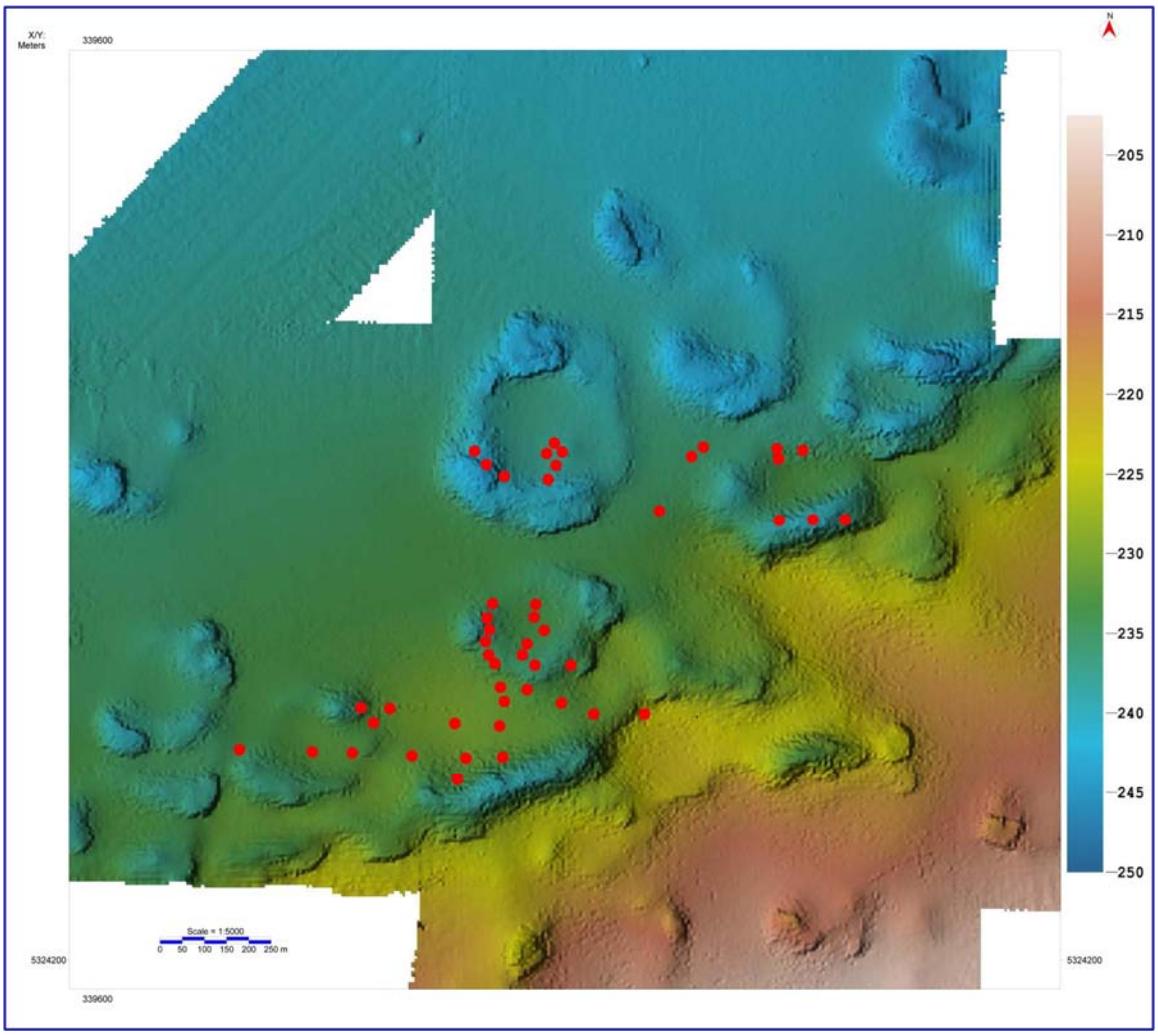

Figure 4.15 Diffuse chimney location map. Diffuse chimney's outer edges as marked determined from the CHIRP data is marked by red dots. These features picked without referencing the bathymetric rings to avoid bias. The resolution of the east-west survey lines is typically better than the north-south survey because of the lake conditions.

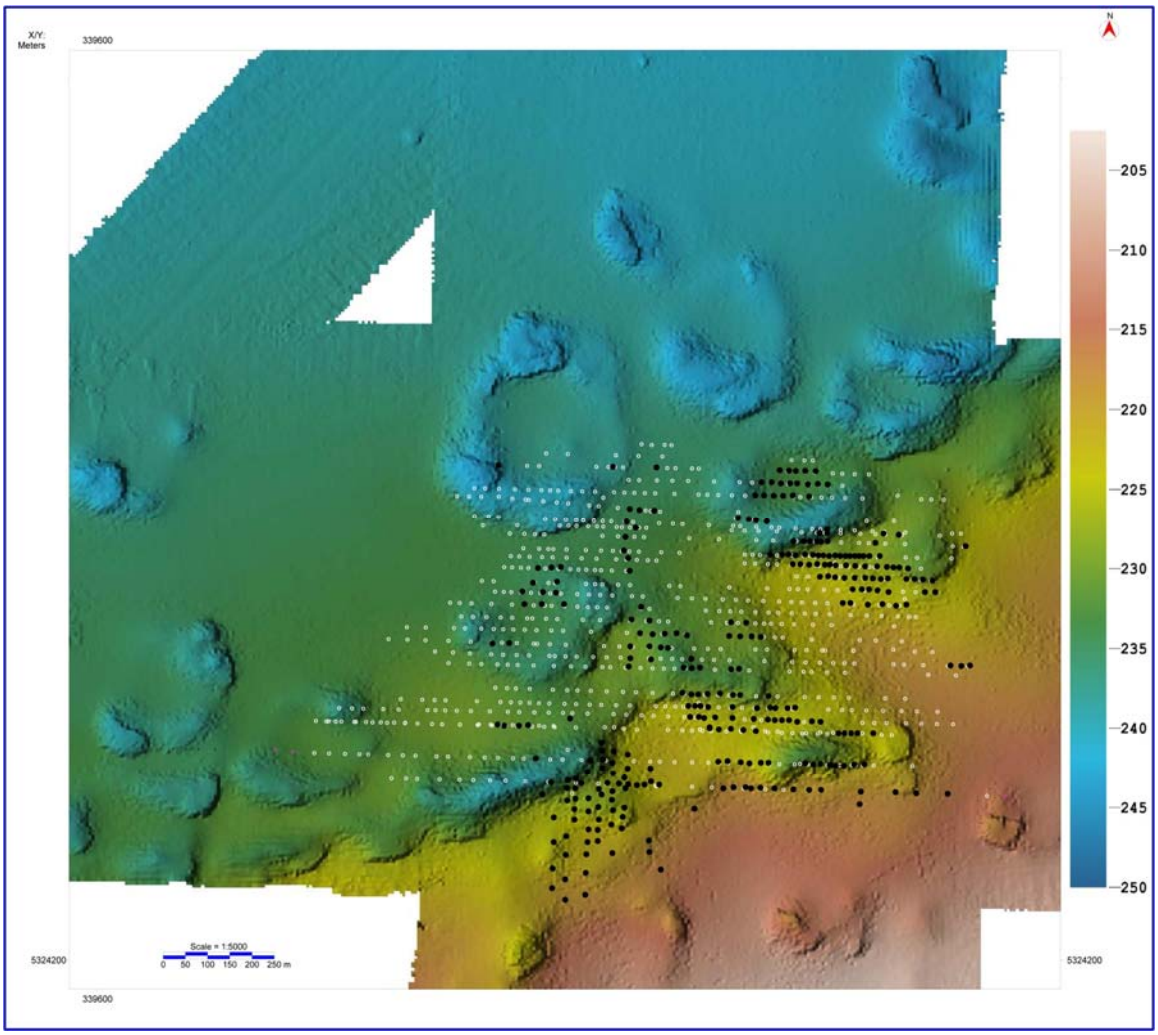

Figure 4.16 Short chimney location map. Locations of short chimneys marked by black dots and suspected short chimneys by white dots. The resolution of the east-west survey lines is typically better than the north-south survey because of the lake conditions. The short chimneys are typically not resolvable in lower resolution north-south survey lines.

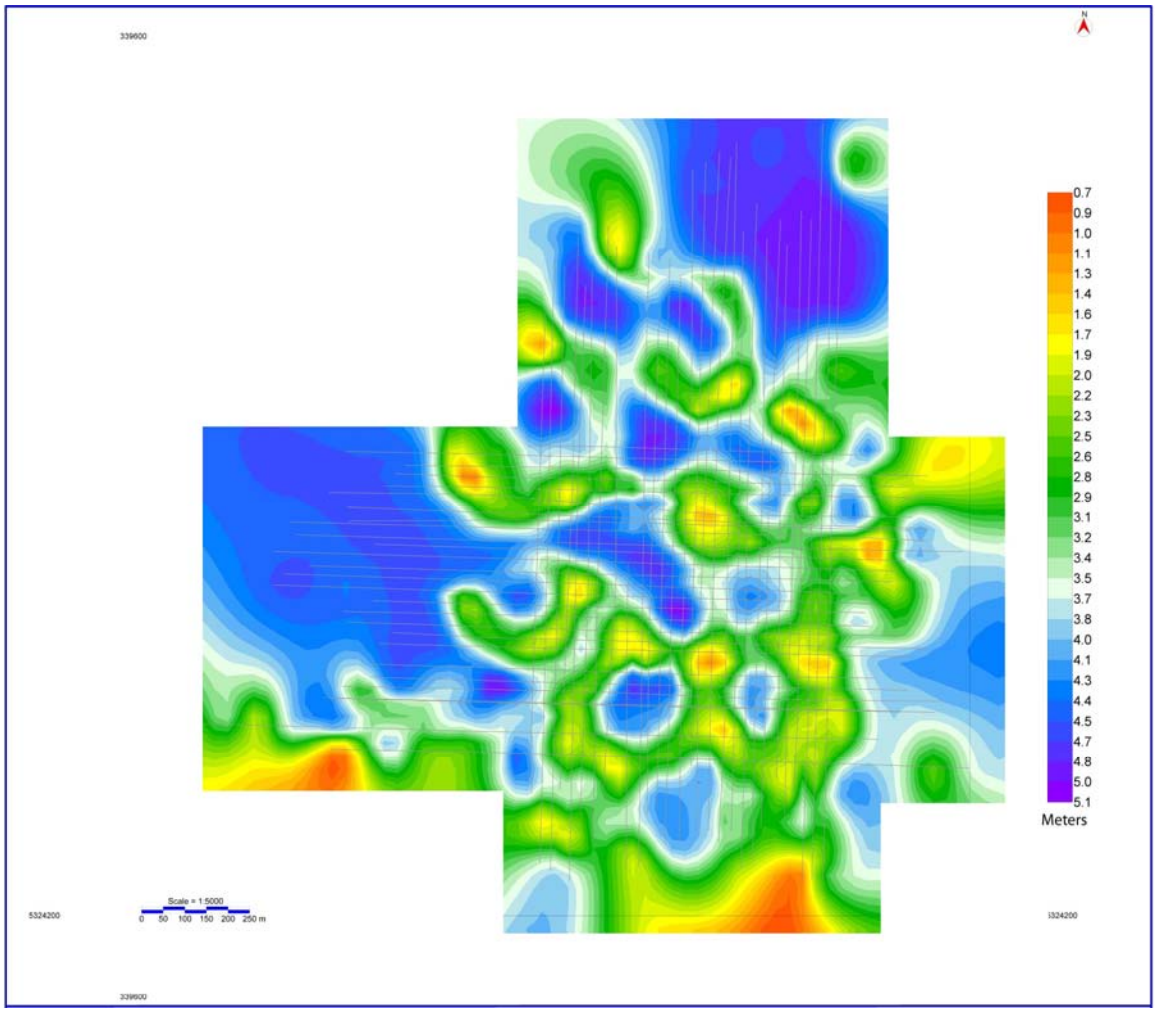

Figure 4.17 Seismic facies D isopach map. This isopach map was created using an assumed seismic velocity of 1500 m/s. Unit thicknesses are given in the scale bar on the right in meters. Seismic facies A is typically between 1-5 meters thick. This unit thins in the troughs that define the bathymetric lake floor rings. The two anomalously thin areas along the southern edge of the map are erroneous. The gridding algorithm (gradient projection) filled in these areas.

Chapter 5: Discussion

5.1 Geologic Interpretation of Seismic Facies

5.1.1 Seismic Facies A

Comprising the acoustic basement, seismic unit A is interpreted to be bedrock, specifically the sedimentary and volcanic rocks of the Keweenawan Supergroup (Huber, 1975). The time map of the upper surface of unit A (Fig. 4.6) illustrates the bedrock topography in the survey area, which is interpreted to be the result of glacial erosion.

5.1.2 Seismic Facies B

Seismic facies B is found above seismic facies A throughout the entire survey area and interpreted to be glacially sourced material that was deposited and reworked as the Superior Lobe advanced and subsequently retreated northward. This interpretation that seismic facies B is glacial in origin, is in agreement with previously published work (Dell, 1971;Breckenridge, 2005; Gary, 2010; Voytek, 2010).

The uppermost bounding reflectors generally dip obliquely towards the northwest (away from Isle Royale), whereas the internal reflectors can be either chaotic or somewhat stratified. The stratified reflectors occur in low lying areas within the survey area. This behavior was also observed by Voytek (2010) who

questioned whether the stratified reflectors were associated with a till. It has been suggested that they may be glacial underflow deposits (Colman, pers. comm.) For the purposes of this thesis all the sediments in this unit will be considered of glacial origin, as they are bounded by Precambrian basement rock below and seismic facies C above.

A time map (Fig. 4.8) of the upper surface of seismic unit B is dominated by two ridges that plunge to the northwest. Due to the limited extent of the survey, the exact nature of the structures observed in Figure 4.8 is difficult to surmise.

5.1.3 Seismic Facies C

Seismic facies C is interpreted to be glaciolacustrine sediments deposited as the Superior lobe made it's final retreat from the basin. The highly-stratified and draped nature of the internal reflectors, observed in seismic facies C, is indicative of a calm or low-energy depositional environment (Stoker et al., 1997). The closely spaced low to moderate amplitude reflections are likely the product of moderate changes in acoustic impedances associated with subtle density changes associated with the annual varves found within this unit (Breckenridge, 2005). The glaciolacustrine sediment package is capped by several strong and distinct reflectors within CHIRP profiles. Two representative marker horizons, labeled GL1 and GL2 are used to characterize the upper surface of seismic facies C. Careful examination of the CHIRP data shows that these marker

horizons are abruptly truncated indicating that the upper boundary of this unit is erosional.

An isochron map made from GL1 (the uppermost glaciolacustrine reflector) to the maximum depth of reflector truncations (missing reflectors) can be used to produce an estimate of how much material was removed (Figure 5.1). This is a rough estimate as the map shows sediment removal outside the ring areas where there is clearly no evidence of sediment excision (truncated reflectors) in cross-sectional profiles. A possible explanation for this is that the gridding algorithm used to fill in the survey line gaps could not account for the naturally occurring slope of the basin. To minimize this error, a strong ubiquitous reflector was selected at depth and used as a datum. This time map shows ring-shaped structures which suggests that it is the result of post-depositional removal of lake sediments by the upward migration of pore fluids.

It is important to note that the material appears to have been removed not only from the troughs defining the rings, but also from within the center of the rings. This suggests that the rings observed in the multibeam data are actually much more complex, representing the integrated expression of an evolving pock-forming process. The term lake floor ring will not be changed as these structures unequivocally express themselves as rings, both here and in other areas of the lake (Wattrus, pers. comm.; Wattrus et al., 2005; Sharpe, 2008).

5.1.3.1 Pockmarks

Before beginning any lengthy discussion of the pockmarks observed in this study, a cursory review of pockmark morphologies is required. Early work on seabed pockmarks classified them as conically shaped depressions that appear circular in map view (King and MacLean, 1970; Berkson and Clay, 1973; Flood, 1984). Research has subsequently shown that pockmarks come in a wide variety of shapes and sizes. The following is a summary of the various pockmark morphologies as defined by Judd and Hovland (2007).

Standard and Elliptical Pockmarks are probably the most common, with a variety of length to width ratios from 1 (circular) to 1.25 or more. Possible reasons for the elongated axis include seafloor slope, tidal currents, and/or slope-normal bottom currents.

Asymmetric Pockmarks often appear to have a long and distinct 'tail' with a strong back wall reflection occurring on only one side. The orientation and scale of the asymmetry can be uniform in localized areas and vary widely regionally.

Pockmark Strings are composed of individual pockmarks, often symmetrical, evenly spaced and arranged in strings or chains. A larger single standard pockmark is sometimes observed at the end of a string, or at the center of several strings radiating outwards.

Giant Pockmarks are anomalously large when compared to other pockmarks in the same vicinity. For example, typical pockmarks may be < 150

meters in diameter and less than 5 meters deep, where giant pockmarks would be on the scale of greater than 500 meters in diameter and greater than 20 meters deep.

Composite Pockmarks are recognized as the amalgamation of two or more standard pockmarks or groups of pockmarks to form a single pock-like structure with a complex shape.

Unit Pockmarks are very small depressions (less than 5 meters) found individually, in groups and are sometimes associated with larger pockmarks. Unit pockmarks can also coalesce to form a composite pock.

5.1.3.2 Pockmark Rings

A review of the CHIRP profiles show that the post-glacial Holocene sediments rest unconformably atop the glaciolacustrine varved sediments. The abruptly truncated reflectors near the top of the glaciolacustrine sediment package define this erosional unconformity. The following discussion on the pockmarks observed in this study will use three representative pockmark ring features (identified in Figure 5.2 as Ring A, B and C), to illustrate the key characteristics of these features in the field area. Two principle pockmark types (standard/asymmetric and composite) were observed in the high-resolution CHIRP profiles.

For the purpose of clarity, the following figures will be subsets of complete survey lines that illustrate these features in cross-sectional CHIRP profiles.

Rings A, B, and C

Several east-west survey lines that intersected Ring A and B exemplify the subsurface characteristics of the pockmarks that define the lake floor rings. Rings A and B show somewhat uniform relief with the exception of two deep pits that dominate Ring A (eastern edge) and Ring B (southern edge) (Fig. 5.1). The CHIRP profiles show that up to 10 meters of glaciolacustrine sediment has been removed in the western and southern edge of Ring A and B.

These deep pits are interpreted to be crescent shaped (Ring A) and elongated (Ring B) asymmetric pocks. Several profiles show that material has been removed from within the center of Ring A – not just along the ring's perimeter. The upper marker reflector (GL1) in seismic facies B is not present in the center of Ring A or B. CHIRP profile cdw13 (Fig 5.3) shows absences of the marker reflectors. Both of the marker reflectors have been removed from the center of Ring A in CHIRP profile cdw13. CHIRP profiles cdw12, cdw13, cdw14, and cdw15 all intersect Ring A and Ring B. They all show similar pockmark morphologies within the lake floor rings. Rings A and B are interpreted to be the expression of a complex-composite pock comprised of smaller unit pocks joined with a larger asymmetric pock. Ring C differs from Ring A and B in that it does not have a deep well developed pit associated with it. CHIRP profile cdw26 (Fig. 5.4) intersects the center of Ring C and shows similar sediment excision throughout the center of the ring as seen in Rings A and B. Ring C is interpreted

to be a complex-composite pock comprised of smaller unit pocks. CHIRP profile cdw69 runs north-south through Rings A and C (Fig. 5.5) and shows similar pockmark morphologies as the east-west CHIRP profiles (cdw13 and cdw26).

Rings A, B, and C are typical of the lake floor rings observed within this survey area. All the rings in this survey show evidence of sediment excision (of varying degrees) within the center of the ring. Some rings (i.e. Rings A and C) have larger/deeper pits (asymmetric pocks) within them. The southeastern half of the survey area is clearly more densely populated with lake floor rings. Individual-isolated rings are apparent in both the multibeam and CHIRP data but the southeastern half of the survey area is dominated by closely-spaced or networked rings.

In fact, it is important to note that CHIRP profiles throughout the networked ring area show widespread sediment excision. Figure 5.5 is a typical CHIRP profile (cdw26) across the southeastern half of the survey area. This profile shows evidence of sediment excision throughout most the lateral extent of the profile.

The complex nature of the lake floor rings in the study area is not clearly articulated in the multibeam data. This could be the result of bottom currents infilling the lake floor rings with Holocene sediments muting their more complex topographic expression. Flood and Johnson (1984) described what they believed to be strong bottom currents reshaping the crescent shaped side-scan bathymetric features on Lake Superior's "modern" lake floor off the Keweenaw

Peninsula. Additionally, the survey line spacing of approximately 20 meters limits the ability of the survey to resolve what is happening within the ring centers. An alternate interpretation of the data might be that, the rings represent the integrated expression of an evolving drainage system that changes over time. That is during the drainage event as lake floor sediments are depleted.

The mechanism, responsible for causing the rings to form networks, or that prevents intersection between adjacent rings is not known. The rings could be the integrated expression of evolving drainage systems resulting in rings comprised of smaller pocks. As the fluid migration pathways migrated/evolved it is possible that smaller fluid flows were captured and integrated into larger flows. This would effectively shut off the fluid flows below smaller pocks and redirect that pore water towards the larger more well developed fluid flow pathways beneath larger pocks.

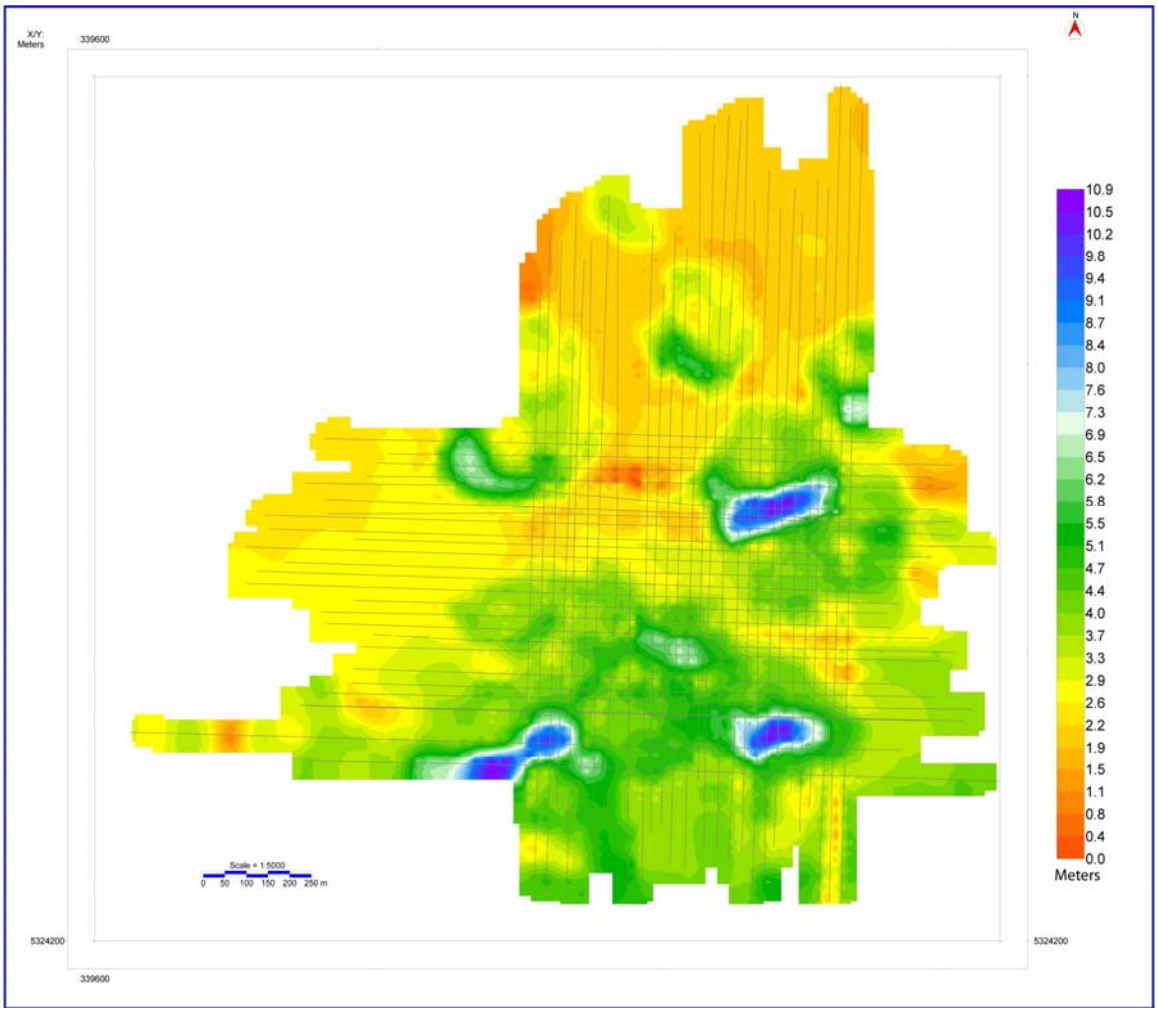

Figure 5.1 Missing glaciolacustrine sediment isochron map. This time map was created by calculating the distance from the uppermost glaciolacustrine reflector GL1 to the maximum depth of erosion (missing reflectors) using an assumed seismic velocity of 1500 m/s. This time map provides an estimate as to how much glaciolacustrine sediment was removed. This map shows "missing" sediment where there is no evidence of erosion (where the GL1 marker reflector is intact).

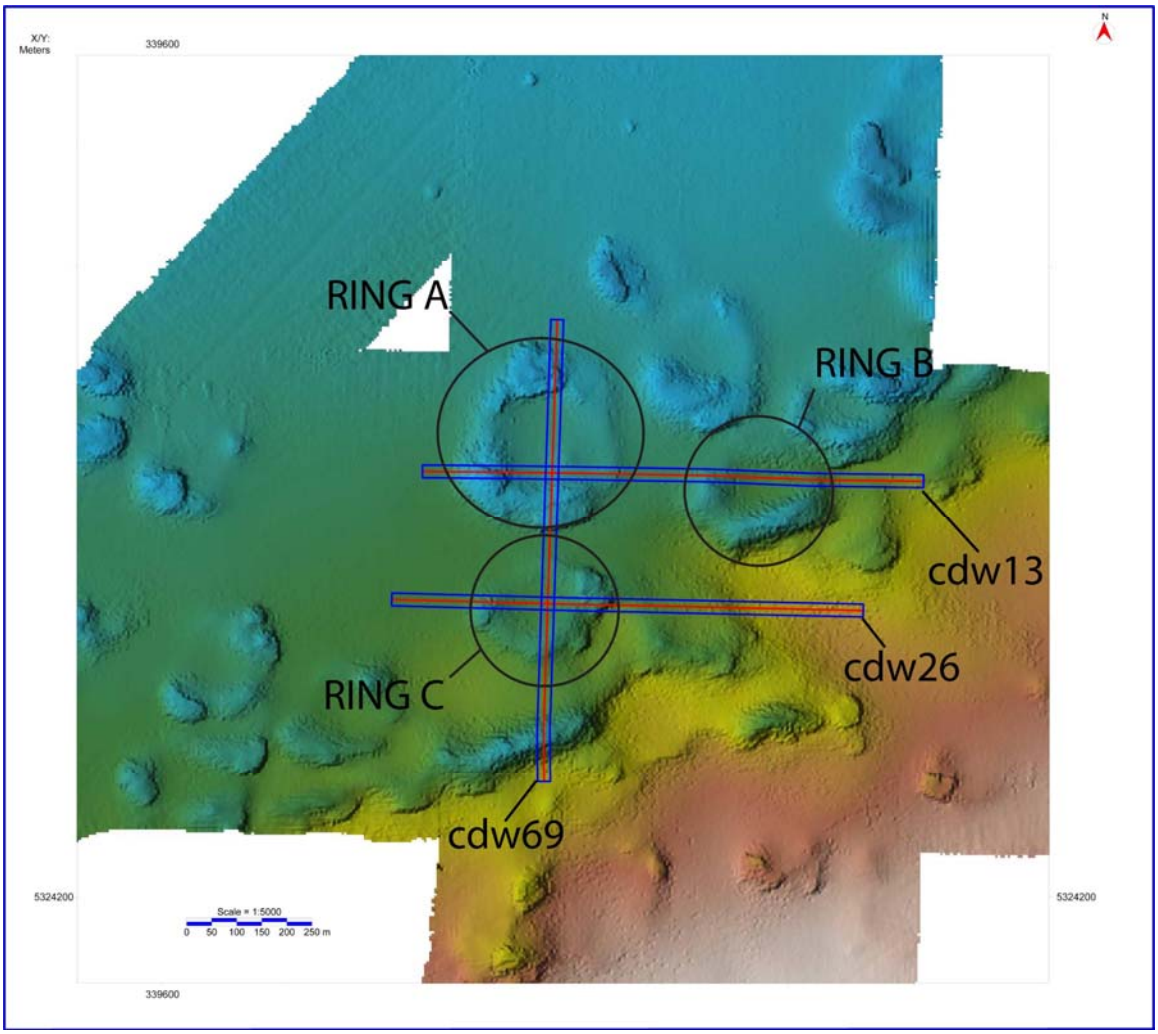

Figure 5.2 Bathymetric ring location map. Three primary bathymetric rings are labeled on this map along with three CHIRP survey lines that intersect them.

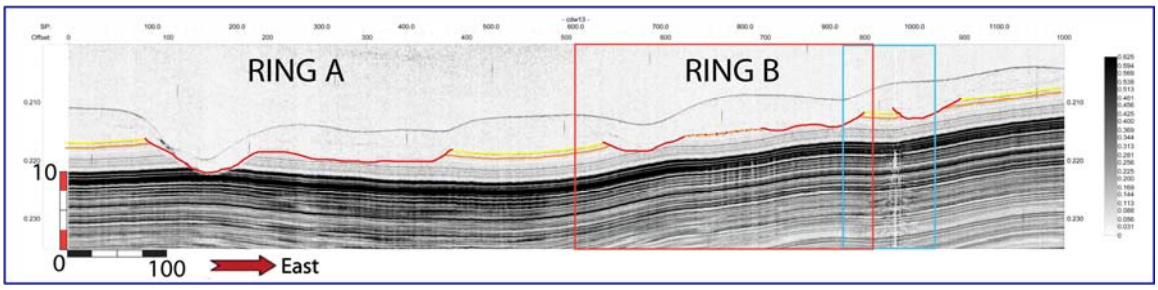

Figure 5.3 CHIRP profile cdw13. CHIRP profile with uppermost glaciolacustrine reflectors (GL1 yellow and GL2 orange). The areas where glaciolacustrine reflectors have been removed is marked by a red line. This CHIRP profile transected Ring A and Ring B (see figure 5.2). Both ring A and ring B show evidence of erosion in their relative centers. Ring A and B are interpreted to be composite pocks. The blue and red boxes depicts the location of figures 5.6 and 5.7.

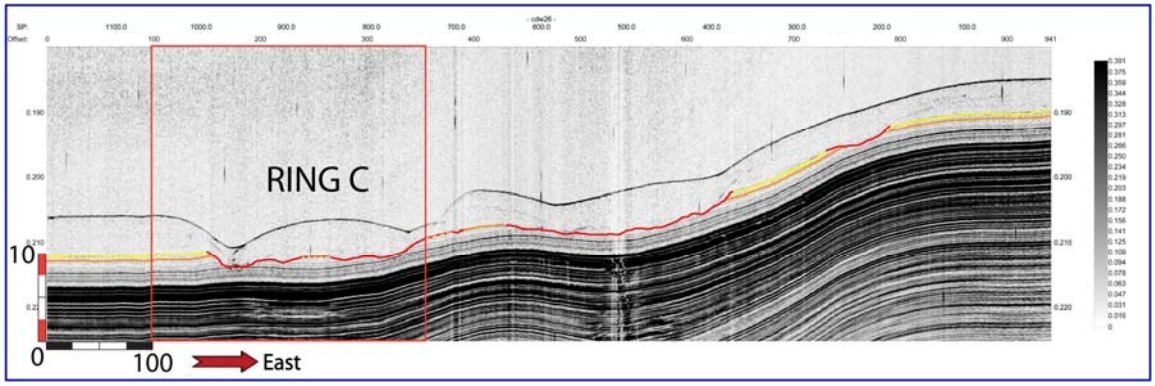

Figure 5.4 CHIRP profile cdw26. CHIRP profile with uppermost glaciolacustrine reflectors (GL1 yellow and GL2 orange). The areas where glaciolacustrine reflectors have been removed is marked by a red line. This CHIRP profile transected ring C. The red box depicts the location of figure 5.8.

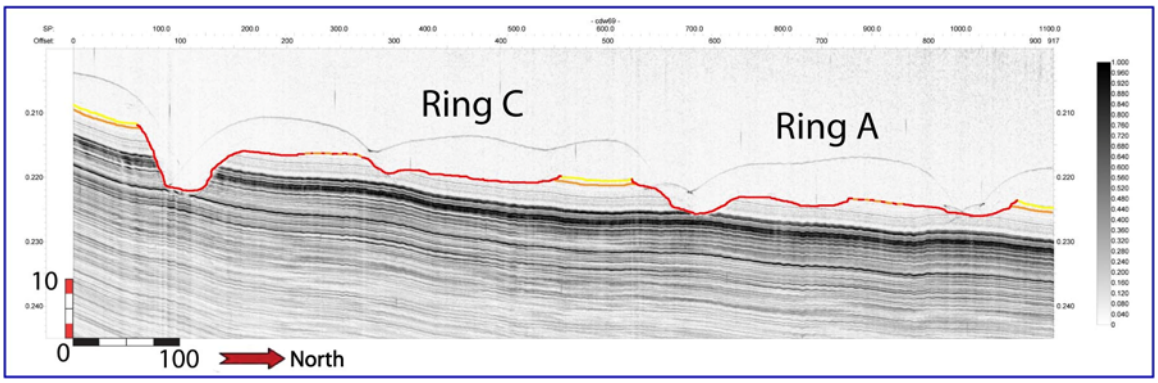

Figure 5.5 CHIRP profile cdw69. CHIRP profile with uppermost glaciolacustrine reflectors (GL1 yellow and GL2 orange). The areas where glaciolacustrine reflectors have been removed is marked by a red line. This CHIRP profile transected ring A and ring C. This north-south CHIRP profile shows similar pockmark ring morphologies to the east-west chirp profiles.

5.1.3.3 Dewatering Structures

Seismic chimneys (sometimes called acoustic chimneys or seismic pipes) have been widely observed globally and are typically thought to be the result of the upward migration of buoyant fluids/gasses (King and MacLean, 1970; Judd and Hovland, 2007; Moernaut et al., 2010). The seismic chimneys described in the previous section are interpreted to be dewatering structures. Subtle changes in acoustic impedance overprinting and in some cases destroying the existing stratified-parallel reflectors.

In this survey, deep-chimneys (Fig. 5.6) were imaged within the glaciolacustrine package down to the acoustic basement. They form two linear trends that correlate with the two topographic lows expressed in the top of the glacial (till) section (Fig. 4.14). These deep structures terminate at the Holocene-

glaciolacustrine unconformity and are typically found below (or in close proximity) to well developed standard/asymmetric pocks.

The fact that the characteristics of the central shafts of drainage features can vary between chimneys could be the result of several factors including: different magnitudes of drainage (fluid volume per unit time); varying orientations of the central shaft; naturally occurring heterogeneity within the sediment package, or how the survey line intersects/transects the structure. Even though this is high-resolution data, our ability to resolve structures and their spatial distribution is still limited by the horizontal resolution of the data. In this case the Fresnel zone is approximately half the width of the central shaft. The deep chimneys observed in this study are dimensionally very similar. This does not support varying scales of drainage among the deep chimneys, however, smaller chimneys may not have been imaged because of the limited resolution of the CHIRP data.

Another possible configuration is that the central shafts need not be completely vertical. Specifically the central shaft is not completely straight, but changes direction or migrates as it develops. Migrating fluids or gases often exploit pre-existing structures or weaknesses (cracks and faults) (Fetter, 2001). An example of this are the migrating fluids that take advantage of polygonal fault systems (PFS) (Cartwright, 1996; Cartwright et al., 2003; Cartwright et al., 2004). No visible evidence of cracks or faults was observed in this survey.

There are several mechanisms that could be responsible for the acoustic-blanking of the central-shafts observed in this data. These include: signal starvation; the presence of gas or gas-hydrates; or the mechanical destruction of pre-existing sedimentary layering. Signal starvation occurs when strong changes in acoustic impedance reflect more acoustic energy than the “typical” material of the surrounding area. This limits the amount of energy available to image deeper layers below (Judd and Hovland, 2007). While signal starvation is possible and could result from ice-rafted glacial dropstones, it is an unlikely cause for the acoustic-blanking with depth observed in this survey. The absence of a strong reflection or diffraction hyperbola strongly argues against this. The presence of gas or gas-hydrates is also not likely the reason for the acoustic-blanking, as Lake Superior’s sediments are very low in source material and neither are they deep enough to facilitate the formation of gas hydrates (Judd and Hovland, 2007).

The glaciolacustrine package in which the dewatering structures are observed is varved. It is likely that the individual sedimentary layers (varves) would have been destroyed during the dewatering process, thereby eliminating the acoustic impedance changes necessary to generate seismic reflections. In these data individual varves are imaged in the upper portions of the glaciolacustrine package. These varves do appear to be disturbed. It is possible that they are thicker and thus more "resistant" to erasure or that they are "out of the plane" reflections. This interpretation explains why varves are recognizable,

albeit disturbed, in the upper ~20 meters of most of the central shafts. It is unlikely that a process that could destroy deeper varves would leave overlying varves intact.

The disturbed/upturned zones of reflectivity are interpreted to represent the lateral extent of the drainage volume, similar to a representative drainage volume in well-hydraulics. An important point to note is that these features often show a persistent underlying “varved “ reflectivity – in other words the drainage related reflections that appear to arc up towards the central shaft/chimney are overlain on top of the original reflections. This is interpreted to mean that drainage to the chimney DOES NOT destroy the fabric of the clays so that, if you were to sample them they would visually look like regular undisturbed varves. In this scenario, the drainage reflectivity is produced by subtle density variations created by the migrating pore water.

CHIRP profile cdw22 (Fig. 4.14) is interpreted to be the result of a survey line tangentially intersecting a central shaft and not a fourth type of dewatering structure. Because the pseudo -3D survey was acquired with a survey line spacing of ~20 m, it is likely that in some cases the central shaft is only tangentially intersected or missed altogether and only the adjoining disturbed/upturned portion of the deep chimney is intersected by a line. This is one way to explain the origin of the diffuse chimneys, which will be discussed in greater detail later in the following section.

5.1.3.4 Diffuse Chimneys

The acoustic turbidity observed in the diffuse chimneys is interpreted to be the result of subtle changes in density due to migrating pore water. They are deep-sourced features that often extend to the acoustic basement. These features typically have upper terminations that occur below what is interpreted to be reflectors GL1 or GL2, implying that they are buried.

One possible explanation for these structures is that they are actually the result of the survey line not intersecting the central shaft of a deep chimney. However this interpretation is not supported when the spatial distribution of these features and the deep-sourced chimneys show that they do not always occur in association with each other. The deep-sourced chimneys are much more restricted in their distribution. This argues against this explanation. Alternatively the diffuse chimneys may be the result of drainage associated with multiple or migrating drainage pathways. The structure today therefore represents the integrated expression of unfocussed flow. The disturbed boundary reflectors could be the result of lateral fluid migration to the central diffuse chimney. Diffuse chimneys are often observed below the lake floor rings in this study (Fig. 5.7), however, the disturbed reflectors bounding these areas of acoustic turbidity often do not correspond directly with the edges of the bathymetric relief found on the lake floor and are often present where little or no relief exists. This suggests that the diffuse chimneys are representative of a physical process and not the

result of seismic wave perturbations induced by surface topography (i.e. a distortion induced by the overlying topography).

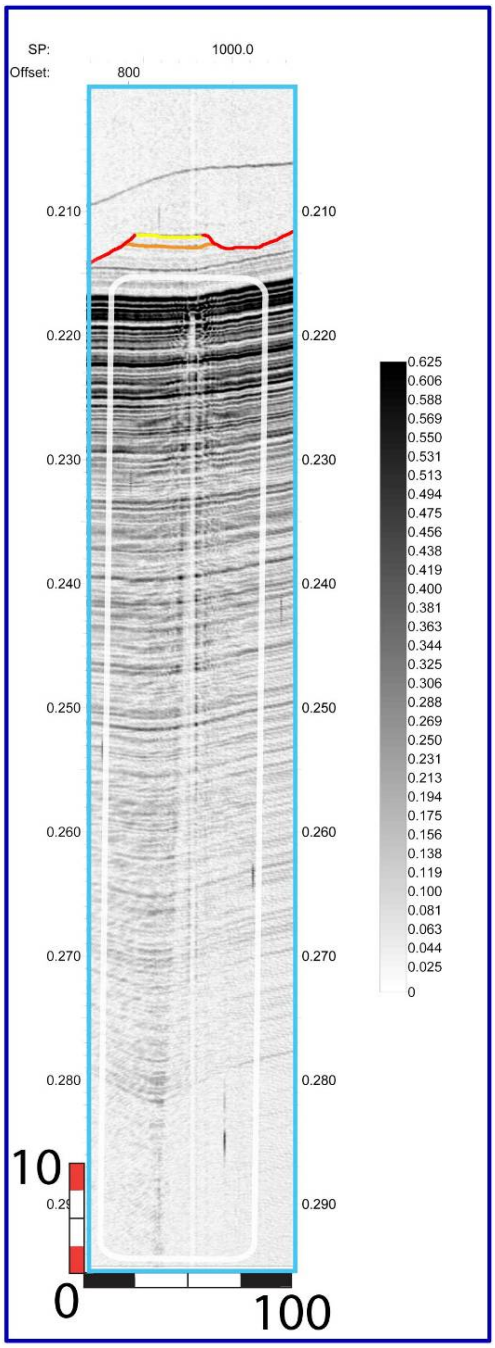

Figure 5.6 Deep Chimney. An example of a deep chimney taken from CHIRP profile cdw13 (Fig. 5.3).

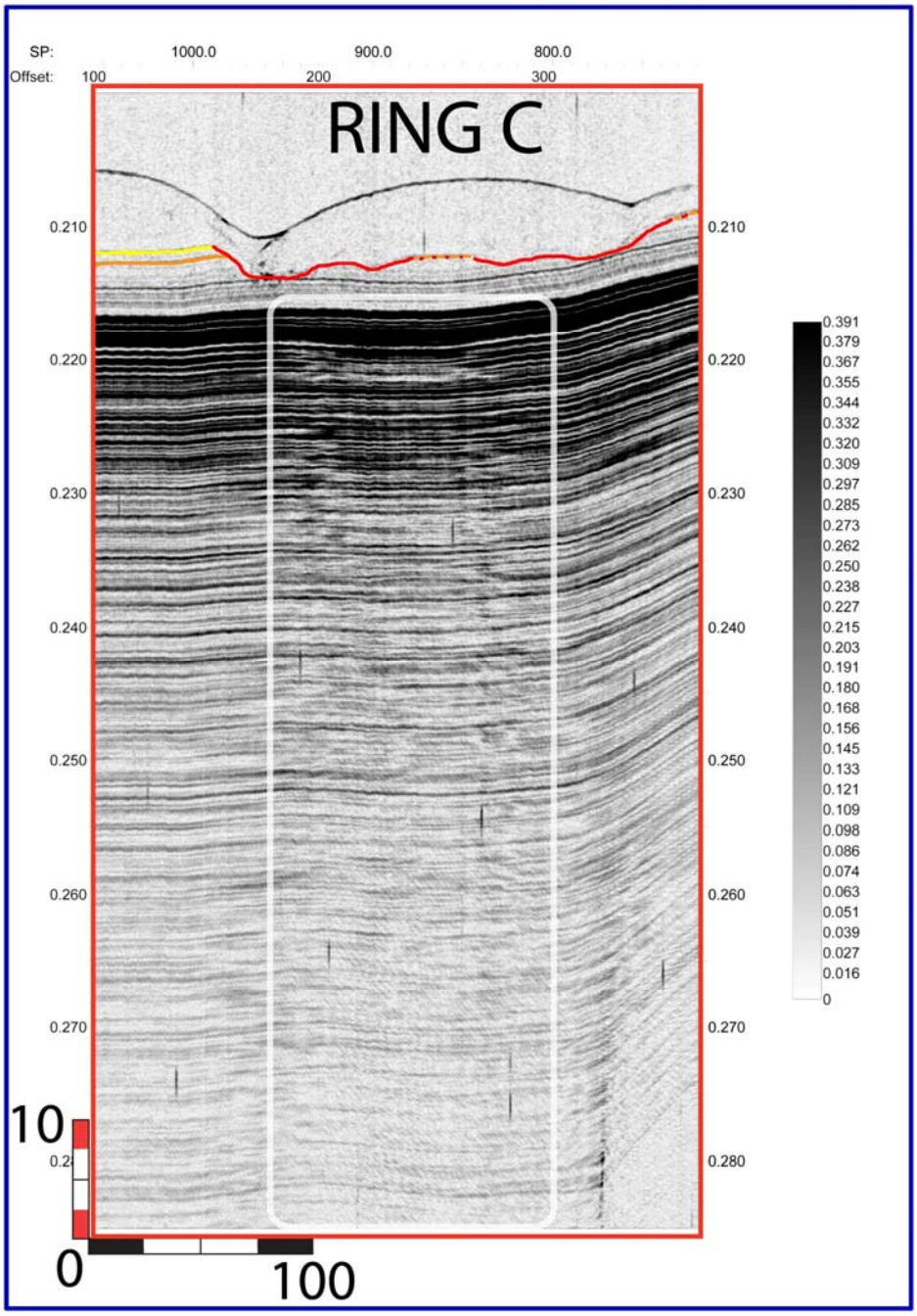

Figure 5.7 Diffuse Chimney. An example of a diffuse chimney taken from CHIRP profile cdw26 (Fig. 5.4).

5.1.3.5 Short Chimneys

A map depicting the distribution of short chimney structures show that they are very densely concentrated in the south eastern half of the survey area where a majority of the bathymetric relief is expressed in the lake floor (Fig. 4.1). The seismic amplitude variation associated with these short chimneys may reflect variations intensity of fluid flow during their formation or possibly the degree of flow localization or spatial stabilization (i.e. did the flow remain spatially fixed or did it move about the space?).

The fact that many short chimney structures terminate below what is interpreted to be the uppermost glaciolacustrine reflector indicates that these drainage structures were actively draining near the end of glaciolacustrine sedimentation, and that this drainage waned prior to the end of glaciolacustrine deposition (Fig. 5.8). Many of the suspect or poorly developed short chimneys are found beneath areas that show no discontinuity in the upper glaciolacustrine reflectors. This implies that in some areas flow was not sufficient enough to facilitate significant erosion. The deep chimneys and the most prominent short chimneys abruptly terminate against the unconformable glaciolacustrine-Holocene boundary. This implies continued drainage through the end of glaciolacustrine sedimentation and possibly for some time into the Holocene. Under high gain weak internal reflectors can be seen above many of the drainage features. This suggests that in some areas (above the most pronounced drainage structures) sediment dewatering within the basin could

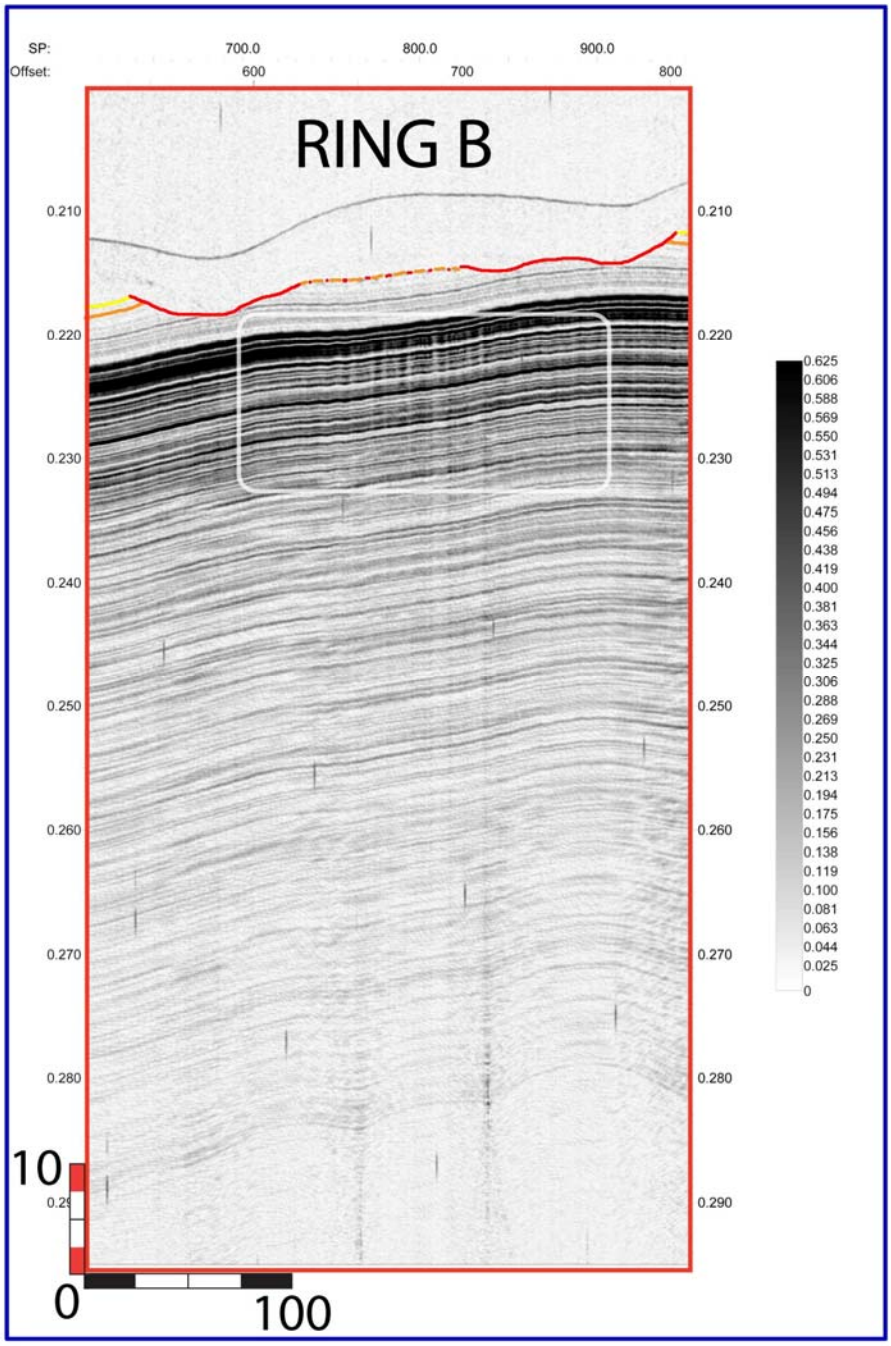

Figure 5.8 Short Chimneys. Examples of a short chimneys taken from CHIRP profile cdw13 (Fig. 5.3).

have been ongoing at the onset of and well into Holocene post-glacial sedimentation of the basin.

Sidescan sonar data collected on other parts of the Superior basin exhibit amplitude variations about pockmarks. These have been interpreted to represent lag surfaces resulting from the winnowing of ultra fines by the expulsion of sediment pore water (Wattrus, pers. comm.). This suggests that in some cases these structures, may still be actively draining, though possibly at a much reduced rate.

5.1.4 Seismic Unit D

Seismic unit D is interpreted to be post-glacial Holocene lacustrine deposits. The draped morphology of this unit is indicative of a low-energy depositional environment, and the absence of internal reflectors implies a rather homogenous composition (Stoker et al., 1997). When the gain is turned up, very-low amplitude internal reflectors can occasionally be recognized, but this is the exception and not the rule. These internal reflectors are typically imaged in close proximity to the lake floor ring edges but are also sometimes seen in areas where there is no present day bathymetric relief. The weak internal reflectors are interpreted to be the result of subtle changes in density associated with ongoing fluid flow from the glaciolacustrine sediments below. The thickness of the Holocene unit varies across the survey area and it frequently thins within the lake floor rings (Fig. 4.17). The fact that the Holocene unit thickness decreases within

the rings supports the idea that the sediments were dewatering, possibly well into the Holocene sedimentation of the basin.

5.2 Fluid Flow

There are numerous physical mechanisms that can induce fluid flow in earthen materials. When sediments are deposited in an aqueous setting, water is trapped in the pore spaces between the individual sediment grains. Fluids or gases can also be introduced to a system after deposition as the result of tectonic processes, diagenetic changes, hydrocarbon generation, or as the result of fluid/gas migration. A comprehensive review of the many mechanisms capable of generating fluid flow discussed below can be found in *Seabed fluid flow; the impact on geology, biology, and the marine environment* by Judd and Hovland (2007).

The intent of this section is to introduce the major mechanisms that are responsible for fluid flow in lake floor sediments and it’s possible role in the formation of Lake Superior's Rings. If a flow mechanism is unlikely to have influenced lake floor ring formation, reasons will be stated for it’s dismissal. The section will end with the favored flow mechanism(s) and a potential trigger.

5.2.1 Heated Fluids

Fluid flow associated with geothermal and hydrothermal systems resulting from magma or volcanic activity (Hovland and Judd, 1988; Pickrill, 1992, 1993) have been shown to induce fluid flow. A detailed review of fluid flow linked to

heated fluids associated geothermal and hydrothermal system is provided by Judd and Hovland (2007). The Lake Superior region was tectonically and volcanically active in its past (Huber, 1975; Klasner, 1982; Ojakangas and Dickas, 2002; Schulz and Cannon, 2007), however, this activity ceased over a billion years before the deposition of the modern day lake's Quaternary sediments. As a result there is no evidence that fluid generation or flow has occurred in the lake floor sediments as a result of this type of activity.

5.2.2 Hydrocarbons

Hydrocarbons are often associated with fluid and gas migration in marine and lacustrine environments (Judd and Hovland, 2007; Sahling, 2008; Webb, 2008; Hustoft et al., 2009).There is little evidence that there is any significant gas generated in the deep lake floor clays. They contain very little source material, (<1.0% TOC) (Johnson et al., 1982; Cartwright et al., 2004) and seismic data collected in the lake shows no sign of gas wipeout (Hovland and Judd, 1988; Cartwright et al., 2004; Wattrus, pers. comm.). For these reasons, Lake Superior's pockmark-rings are not thought to be related to migrating hydrocarbons.

5.2.3 Submarine Groundwater Discharge (SGD)

Submarine groundwater discharge (SGD) is the expulsion of connate or meteoric fresh water from below the sea/lake-floor (Burnett et al., 2003; Judd and Hovland, 2007). Although there are local examples of pockmarks tied to ground

water seepage along underlying fractures in the bedrock, Lake Superior's pockmark rings are very large and widespread. As such there is little evidence to support large scale and wide spread SGD throughout the Lake Superior Basin (Wattrus, pers. comm.).

5.2.4 Syneresis

Syneresis is the process by which gel-like materials (often water saturated-clays) spontaneously expel pore fluid associated with the volumetric contraction of the material. Often this is in response to a chemical trigger. A key characteristic of this process is that it can occur even when sediment is not sub-aerially exposed i.e. while it is submerged. Sediments that have experienced syneresis often exhibit polygonal fracturing and faulting as a result of the volumetric contraction that the process generates (Cartwright and Lonergan, 1996). Triggers for syneresis include a salinity change in surrounding fluids, diagenesis, seismic shaking, compaction, and/or gravitational loading (Pratt, 1998; Boggs, 2005; Hustoft et al., 2009). Lake Superior's polygonal pockmark rings were first described by Berkson and Clay (1973) who invoked large scale syneresis to explain their polygonal organization. It should be noted however, that they failed to provide a mechanism for triggering the contraction of the lake floor sediments.

The volumetric contraction of clays experiencing syneresis is accommodated by the formation of polygonal fault systems (PFS) (Wattrus et al., 2000; Cartwright et al., 2003; Wattrus et al., 2003; Cartwright et al., 2004). The

development of PFS in an oil field can be economically significant because these faults can then be exploited by migrating fluids or gasses within the sediments. Lake Superior's rings have been suggested to be the expression of an immature polygonal fault system by Wattrus (2000, 2003) and then by Cartwright et al. (2004). The lake floor rings are no longer believed to be associated with PFS because the rings have been observed in the absence of any visible faulting (Wattrus, pers. comm.).

5.2.5 Faulting and Debris Flows

Faults increase secondary porosity and permeability in sediments (Fetter, 2001). They are often exploited by migrating fluids and gases (Wattrus et al., 2003; Cartwright et al., 2004). Faults (slip planes) in marine or lacustrine sediments can result from: syneresis as previously discussed, debris flows; slumps, turbidite deposits, or block-landslides. This phenomenon has been observed globally (Lastras, 2004, Berndt, 2005; Guillaume et al., 2011). There is no evidence of faulting or debris flows observed in this survey area however there are some beautiful and large debris flows elsewhere in the Thunder Bay Trough (Wattrus, pers. comm.).

5.2.6 Seismic Shaking

Seismic shaking has been shown to induce fluid flow in lacustrine and marine settings (Lastras, 2004; Chapron et al., 2004; Fanetti et al., 2008; Guillaume et al., 2011) . Although the Great Lakes are not particularly seismically

active, earthquakes are often triggered during isostatic rebound following deglaciation (Wu and Johnston, 2000). In such cases the frequency of occurrence and magnitude of the seismic events is greatest immediately after deglaciation, although seismic events can still occur several thousand years after deglaciation (Mohajer et al., (1992)). If localized seismicity is responsible for inducing fluid flow in Lake Superior's sediments, sediment dewatering would be expected to be episodic if not ongoing (as the basin is still rebounding). Seismic shaking is not likely involved in the dewatering of Lake Superior's sediments and the formation of the lake floor rings. If it were then one would expect to find buried pocks and dewatering structures at various intermittent depths within the glaciolacustrine sediment package. All of the buried pocks observed in this study occur at the similar depths, which argue against episodic drainage.

5.2.7 Over-pressure in Lacustrine/Marine Sediments

Internal pore-fluid pressure controls the strength of sediments and their behavior. Over-pressurization of sea/lake-floor sediments has been identified as a principle (necessary) component in fluid escape(s) and submarine-slope failures (soft-sediment deformation) (Hampton et al., 1996; Berndt, 2005; Fanetti et al., 2008; Flemings, 2008; Long et al., 2011; Dugan, 2012). The presence of gas or gas-hydrates exacerbates basin over-pressurization (Judd and Hovland, 2007). Two principle causal mechanisms for marine and lacustrine sediment-over-pressurization are: the rapid deposition of fine-grained low-permeability sediments; or a reduction in confining pressure (sea/lake-level drop).

5.2.7.1 Rapid Sedimentation

Fine grained sediments have high porosities and low permeabilities (Fetter, 2001). Sediment permeability can vary widely (by 13 orders of magnitude) from pervious-to-impervious. Clay permeability can vary by seven orders of magnitude (Bear, 1988; Fetter, 2001). Clayey sediments are prone to developing overpressure during and after deposition because they do not efficiently dewater at a rate proportionate with overburden loading and compaction (Bolton et al., 1998; Trincardi et al., 2004; Judd and Hovland, 2007; Plaza-Faverola et al., 2011). The rapid deposition of low-permeability fine-grained silts and clays effectively seal the sediment column during deposition and compaction. The increased overburden load is distributed to the incompressible pore-fluid, (water), and as a result the sediment's porosity does not decrease as much as it would have had the trapped pore water been able to freely move through and out of the sediments. These sediments are referred to as being over-pressured or under-consolidated (Bitzer, 1996; Bolton et al., 1998; Berndt, 2005; Behrmann et al., 2006; Judd and Hovland, 2007). The magnitude of modeled overpressure resulting from the rapid deposition of fine grained sediments has been shown to reach pressures approaching 95% of lithostatic pressure (Flemings et al., 2003).

While these fine-grained sediments are over-pressured and effectively sealed over decadal to century time scales, given sufficient time (multiple millennia) they are able to dewater via compaction and achieve equilibrium with

their environment. Variations in sedimentation rates (differential sedimentation) can shift the sediment dewatering regime from a homogeneous compaction-driven system to more-focused flow regimes (Dugan and Flemings, 2000a; Dugan and Flemings, 2000b; Berndt, 2005; Behrmann et al., 2006; Judd and Hovland, 2007).

As previously noted, the varved-clayey sediments in the survey area are ultra-fined grained (< 2 μm), and were deposited very rapidly. Correlated varve thicknesses vary throughout the lake and are observed but are commonly greater than one or two centimeters (Breckenridge et al., 2004; Breckenridge, 2005). If these varves do in fact represent an annual record, then they show glaciolacustrine sedimentation rates can exceed five cm per year. In contrast the Holocene sedimentation rates are often measured in tenths of a millimeter per year (Breckenridge et al., 2004) and sedimentation rates of fine grained sediments in excess of one millimeter per year are known to induce over-pressurization in sedimentary basins (Walter, 1975; Behrmann et al., 2006).

The sediment piston core taken from within the survey area has not been split or subsequently photographed; however, the X-Radiographic image exhibits light and dark rhythmites are present in the core. The metadata (acoustic impedance, bulk density and to a lesser degree P-wave velocity) obtained for this core shows local maxima and minima associated with the light-dark rhythmites. The light-dark couplets are believed to be annual varves (Breckenridge, pers. comm.). These varves have not been correlated with the known Lake Superior

varve stratigraphy and are not useful for the purpose of dating the sediments. They do however suggest that these sediments were deposited very rapidly, on the order of four or five centimeters per year. Because of the ultra-fine grained nature of the sediment and the extremely high sedimentation rates, the system in which these rings formed is interpreted to be significantly over-pressured. Examples of focused fluid-flow resulting from rapid sedimentation include the Nyegga pockmark field in the mid-Norwegian margin (Reiche et al., 2011) and in the Gulf of Mexico Continental Margin (Behrmann et al., 2006).

The deep chimneys are primarily restricted to linear trends that follow topographic lows observed in the glacial unit. It is possible that sediments were focused within these valleys effectively increasing the rate of sedimentation. The CHIRP did not image the glacial unit or the lower portion of the glaciolacustrine unit. There is no evidence of sediment slumping or debris flows in the airgun SCS data.

5.5.7.2 Change in Confining Pressure

Open systems that are under hydrostatic conditions will not develop over-pressure in response to sea/lake-level fluctuations because the pore pressure in these systems varies with water depth (Fetter, 2001; Fanetti et al., 2008). If low or impermeable layers are present, however, the sediment is no longer open and a reduction in sea/lake-level (confining pressure) can induce pore-fluid overpressure at depth (Hampton et al., 1996). A rapid drop in sea/lake-level can lead to the over-pressurization of unconsolidated water-charged sediments

resulting in focused-fluid flow and soft sediment deformation (Lee et al., 1996; Fanetti et al., 2008).

Low permeability sediments (clays) are typically unable to express pore water at a rate proportionate to the rate of sea/lake-level drop. Specifically, the faster sea/lake level drops (which is directly linked to the reduction in confining pressure), the coarser the material needs to be to avoid becoming over-pressurized. This inability to depressurize creates a pressure gradient between the sediment and water column interface, triggering fluid flow.

A reduction in sea or lake level can in itself induce overpressure in fine grained (tight) systems. If a system is already over-pressured as the result of the rapid deposition of fine grained clays, then a subsequent drop in confining pressure (lake level) would compound pore-fluid overpressure.

5.2.7.3 Lake Superior Trigger

The failure of ice dams containing Lake Agassiz's resulted in several catastrophic flood outbursts during the last de-glaciation (Farrand and Drexler, 1985; Teller et al., 2002; Teller, 1995, 2003, 2005; Gary, 2010). Catastrophic eastward Agassiz flood outbursts during the deglaciation of the region are well documented, but their exact routings is still a subject of debate (Teller, 1995; Leverington, 2003; Fisher, 2005; Fisher et al., 2006; Fisher et al., 2008; Gary, 2010; Yu et al., 2010).

A catastrophic Agassiz flood outburst could act as an ideal trigger for the wide-spread dewatering of the Lake Superior sediments. Towards the end of the

last glacial maximum, around 9300 calibrated years before present (Yu et al., (2010)) a catastrophic eastward Agassiz drainage is believed to have entered Lake Superior. The proposed routing of this Agassiz flood outburst is thought to have been routed through the Lake Superior basin through Lake Huron >> North Bay >> Ottawa River >> St. Lawrence River Valley (Yu et al., 2010). This led to a short-term lake level rise and the overtopping and rapid incision of the drift moraine sill near Sault Ste. Marie resulting in a ca. 45 meter reduction in lake level (Saarnisto, 1974; Farrand and Drexler, 1985). The speed of this lake level change was probably extremely fast and may have been achieved in less than a year (Yu et al., 2010). Which in geologic time one year is effectively instantaneous.

5.2.7.4 1D-Flow Model

A one-dimensional numerical model was used to further investigate the effects of rapid sedimentation and confining pressure reductions. The model is run in MATLAB and a copy of the code used is included in Appendix-I. This model calculates simulated pore pressure in terms of excess hydraulic head. These hydraulic head values are converted to pressure prior to plotting the model results. This model is governed by the Gibson diffusion equation shown below. This is a small-strain model, where k = hydraulic diffusivity (meters/year), S_S = specific storage (meters^{-1}), ρ_b = bulk sediment density, ρ_w = fluid density, l = sediment pile thickness (meters), and $\dot{\ell}$ = sedimentation rate (meters/year). It is

assumed that water is incompressible and that the system behaves diffusively. It does not consider explicitly the collapse of internal pore space (compaction). It is assumed that the length changes that result from compaction are significantly smaller than the overall thickness of the sediment pile.

$$k\frac{\partial^2 h}{\partial z^2} = S_S\frac{\partial h}{\partial t} - S_S\frac{\rho_b}{\rho_w}\dot{\ell}$$

The physical system modeled using this equation models how internal pressure changes in space and time within a sediment pile. Hydraulic diffusivity is obtained by dividing the sediment's hydraulic conductivity by its specific storage. Reasonable real world values were selected for the various physical parameters in the model. The most important parameters are hydraulic conductivity (a function of intrinsic permeability), and specific storage (a measure of the material's bulk compressibility). Hydraulic conductivities (K) between 10^{-6} and 10^{-11} m/s were used, which represent silty-sand and clay respectively. A fairly large specific storage (S_s) value of 10^{-3} m^{-1} was chosen for this simulation. This was because clays are relatively compressible.

This survey was conducted in an area of Lake Superior where the sediments are primarily clays and were deposited very rapidly. Intuitively Lake Superior's sediments were over-pressured as a result. A subsequent lake level drop (loss of confining pressure) would further stress the system and effectively over-pressure an already over-pressured system and could trigger fluid expulsion. This is a complex physical system being represented by a "simple"

1D-model. The model behaved as expected, with the onset of overpressure occurring more rapidly with lower (tighter) hydraulic conductivities.

The model simulated the onset of over-pressure in the sediment pile with sedimentation rates between 1 mm/yr and 1.5 cm/yr. Modeled results for a sedimentation rate of 5 mm/yr are shown in Figure 5.10. This behavior does not change with reasonable perturbations in hydraulic conductivity. Simulations with sedimentation rates in excess 1.5 cm/yr still develop reasonable over-pressure initially but the simulated pore-pressures quickly exceed lithostatic pressure. This is a scenario that would lead to the bulk failure of the sediment package in a natural system. This model lacks physical feedbacks (i.e. failure) found in natural systems. These physical feedback are difficult to model and would be at best, poorly constrained.

If the lake level remains steady after the cessation of sedimentation, the simulated overpressure diffuses on a millennial time scale. If the modeled system is at hydrostatic pressure and then experiences a reduction in confining pressure in the form of a lake level drop the simulated system becomes over-pressured. The model shows that a 40 meter drop in lake level produces significant over-pressure in the sediment pile. Simulations where a lake level drop was applied to already over-pressured sediments, showed failure (pore pressure = lithostatic pressure) to be effectively instantaneous in the upper portion of the modeled sediment pile. While this model is not empirical proof that the lake floor rings are

the result of sediment dewatering triggered by a drop in lake level, it does show a proof of concept.

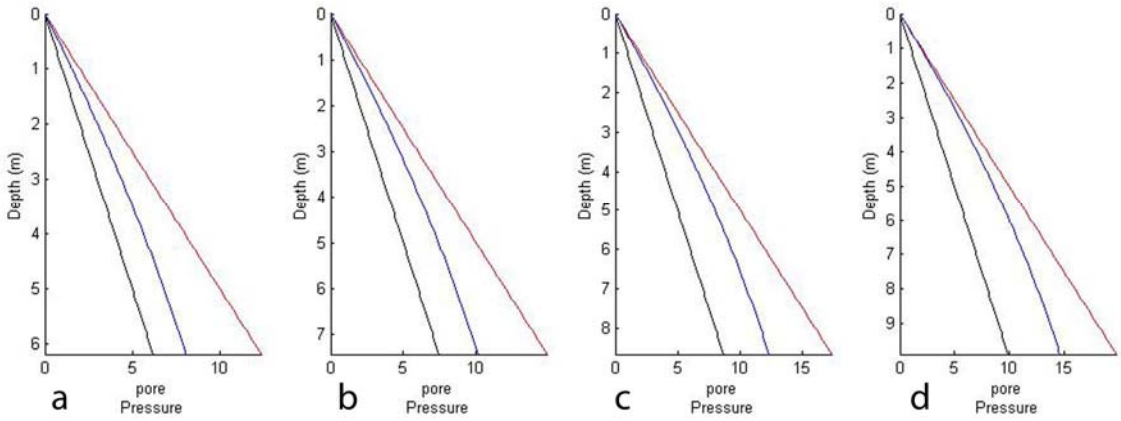

Figure 5.9 a,b,c,d MATLAB simulation results. Four snapshots in time (a,b,c,d) with a sedimentation rate of 5 mm/yr. Vertical axis represents sediment pile thickness in meters. The sediment pile grows in time and the 4 plots are not the same thickness. Horizontal axis is pressure in Newtons. Hydrostatic pressure (black), simulated pore pressure (blue), and lithostatic pressure (red). Simulated pore pressures are closest to lithostatic pore pressures in the upper 1-2 meters of the sediment column.

Chapter 6: Conclusions

The primary objectives of this project were to: compile a detailed morphologic picture of the subsurface plumbing associated with the lake floor rings using seismic reflection methods; establish a relative chronology for their formation; and propose a rudimentary physical model that explains their formation. This study set out to do this by testing three proposals:

a. The lake floor rings are comprised of polygonal ring-like chains of individual pockmarks.
b. Dewatering structures that terminate below or in close proximity to individual pockmarks, should be present in high resolution CHIRP profiles.
c. The lake floor bathymetric features are not controlled or influenced by the underlying till or bedrock topography.

The following conclusions were drawn from this study.

1. Lake Superior's glaciolacustrine sediments were significantly over-pressured, the direct result of extremely rapid sedimentation of fine-clays. These high sedimentation rates were facilitated by the proximity of the site to sediment-laden glacial water sources and, sediment focusing in the Thunder Bay Trough near Isle Royale.
2. The existing over-pressures were then intensified by a ca. 45 meter drop in lake level, (confining pressure) facilitated by eastward Agassiz drainage triggering the overtopping and incision of the

morainic barrier near Sault Ste Marie. This over-pressurization of already over-pressured sediments triggered the onset of rapid widespread sediment dewatering (expulsion of pore-water) in the basin.

3. The expulsion of pore-water led to the development of sub-surface dewatering structures and the associated erosional bathymetric pocks (lake floor rings).

This study has revealed that the lake floor rings observed in the survey area are not polygonal chains of individual well-defined standard pocks that evolved during the course of the drainage event. They are instead interpreted to be large polygonal ring-shaped composite pocks, comprised of small unit pocks and larger standard/asymmetric pocks. The high-resolution CHIRP data reveal that three distinct types of dewatering structures (deep-chimney, diffuse-chimney, and short chimney) are developed in the very fine grained glaciolacustrine clays below the lake floor.

The well defined deep chimneys are not directly associated with the lake floor rings. They follow a pair of NW-SE linear trends that overlie topographic lows in the top of the glacial unit, on which the glaciolacustrine sediments rest. They are interpreted to be the result of deep-sourced extreme over-pressure facilitated by an increase in effective sedimentation rates resulting from sediment focusing within the topographic lows. They often terminate below or in close

proximity to deep, well defined standard pocks. Although these two linear trends intersect several lake floor rings, well developed deep chimneys are not commonly found beneath the rings in general.

Diffuse chimneys are found below individual lake floor rings. These are again deep-sourced dewatering structures but, unlike the previously described chimney structures, they are not associated with topographic relief on the surface of the underlying glacial section. These features are interpreted to be the result of either:

1. dewatering that either did not evolve and develop a strong central shaft;
2. dewatering associated with a continuously migrating dominant fluid pathway below the rings.

Diffuse chimneys are highly speculative dewatering structures and require further study.

Simple numerical modeling of pore pressure profile evolution in a clay dominated sedimentary package subject to extremely high sedimentation rates show that such a system will be over-pressured. The results suggest that the pore pressure profile in the near surface portion of the sedimentary pile tends to most likely intersect the lithostatic profile. This makes these sediments most susceptible to failure and drainage if the ambient confining pressure is abruptly decreased as a result of a lake level drop. The observation of short chimneys throughout the survey area suggests that this indeed happened. These drainage

features are particularly well developed in the southern portion of the survey area where they occur below a well developed network of lake floor rings.

The trigger for the abrupt release of stored pore water was probably an abrupt drop in lake level that occurred close to the termination of glaciolacustrine sedimentation in the basin when water overflowing into Superior from glacial Lake Agassiz overtopped and then rapidly incised a morainal sill at Superior's outlet near the lake's present day outlet at Sault St Marie. Recent work by Yu et al. (2010) suggest that this produced a ca. 45 meter drop which they suggest may have occurred in less than a year. Sensitivity studies using the one-dimensional model developed for this study suggest that fine-grained clays are so "tight" that failure would have been expected even if the drop in lake level had taken several decades or even centuries.

The high resolution CHIRP data shows that the structure of the lake floor rings is more complex than their expression in multibeam bathymetric images might suggest. The CHIRP data suggests that the area inside the ring has also been excavated, presumably by fluid draining from the lake floor as a result of the over-pressured sediments responding to rapid lake level change. One scenario that might explain the ring's complex structure envisions early dewatering removing material from the interior of the ring to form a simple pock. As time passes and drainage proceeds, the focus of the drainage event migrates outward to tap as yet undrained sediments. This would result in the previously excavated pock being buried by sediment mobilized by fluid flowing from the

newly developed pocks. This model also might explain why individual rings in networked systems never appear to intersect each other. Once a volume of sediment has been drained there is no reason why a migrating drainage system would migrate into that space. In a sense then, the drainage system would tend to self-organize itself into a network of polygonal pocks.

This study set out to study the origin and development of Lake Superior's lake floor rings, and to do this several high resolution datasets were acquired. The new data has answered some questions and raised new ones. In particular, although a model for the formation of the rings has been proposed, the present study has been unable to definitively answer the question why the rings are polygonal or why when they form networks, adjacent rings in the network never intersect each other. Presumably, as previously noted, the drainage system is self-organized. Finally, the present study has not been able to explain why similar features have not been observed elsewhere. There may be two reasons why this is so. Firstly, the circumstances required to produce these type of features are rather unusual (over-pressure generation followed by a basin-wide trigger). Secondly, the features are relatively small and require high-resolution techniques to study. This would not be possible for buried ancient systems where seismic surveying methods, even the advanced 3D techniques used by the oil and gas industry, lack the high frequencies necessary to image them.

The new CHIRP data has shed new light on the morphology of the rings and their relationship to underlying drainage features. The model outlined should

be tested and to do this further work is required. This should include the collection of true 3D high-resolution data over a larger area of rings. Ideally this survey should be conducted with a high frequency source to obtain the highest possible resolution. Since high frequency sources are typically depth-limited, that is their energy is rapidly attenuated, a near-lake floor survey from an autonomous underwater vehicle (AUV) would be highly desirable. Such a survey platform would be able to collect high quality data without concerns about the sea state which otherwise could frustrate surface based attempts to collect high-resolution data. Secondly a detailed program of piston coring in and across selected lake floor rings would be extremely beneficial when attempting to reconstruct the architecture and development of these features. Hopefully such a program would make it possible to test the validity of the model outlined above for the development of the rings. Lastly it would be extremely interesting to see if these pocks are still active. In order to do this seep meters could be installed above/in pockmarks identified by high-resolution multibeam bathymetric surveying. This would probably require the use of remotely operated vehicles (ROVs) to ensure accurate installation on the lake floor.

References

Bear, J., 1988, Dynamics of fluids in porous media: New York, New York : Dover.

Behrmann, J.H., Flemings, P.B., John, C.M., Iturrino, G.J., Aizawa, Y., Binh, N.T.T., de Silva, N., Dugan, B., Edeskar, T.M., Franke, C., Gay, A., Gilhooly, W.P., III, Gutierrez-Pastor, J., Jiang, S.Y., Long, H., Moore, J.C., Nonoura, T., Pirmez, C., Reichow, M., Sawyer, D.E., Schneider, J., Shumnyk, A.V., Suzuki, T., Takano, Y., Urgeles, R., Yamamoto, Y., and Zampetti, V., 2006, Rapid sedimentation, overpressure, and focused fluid flow, Gulf of Mexico continental margin: Scientific Drilling, v. 3, p. 12-17.

Berkson, J.M., and Clay, C.S., 1973, Microphysiography and Possible Iceberg Grooves on the Floor of Western Lake Superior: Geological Society of America Bulletin, v. 84, p. 1315-1328.

Berndt, C., 2005, Focused fluid flow in passive continental margins: Philosophical Transactions - Royal Society. Mathematical, Physical and Engineering Sciences, v. 363, p. 2855-2871.

Bitzer, K., 1996, Modeling consolidation and fluid flow in sedimentary basins: Computers & Geosciences, v. 22, p. 467-478.

Boggs, S., Jr., 2005, Principles of sedimentology and stratigraphy: United States, Merrill Publ. Co. : Columbus, OH, United States.

Bolton, A.J., Maltman, A.J., and Clennell, M.B., 1998, The importance of overpressure timing and permeability evolution in fine-grained sediments undergoing shear: Journal of Structural Geology, v. 20, p. 1013-1022.

Breckenridge, A., 2005, Lake Superior Varves: Records of Lake Agassiz Overflow and Ice Sheet Dynamics, Ph.D. Dissertation, University of Minnesota.

Breckenridge, A., Johnson, T.C., Beske-Diehl, S., and Mothersill, J.S., 2004, The timing of regional Lateglacial events and post-glacial sedimentation rates from Lake Superior: Quaternary Science Reviews, v. 23, p. 2355-2367.

Broecker, W.S., 1989, Routing of meltwater from the Laurentide ice sheet during the Younger Dryas cold episode: Nature [London], v. 341, p. 318-321.

Burnett, W.C., Bokuniewicz, H., Huettel, M., Moore, W.S., and Taniguchi, M., 2003, Groundwater and pore water inputs to the coastal zone: Biogeochemistry [Dordrecht], v. 66, p. 3-33.

Card, K.D., 1990, A review of the Superior Province of the Canadian Shield, a product of Archean accretion: Precambrian Research, v. 48, p. 99-156.

Carney, S.J., 1996, Paleohydrology of the Western Outlets of Glacial Lake Duluth. Ph.D. Dissertation, University of Minnesota.

Cartwright, J., James, D., and Bolton, A.J., 2003, The genesis of polygonal fault systems; a review: Geological Society Special Publications, v. 216, p. 223-243.

Cartwright, J., and Lonergan, L., 1996, Volumetric contraction during the compaction of mudrocks; a mechanism for the development of regional-scale polygonal fault systems: Basin Research, v. 8, p. 183-193.

Cartwright, J., Wattrus, N., Rausch, D., and Bolton, A., 2004, Recognition of an early Holocene polygonal fault system in Lake Superior: Implications for the compaction of fine-grained sediments: Geology, v. 32, p. 253-256.

Cartwright, J.A., 1996, Polygonal fault systems; a new type of fault structure revealed by 3-D seismic data from the North Sea basin: AAPG Studies in Geology, v. 42, p. 225-230.

Chapron, E., van Rensbergen, P., De Batist, M., Beck, C., and Henriet, J.P., 2004, Fluid-escape features as a precursor of a large sublacustrine sediment slide in Lake Le Bourget, NW Alps, France: Terra Nova, v. 16, p. 305-311.

Clark, P.U., 2001, Freshwater forcing of abrupt climate change during the last glaciation: Science, v. 293, p. 283-287.

Clayton, L., and Moran, S.R., 1983, Chronology of late wisconsinan glaciation in middle North America: Quaternary Science Reviews, v. 1, p. 55-82.

Colman, S.M., 2002, A fresh look at glacial floods: Science, v. 296, p. 1251-1252.

Davy, B., Pecher, I., Wood, R., Carter, L., and Gohl, K., 2010, Gas escape features off New Zealand: Evidence of massive release of methane from hydrates: Geophys. Res. Lett., v. 37, p. L21309.

Dell, C.I., 1971, Late Quaternary sedimentation in Lake Superior: United States.

—, 1972, The origin and characteristics of Lake Superior sediments: Proceedings - Conference on Great Lakes Research, p. 361-370.

—, 1974, The stratigraphy of northern Lake Superior late-glacial and postglacial sediments: Proceedings - Conference on Great Lakes Research, p. 179-192.

Drexler, C.W., Farrand, W.R., and Hughes, J.D., 1983, Correlation of glacial lakes in the Superior Basin with eastward discharge events from Lake Agassiz: Special Paper - Geological Association of Canada, v. 26, p. 309-329.

Dugan, B., 2012, A Review of Overpressure, Flow Focusing, and Slope Failure Submarine Mass Movements and Their Consequences, *in* Yamada, Y., Kawamura, K., Ikehara, K., Ogawa, Y., Urgeles, R., Mosher, D., Chaytor, J., and Strasser, M., eds., Volume 31: Advances in Natural and Technological Hazards Research, Springer Netherlands, p. 267-276.

Dugan, B., and Flemings, P.B., 2000a, The New Jersey margin; compaction and fluid flow: Journal of Geochemical Exploration, v. 69-70, p. 477-481.

—, 2000b, Overpressure and fluid flow in the New Jersey continental slope; implications for slope failure and cold seeps: Science, v. 289, p. 288-291.

Fanetti, D., Anselmetti, F.S., Chapron, E., Sturm, M., and Vezzoli, L., 2008, Megaturbidite deposits in the Holocene basin fill of Lake Como (southern Alps, Italy): Palaeogeography, Palaeoclimatology, Palaeoecology, v. 259, p. 323-340.

Farrand, W.R., 1969, The Quaternary history of Lake Superior, p. 181-197.

Farrand, W.R., and , Drexler, C.W.,1985, Late Wisconsinan and Holocene history of the Lake Superior Basin: Special Paper - Geological Association of Canada, v. 30, p. 17-32.

Fetter, C.W., 2001, Applied hydrogeology: United States, Prentice-Hall : Upper Saddle River, NJ, United States.

Fisher, T.G., 2002, Chronology of glacial Lake Agassiz meltwater routed to the Gulf of Mexico: Quaternary Research, v. 59, p. 271-276.

—, 2005, Deglaciation west of Thunder Bay, Ontario; a conundrum for eastern Lake Agassiz drainage: Abstracts with Programs - Geological Society of America, v. 37, p. 5-5.

—, 2006, Abandonment chronology of glacial Lake Agassiz's Northwestern outlet: Palaeogeography, Palaeoclimatology, Palaeoecology, v. 246, p. 31-44.

Fisher, T.G., Lowell, T.V., and Loope, H.M., 2006, Comment on "Alternative routing of Lake Agassiz overflow during the Younger Dryas: New dates, paleotopography, and a re-evaluation" by: Quaternary Science Reviews, v. 25, p. 1137-1141.

Fisher, T.G., and Whitman, R.L., 1999, Deglacial and Lake Level Fluctuation History Recorded in Cores, Beaver Lake, Upper Peninsula, Michigan: Journal of Great Lakes Research, v. 25, p. 263-274.

Fisher, T.G., Yansa, C.H., Lowell, T.V., Lepper, K., Hajdas, I., and Ashworth, A., 2008, The chronology, climate, and confusion of the Moorhead Phase of glacial Lake Agassiz: new results from the Ojata Beach, North Dakota, USA: Quaternary Science Reviews, v. 27, p. 1124-1135.

Flemings, P., 2008, Rapid sedimentation drives overpressure and submarine landslides in the deepwater Gulf of Mexico; IODP Expedition 308: International Geological Congress, Abstracts = Congres Geologique International, Resumes, v. 33, p. @Abstract1353225-@Abstract1353225.

Flemings, P.B., Liu, X., and Winters, W.J., 2003, Critical pressure and multiphase flow in Blake Ridge gas hydrates: Geology [Boulder], v. 31, p. 1057-1060.

Flood, R.D., 1984, Side-scan targets in Lake Superior; evidence for bedforms and sediment transport: Sedimentology, v. 31, p. 311-333.

Gary, J.L., 2010, Characterizing the Discharge Features of Glacial Lake Agassiz Durring The Post-Marquette Period Using Marin Seismic-Reflection Methods, [Masters Thesis], Duluth, University of Minnesota. 79 p.

Green, J.C., 1995, Volcanic rocks of the Midcontinent Rift System; a review: Proceedings of the International Conference on Basement Tectonics, v. 10, p. 65-67.

Guillaume, S.-O., Mathieu, J.D., and Patrick, L., 2011, Marine geology of the St. Lawrence Estuary: IOP Conference Series: Earth and Environmental Science, v. 14, p. 012003.

Hampton, M.A., Lee, H.J., and Locat, J., 1996, Submarine landslides: Reviews of Geophysics, v. 34, p. 33-59.

Hovland, M., and Judd, A.G., 1988, Seabed pockmarks and seepages; impact on geology, biology and the marine environment: United Kingdom, Graham & Trotman : London, United Kingdom.

Hovland, M., Judd, A.G., and Burke Jr, R.A., 1992, The global flux of methane from shallow submarine sediments: Chemosphere, v. 26, p. 559-578.

Huber, N.K., 1975, The geologic story of Isle Royale National Park: U. S. Geological Survey Bulletin.

Hustoft, S., Dugan, B., and Mienert, J., 2009, Effects of rapid sedimentation on developing the Nyegga pockmark field; constraints from hydrological modeling and 3-D seismic data, offshore mid-Norway: Geochemistry, Geophysics, Geosystems - G [super 3], v. 10

Johnson, T.C., 1980, Late-glacial and postglacial sedimentation in Lake Superior based on seismic-reflection profiles: Quaternary Research, v. 13, p. 380-391.

Johnson, T.C., Evans, J.E., and Eisenreich, S.J., 1982, Total organic carbon in Lake Superior sediments; comparisons with hemipelagic and pelagic marine environments: Limnology and Oceanography, v. 27, p. 491-491.

Judd, A., Long, D., Sankey, M., 1994, Pockmark formation and activity, U. K. Block 15/25, North Sea: Bulletin of the Geological Society of Denmark, v. 41, Part 1, p. 34-49.

Judd, A. and Hovland, M., 2007, Seabed fluid flow; the impact on geology, biology, and the marine environment: United Kingdom, Cambridge University Press : Cambridge, United Kingdom.

King, L.H., and MacLean, B., 1970, Pockmarks on the Scotian Shelf: Geological Society of America Bulletin, v. 81, p. 3141-3148.

Klasner, J.S., 1982, The pre-Keweenawan tectonic history of southern Canadian Shield and its influence on formation of the Midcontinent Rift: Memoir - Geological Society of America, v. 156, p. 27-46.

Landmesser, C.W., 1982, Seismic reflection study of recessional moraines beneath Lake Superior and their relationship to regional deglaciation: Quaternary Research, v. 17, p. 173-190.

Lastras, G., 2004, Shallow slides and pockmark swarms in the Eivissa Channel, western Mediterranean Sea: Sedimentology, v. 51, p. 837-850.

Lee, H.J., Chough, S.K., and Yoon, S.H., 1996, Slope-stability change from late Pleistocene to Holocene in the Ulleung Basin, East Sea (Japan Sea): Sedimentary Geology, v. 104, p. 39-51.

Leverington, D.W., 2003, Paleotopographic reconstructions of the eastern outlets of glacial Lake Agassiz: Canadian Journal of Earth Sciences = Revue Canadienne des Sciences de la Terre, v. 40, p. 1259-1278.

Leverington, D.W., Mann, J.D., and Teller, J.T., 2000, Changes in the Bathymetry and Volume of Glacial Lake Agassiz Between 11,000 and 9300 14C yr B.P: Quaternary Research, v. 54, p. 174-181.

Long, H., Flemings, P.B., Germaine, J.T., and Saffer, D.M., 2011, Consolidation and overpressure near the seafloor in the Ursa Basin, Deepwater Gulf of Mexico: Earth and Planetary Science Letters, v. 305, p. 11-20.

Lowell, T.V., 1999, Age verification of the Lake Gribben Forest Bed and the Younger Dryas advance of the Laurentide ice sheet: Canadian Journal of Earth Sciences = Revue Canadienne des Sciences de la Terre, v. 36, p. 383-393.

Lowell, T.V., and Fisher, T.G., 2009, Reply to comments by Carlson et al., (2009) on "Radiocarbon deglaciation chronology of the Thunder Bay, Ontario area and implications for ice sheet retreat patterns": Quaternary Science Reviews, v. 28, p. 2548-2550.

Lowell, T.V., Fisher, T.G., Hajdas, I., Glover, K., Loope, H., and Henry, T., 2009, Radiocarbon deglaciation chronology of the Thunder Bay, Ontario area and implications for ice sheet retreat patterns: Quaternary Science Reviews, v. 28, p. 1597-1607.

Lowell, T.V., Larson, G.J., Hughes, J.D., and Denton, G.H., 1998, Age verification of the Lake Gribben Forest Bed and the Younger Dryas advance of the Laurentide ice sheet: Canadian Journal of Earth Sciences = Revue Canadienne des Sciences de la Terre, v. 36, p. 383-393.

Moernaut, J., Verschuren, D., Charlet, F., Kristen, I., Fagot, M., and De Batist, M., 2010, The seismic-stratigraphic record of lake-level fluctuations in Lake Challa; hydrological stability and change in equatorial East Africa over the last 140 kyr: Earth and Planetary Science Letters, v. 290, p. 214-223.

Mohajer, A., Eyles, N., and Rogojina, C., Neotectonic faulting metropolitan Toronto: Implications for earthquake hazard assessment in the Lake Ontario region, Geology, November, 1992, v. 20, p. 1003-1006.

Mooers, H.D., 2005, Ice advances in the western Lake Superior region; a reevaluation of the St. Louis Sublobe and the Marquette Phase of the Superior Lobe: Abstracts with Programs - Geological Society of America, v. 37, p. 92-92.

Mothersill, J.S., 1979, The paleomagnetic record of the late Quaternary sediments of Thunder Bay: Canadian Journal of Earth Sciences = Revue Canadienne des Sciences de la Terre, v. 16, p. 1016-1023.

Murton, J.B., 2010, Identification of Younger Dryas outburst flood path from Lake Agassiz to the Arctic Ocean: Nature [London], v. 464, p. 740-743.

Ojakangas, R.W., and Dickas, A.B., 2002, The 1.1-Ga Midcontinent Rift System, central North America: sedimentology of two deep boreholes, Lake Superior region: Sedimentary Geology, v. 147, p. 13-36.

Ojakangas, R.W., Morey, G.B., and Green, J.C., 2001a, The Mesoproterozoic Midcontinent Rift System, Lake Superior Region, USA: Sedimentary Geology, v. 141-142, p. 421-442.

Ojakangas, R.W., Morey, G.B., and Southwick, D.L., 2001b, Paleoproterozoic basin development and sedimentation in the Lake Superior region, North America: Sedimentary Geology, v. 141-142, p. 319-341.

Pickrill, R.A., 1992, Shallow seismic stratigraphy of a hydrothermally-influenced lake, Lake Rotoiti, New Zealand: Geological Society of New Zealand Miscellaneous Publication, v. 63A, p. 125-125.

—, 1993, Shallow seismic stratigraphy and pockmarks of a hydrothermally influenced lake, Lake Rotoiti, New Zealand: Sedimentology, v. 40, p. 813-828.

Plaza-Faverola, A., Bünz, S., and Mienert, J., 2011, Repeated fluid expulsion through sub-seabed chimneys offshore Norway in response to glacial cycles: Earth and Planetary Science Letters, v. 305, p. 297-308.

Pratt, B.R., 1998, Syneresis cracks; subaqueous shrinkage in argillaceous sediments caused by earthquake-induced dewatering: Sedimentary Geology, v. 117, p. 1-10.

Reiche, S., Hjelstuen, B.O., and Haflidason, H., 2011, High-resolution seismic stratigraphy, sedimentary processes and the origin of seabed cracks and pockmarks at Nyegga, mid-Norwegian margin: Marine Geology, v. 284, p. 28-39.

Saarnisto, M., 1974, The deglaciation history of the Lake Superior region and its climatic implications: Quaternary Research, v. 4, p. 316-339.

Sahling, H., 2008, Pockmarks in the northern Congo Fan area, SW Africa; complex seafloor features shaped by fluid flow: Marine Geology, v. 249, p. 206-225.

Sharpe, A.T., 2008, Evidence of Soft-Sediment Post-Depositional Deformation in Lake Superior [Masters Thesis]: Duluth, University of Minnesota, 82 p.

Schulz, K.J., and Cannon, W.F., 2007, The Penokean orogeny in the Lake Superior region: Precambrian Research, v. 157, p. 4-25.

Smith, D.G., 1993, Glacial Lake Agassiz; the northwestern outlet and paleoflood: Geology [Boulder], v. 21, p. 9-12.

Stoker, M.S., Pheasant, J.B., and Josenhans, H., 1997, Seismic Methods and Interpretation. in Davies, T.A., et al., eds., 1997 Glaciated Continental Margins: An Atlas of Acoustic Images: London, Chapman & Hall, 315 p.

Stouffer, R.J., 2007, Climate response to external sources of freshwater; North Atlantic versus the Southern Ocean: Journal of Climate, v. 20, p. 436-448.

Teller, J.T., 1985, Glacial Lake Agassiz and its influence on the Great Lakes: Special Paper - Geological Association of Canada, v. 30, p. 1-16.

—, 1995, History and drainage of large ice-dammed lakes along the Laurentide Ice Sheet: Quaternary International, v. 28, p. 83-92.

—, 2003, Controls, history, outbursts, and impact of large late-Quaternary proglacial lakes in North America, *in* A.R. Gillespie, S.C.P., and Atwater, B.F., eds., Developments in Quaternary Sciences, Volume Volume 1, Elsevier, p. 45-61.

—, 2005, Alternative routing of Lake Agassiz overflow during the Younger Dryas; new dates, paleotopography, and a re-evaluation: Quaternary Science Reviews, v. 24, p. 1890-1905.

Teller, J.T., Leverington, D.W., and Mann, J.D., 2002, Freshwater outbursts to the oceans from glacial Lake Agassiz and their role in climate change during the last deglaciation: Quaternary Science Reviews, v. 21, p. 879-887.

Teller, J.T., and Thorleifson, L.H., 1983, The lake Agassiz-Lake Superior connection: Special Paper - Geological Association of Canada, v. 26, p. 261-290.

Trincardi, F., Cattaneo, A., Correggiari, A., and Ridente, D., 2004, Evidence of soft sediment deformation, fluid escape, sediment failure and regional weak layers within the late Quaternary mud deposits of the Adriatic Sea: Marine Geology, v. 213, p. 91-119.

Voytek, E., 2010, Seismic Stratigraphy of Thunder Bay and The Isle Royale Region of Lake Superior, [Masters Thesis], Duluth, University of Minnesota.

Walter H, F., 1975, Geochemistry of oilfield waters. Developments in petroleum science 1: A. Gene Collins. Elsevier, Amsterdam, 1975, XI + 496 pp., Dfl. 95.00: Journal of Geochemical Exploration, v. 4, p. 487-489.

Wattrus, N.J., Cartwright, J.A., and Rausch, D.E., 2000, Lake Superior's rings; clues to the origin of polygonal fault systems, Annual Meeting Expanded Abstracts - American Association of Petroleum Geologists, Volume 2000: United States, American Association of Petroleum Geologists and Society of Economic Paleontologists and Mineralogists (AAPG) : Tulsa, OK, United States, p. 154-154.

Wattrus, N.J., Lewis, C., and Beer, J., 2005, High resolution imaging of de-watering structures in western Lake Superior, Eos, Transactions, American Geophysical Union, Volume 86: United States, American Geophysical Union : Washington, DC, United States, p. @AbstractOS33C-1494.

Wattrus, N.J., Rausch, D.E., and Cartwright, J., 2003, Soft-sediment deformation in Lake Superior: evidence for an immature Polygonal Fault System?: Geological Society, London, Special Publications, v. 216, p. 323-334.

Webb, K.E., 2008, Pockmark ecology in fjords and offshore Norway: International Geological Congress, Abstracts = Congres Geologique International, Resumes, v. 33, p. @Abstract1341399-@Abstract1341399.

Wright, H.E., Jr., 1971, Retreat of the Laurentide ice sheet from 14,000 to 9,000 years ago: United States, Amer. Quat. Ass. : Seattle, WA, United States, 157-159 p.

—, 1973, Superior and Des Moines lobes: Memoir - Geological Society of America, p. 153-185.

Wu, P., and Johnston, P., 2000, Can deglaciation trigger earthquakes in N. America?: Geophysical Research Letters, v. 27, p. 1323-1326.

Yu, S.-Y., Colman,S.M., Lowell, T.V., Miline, G.A., Fisher, T.G., Breckenridge, A. Boyd, M., Teller, J.T., 2010, Freshwater outburst from Lake Superior as a trigger for the cold event 9300 years ago: Science, v. 328, p. 1262-1266.

Zhang, R., 2004, Simulated global response to a substantial weakening of the Atlantic thermohaline circulation: Eos, Transactions, American Geophysical Union, v. 85, p. @AbstractPP31A-0904.

Appendix I

```
pn=1;                    % plot number
dx=.01;                  % spatial step
dt=.0001;                % temporal step
hy(1:1/dx)=[1:1:1/dx];   % initialize hydrostatic plot domain
li(1:1/dx)=[1:1:1/dx];   % initialize lithostatic plot domain
pp(1:1/dx)=[1:1:1/dx];   % initialize pore pressure plot domain
rt(1:1/dx)=[1:1:1/dx];   % initialize real thickness domain
k=10^-8;                 % Hydraulic conductivity (m/s)
Ss=10^-4;                % specific storage (m^-1)
K=k/Ss;                  % physical diffusivity
N=1500/dt;               % # time steps
M=1/dx;                  % # spatial steps
Q=N/4;                   % total number of plots
l=.001;                  % l-dot or rate of deposition
pw=1;                    % density of water
pb=2;                    % density of sediment
L_old=5;                 % initialization of column length

for o=1:1/dx             % initializes column pressure
        h_old(1,o)=0;
end
h=h_old;                 % save head values
STAB=K/(dt/dx^2)         % Stability

for j=1:N;
    L=L_old+l*dt;

h(end)=+h_old(end)+(l*dt*(pb/pw))+(dt*K/(Ss*dx^2*L_old^2)*(2*h_old(end-
1)-2*h_old(end)));
    h(1)=0;
    for i=2:M-1;
        h(i)=K*dt/(dx^2*Ss*L_old^2)*(h_old(i-1)-
2*h_old(i)+h_old(i+1))+l*dx*i*dt/(2*dx*L_old)*(h_old(i+1)-h_old(i-
1))+h_old(i)+(pb/pw)*l*dt;
    end
    rz=L/100;            % real depth incriment on grid
     while Q==j
       for k=0:99        % conversion to pressure and plot
                rt(1,k+1)=rz*k;
                hy(1,k+1)=k*rz;
                li(1,k+1)=(k*pb*rz);
                pp(1,k+1)=(10*pw*(h(1,k+1)))+hy(1,k+1);
                if k==99
                 subplot(1,4,pn)
                 xlabel({'pore';'Pressure'})
                 ylabel('Depth')
                 axis([0 max(li) 0 max(rt)])
                 set(gca,'YDir','reverse')
                 hold on
                    plot(li(:),rt(:),'red')
                    plot(pp(:),rt(:))
```

```
                    plot(hy(:),rt(:),'black')
                end
            end
             Q=Q+N/4;
             pn=pn+1;
         end
        h_old=h;
        L_old=L;
end
```